IBS International Summerschool on Computer Science, Computer Engineering and Education Technology 2017

Wolfram Hardt
(Hrsg.)

TUD*press*

IBS Scientific Workshop Proceedings

Herausgegeben von Stiftung IBS, Wolfram Hardt

Band 4

IBS International Summerschool on Computer Science, Computer Engineering and Education Technology 2017

Wolfram Hardt
(Hrsg.)

TUD*press*
2017

Bibliografische Information der Deutschen Nationalbibliothek
Die Deutsche Nationalbibliothek verzeichnet diese Publikation in der Deutschen Nationalbibliografie; detaillierte bibliografische Daten sind im Internet über http://dnb.d-nb.de abrufbar.

Bibliographic information published by the Deutsche Nationalbibliothek
The Deutsche Nationalbibliothek lists this publication in the Deutsche Nationalbibliografie; detailed bibliographic data are available in the Internet at http://dnb.d-nb.de.

ISBN 978-3-95908-101-6

THELEM Universitätsverlag
GmbH und Co. KG
http://www.tudpress.de

Gesetzt von den Herausgebern.
Printed in Germany.

IBS Scientific Workshop Proceedings

Foundation IBS encourages and supports scientific oriented, interdisciplinary research networks. National and international scientists and experts are brought together for research and technology transfer, where the foundation IBS provides the suitable environment for conferences, workshops and seminars. Especially young researchers are encouraged to join IBS events and benefit by IBS networks.

The *IBS Scientific Workshop Proceedings (IBS-SWP)* publish peer reviewed papers contributed to IBS – Workshops. IBS-SWP are open access publications, i.e. all volumes are online available at IBS website www.ibs-laubuch.de/ibs-swp free of charge.

IBS Scientific Workshop Proceedings aiming to ensuring permanent visibility and access of research results presented during the events organized by Foundation IBS.

Preface

This volume of IBS Scientific Workshop Proceedings presents research contributions to the **International Summer School on Computer Science, Computer Engineering and Education Technologies (ISCSET)** held in Chemnitz and Laubusch (Germany) from 3rd to 7th July 2017. Main goal of this Summer School is to support researchers and students to present their ongoing research ideas to the community. International professors, researchers and industrial experts are invited for key notes and lectures. Key topics are image processing, education technologies, embedded systems and applied computer engineering.

www.ibs-laubusch.de

IBS Scientific Workshop Proceedings

International Summer School on Computer Science, Computer Engineering and Education Technologies (ISCSET)

A Link Density Constrained Walking method for Dynamic Community Detection on Social Network…… 4
Xin Yu, Xie Zhiqiang and Sun Guanglu

A Priori Analysis of Reliability of Radio Engineering Systems with Recovery and Standby……8
Boris I. Filippov and Olga V. Sanina

A web-based application for data visualisation and non-linear regression analysis including error calculation for laboratory classes in natural and life sciences…… 12
Titus Keller and Danny Kowerko

Analysis of Particle Size Distribution of Milk Fat Based on Image Processing……..16
Siqi Zhang, Zhen Zhou, Xu Yang and Xiaotong Na

Automated Noise Analysis for Fault Detection…….. 19
Yanjin Altankhuyag and Wolfram Hard

CCA based Dual Algorithm in a Zigbee transmission under WLAN interference…… 25
Khishigjargal Gonchigsumlaa, Uuganbayar Purevdorj, Narangerel Purevdorj and Young-il Kim

Design of a Laboratory for Audio and Video Based Object Localization and Tracking……..28
Hussein Hussein, Robert Manthey, Abul Hasan, Manuel Heinzig, Marc Ritter, Danny Kowerko and Maximilian Eibl

Designing a Heart Sound Sensor Matrix Structure and Data Processing Platform Using FPGA……..30
Wang Tian, Shi Yunbo and Wolfram Hardt

Device-Independent testsets for inspection of virtual reality devices…….34
Robert Manthey and Danny Kowerko

Digital Learning, Culture and Delivery Mode on E-learning in Mongolia……36
Ariunaa Khashkhuu

FPGA-based Straight Line Detection……...42
Ammad Ali Syed, Stephan Blokzyl and Wolfram Hardt

Generation of Images with Hexagonal Tessellation using Common Digital Cameras……47
Robert Manthey, Tobias Schlosser and Danny Kowerko

Integration of FPGA-based Hardware-acceleration into an Automotive Validation Framework……51
Reham Tallawi, Stephan Blokzyl and Wolfram Hardt

Intersection Point Based Power Lines Detecting and Tracking Algorithm……..55
Batbayar Battseren, Hemanth Patchipala, Uranchimeg Tudevdagva and Wolfram Hardt

Multi-Objective Integrated Scheduling Algorithm Based on Allocation Rule Queue……58
Zhiqiang Xie, Yingchun Xia and Yu Xin

Some experiences of using ICT in active learning……60
Danaa Ganbat and Senden Delgermaa

Support of Inclusive Education of Student with Hearing Disabilities based on Computer Sign Language Translation System……...64
Michael Grif and Yuliya Manueva

The Computational Method for Self-Diagnostical System……67
Yumchmaa Ayush and Michael Grif

The design of high efficiency personal computer power supply……..…70
Yu-Bo Liu, Xu-Dong Wang and Xiao-Li Wang

A Link Density Constrained Walking method for Dynamic Community Detection on Social Network

Xin Yu, Xie Zhiqiang and Sun Guanglu
College of Computer Science and Technology
Harbin University of Science and Technology
Heilongjiang, China
Email: xinyu@hrbeu.edu.cn

***Abstract*—For the problem of dynamic community detection, this paper gives a directed clustering for the nodes on social network, by establishing the tendency of the nodes to their neighboring nodes. By this LDCW (Link Density Constrained Walking) method, the static overlapping communities can be found. For the dynamic evens, we designed the ADCD (Adaptive Dynamic Community Detection) policy, which utilizes the LDCW to adjust the nodes affected by dynamic events adaptively, to detect the dynamic communities. For the ADCD adopts the dynamic adaptive adjustment strategy, the computational cost of ADCD is less. Furthermore, since the ADCD takes the node as the computing unit, the calculation manner of ADCD is not only fit for the distributed computing.**

I. Introduction

Since human social activities are mobile and dynamic, people's thinking habits and hobbies are also slowly changing, which leads to the social network in real life has a dynamic characteristic. There are 3 kinds of individuals on social network: passive, linker and inviters, where the 'passive' individuals appear in a random way, the 'linker' individuals appears in each time, and the 'inviters' individuals appears following the probability which is affected by its neighbor nodes. By adjusting the proportion of the 3 kinds of individuals, the simulation of dynamic social network can be achieved. Therefore, it has the practical significance to study the dynamic evolution of social network. At present, there are a large number of research methods on community evolution, such as tracking and dynamic simulation[1]. On the one hand, it is necessary to ensure that the detected community has a high degree of rationality (such as higher modularity). On the other hand, it is necessary to ensure that the community has dynamic adaptability when a dynamic event occurs. In this paper, we designed the ADCD method based on our previous work[2]. The ADCD has an improvement on the controlling the random walk. When the dynamic event occurs, the dynamic community detection can be achieved by dynamically adjusting the impacted communities.

II. Related Work

The dynamic community detection methods can be classified to 3 categories, containing the dynamic evolution methods, objective function optimization methods, and representative community detection methods.

1) The dynamic evolution methods. These methods are based on the EC(Evolutionary Clustering) methods proposed by Chakrabarti[3]. In the process of community detection, the time slice is a sampling unit for cluster analysis, and the clustering results in time slice t or the global distribution in time slice t-1 are synthetically modeled. In 2007, Chi[4] proposed the PCQ (Preserving Cluster Quality) model and the PCM (Preserving Cluster Membership) model on the basis of the EC algorithm, where PCQ focused on the clustering density, and PCM focused on the node similarity in the same cluster. In 2008, Lin[5] proposed the FacetNet method based on the EC, establishing the snapshot cost function according to the community distribution of the current time slice. In 2009, Kim et al[6] proposed the PDEM (Particle and Density based Evolutionary Clustering) model based on the EC model. The PDEM considered the shortcomings of needing to set the number of communities in advance and not allow the community to dynamically increase or decrease.

2) The Objective Function Optimization Methods. These methods are based on the optimization of modularity[7] or community density function, to make a judgment about the dynamic merging or splitting. In 2011, Nguyen Proposed AFOCS (Adaptive Finding Overlapping Community Structure) algorithm[8] and QCA (Quick Community Adaption) algorithm[9], these two methods divide the dynamic changes of the network into four categories: adding nodes, deleting nodes, adding edges, deleting edges. The AFOCS and QCA have improved the community density function and modularity model respectively, which makes it possible to measure the relationship between the community and the node directly, and takes into account of the increase of modularity to adaptively update detected communities. In 2014, Guo[10] proposed the ECSD (Evolutionary Community Structure Discovery) algorithm for the dynamic community detection problem. The ECSD can be used as the criterion of community merging when the network dynamics changed.

3) The Representative Community Detection Methods. In 2011, Takaffoli[11] proposed a dynamic network analysis method on user nodes. This method has realized the identification of stable nodes and high-impact nodes by establishing the steady-state model and influence model of nodes. In 2012, Duan[12] proposed an incremental k-clique community update method. This method uses the tree in the DFS forest of

the network as the community, and improves the dynamic update strategy of DFS as the dynamic update strategy for the community detection. In 2013, Ma[13] proposed the CUT (Community Update and Tracking) algorithm, which takes the Seed community (the clique community) as the core of the community. This method only updates the Seed community with the changed nodes or edges, when the network topology changes.

This paper is inspired by the adaptive adjustment strategy of AFOCS[8] and QCA[9], combining the adaptive method with the local community detection method. On the dynamic community detection, this article is based on our previous work, namely ANRW[2] walking method, making an improvement on using the link density to control the walking direction. By which the potential community structures are fully walked to improve the accuracy of community detection.

III. Link Density Constrained Walking

A. The description of LDCW

The notations in this article are the following: G represents the network, G_i is the i-th node, L_{ij} is the link between G_i and G_j, C_i represents the i-th community, Ne_i is the neighbors of G_i. There is a network composed by 2 communities C_1 and C_2 in Fig.1, where the nodes G_8 and G_1 are adjacent nodes and these to nodes are the boundary nodes of C_1 and C_2 respectively. For the random walking method, if the node G_1 is the start point of walker, the possibilities of the walker returning the node G_1 through $L_{2,1}$, $L_{3,1}$,$L_{7,1}$ are higher than that through $L_{8,1}$.

The reason is that the node G_1 belongs to the community C_1 and the compactness inside the community is higher than the outside, so when the walker walks into the community C_1, it is not easy to walk out of the community C_1[14]. Similarly, when the walker walk into the community C2 through $L_{1,8}$, it is not easy to return node G_1.

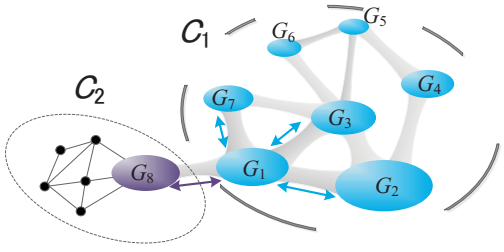

Fig. 1. The random walking example starting from G_1

By analysis we obtain the following conclusions. 1) The possibilities of the walker returning the node G_1 can be obtained by multiple walks. 2) The possibility of walker returning to G_i could reflect the local community structure of the node G_i. 3) The possibility of walker returning to G_i through L_{ji} reflects the importance of G_j to G_i. For the multiple walks, if the number of times of the walker returning to G_i through L_{ji} is more, the tendency of G_i to G_j is more intense. In this paper, we utilize the above 3 characteristics of random walk as the tendency of adjacent nodes modeling method. By which the LDCW (Link Density Constrained Walking) is proposed.

The process of the random walk we designed in this paper is that, when the walker walks into a node G_i, the walker needs to select a neighbor of G_i as the target of the next walk according to the following probabilities.

$$p_j = \frac{ds_j}{\sum_{k \in Ne_i} ds_k} \tag{1}$$

where ds_j is the link density of G_j, B_j is the G_j-center block composed by the nodes of $\{Ne_j \cap G_j\}$.

$$ds_j = \frac{2L(B_j)}{|B_j|(|B_j|-1)} \tag{2}$$

where $L(B_j)$ represents the number of links in B_j, and $|B_j|$ represents the number of nodes in B_j. The Eq(1) and Eq(2) could guide the walker to walk to nodes with high link density, so that the potential community structure can be fully walked.

The process of LDCW is the following:

1) The walker depart from the node G_i for N times, each time walking S step and record the number of times return from each links, denoted by $F_{i,j}$.
2) Calculate the clustering direction of G_i according to $F_{i,j}$, denoted by G_k= argmax($F_{i,k}$, $G_k \in Ne_i$), where G_k is the clustering direction of G_i.
3) Calculate the clustering directions of all the nodes by step 1) and 2), then cluster the directed node and obtained the communities.

Since each node in the LDCW algorithm has only one clustering direction, which causes each node to belong to only one community, so the detected communities by LDCW are hard communities. In order to detect the overlapping community, each node should have multiple clustering directions. By which some nodes must belong to multiple clusters, these nodes are the overlapping nodes, and the overlapping clusters are overlapping communities. The clustering directions of G_i are $Dirs(G_i) = \{G_k, G_{k'}, G_{k''}, \ldots\}$, where G_k=argmax($F_{i,k}, G_k Ne_i$) and $\{(F_{i,k} - F_{i,k'}) < h, (F_{i,k} - F_{i,k''}) < h, \ldots\}$, h is the overlapping tunable parameter, when h=0 the detected communities are hard communities.

B. The Dynamic Adaptive Strategy of LDCW

There are 4 dynamic events in social network, 1) adding nodes; 2) deleting nodes; 3) adding links; 4) deleting links. In order to realize the adaptive dynamic community detection, it is necessary to establish the adaptive strategy for the 4 events. We designed the ADEC (Adaptive Dynamic Community Detection) method, which is based on the LDCW method, to deal with the dynamic events. The basic idea of ADCD algorithm is to only re-walk on the nodes which are intensively influenced by the dynamic events. This method does not make a redirection for all the nodes. So that the ADCD could only adjust the influenced nodes and communities, which could

reduce the calculation cost. The process of ADCD is described as follows.

1) Establish a global adaptive queue Q;
2) Make a judgment on the dynamic event, for adding nodes event go to step 3), for deleting nodes event go to step 4), for adding links event go to step 5), for deleting links event go to step 6).
3) The adding nodes event, node G_i and its neighbor nodes Ne_i are added into the queue Q.
4) The deleting nodes event, the neighbor nodes N_i of G_i are added into the queue$Q$.
5) The adding links event, add the 2 endpoints G_i and G_j of the added link $L_{i,j}$ to the queue$Q$.
6) The deleting links event, Add the 2 endpointsG_i and G_j of the deleted link $L_{i,j}$ to the queue Q.
7) If the queue Q is empty then go to step 9), else go to step 8).
8) Make a calculation on all the elements in Q by LDCW, to adjust the community.
9) End.

The 8) is to adjust the nodes affected by the dynamic event.

The ADCD only re-walks the affected nodes, avoiding the global computation when dynamic events occur, so the time complexity of dynamic community detection can be reduced. Fig.2 intuitively shows the dynamic changes.

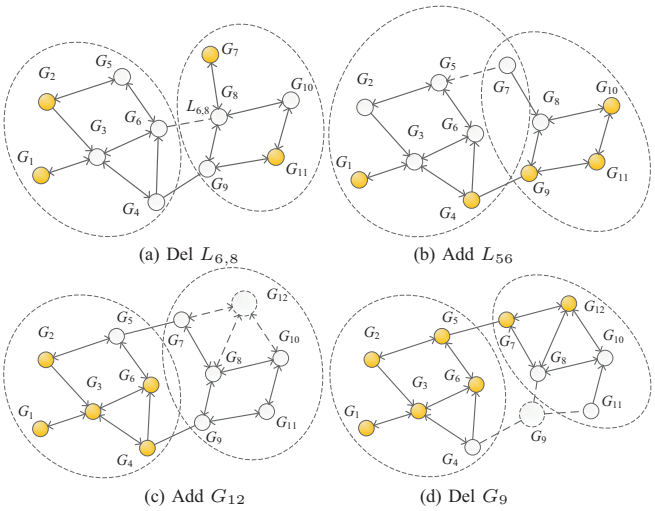

Fig. 2. The illustration of processing the 4 dynamic events by ADCD

IV. Experiment

In this paper, 3 dynamic adaptive methods QCA, AFOCS and MIEN[15] are selected as the comparison methods of this experiment. This experiment uses LFR Benchmark[16] to generate the network containing 1000 nodes as the experimental data, denoted by G_1000. The generation parameters of LFR Benchmark are the following: $|G|$=1000, ad=25, $dmax$=50, $cmin$=40, $cmax$=100, on=130, om=6, mi=2.5). To simulate dynamic changes, we designed the following 8 dynamic change policy:

Policy 1: adding nodes. Select the nodes in the same community as the neighbors, and then increase the links between the added node and the selected nodes.

Policy 2: deleting nodes. Select a node whose neighbors belong to the different communities as the removal node.

Policy 3: adding links. Add the link on the 2 non-adjacent nodes in the same community.

Policy 4: deleting links. Delete the link of the 2 adjacent nodes in the different communities.

Policy 5: adding nodes. Select the nodes in the different communities as the neighbors, and then increase the links between the added node and the selected nodes.

Policy 6: deleting nodes. Select a node whose neighbors belong to the same communities as the removal node.

Policy 7: adding links. Add the link on the 2 non-adjacent nodes in the different communities.

Policy 8: deleting links. Delete the link of the 2 adjacent nodes in the same community.

For the 8 policies, the Policy 1-4 would make the structure of communities become apparent, while the Policy 1-4 would make the structure of communities become blurred.

In this experiment, the dynamic simulation of G_1000 is carried out by the 8 policies, to compare the dynamic adaptive effect of the comparison methods. We utilize the NMI[17] and EQ[18] to measure the performance of the methods. In this experiment, each of the 8 policies is experimented separately, and the experiment process was divided into 10 time slices. Each time slice dynamically changed 200 nodes (links) by the policy. As the application of one policy alone will lead to the NMI and EQ monotonically increasing or decreasing, therefore, we can directly determine the stability of the methods by analyzing the NMI and EQ trends. Fig.3 shows the changes of NMI, where QCA, AFOCS and MIEN have a better performance. It can be seen from Fig. 3 that the NMI of AFOCS and NIEN are getting convergent, which implies the performance of the AFOCS and NIEN algorithms decreases and the 'fatigue' phenomenon occurs, when dynamic events continues to increase. Fig.4 shows the EQ comparison chart of QCA, AFOCS and MIEN, and the results in Fig.4 support the conclusion of Fig.3. Therefore, the ADCD algorithm proposed in this paper has the best stability than the other 3 methods.

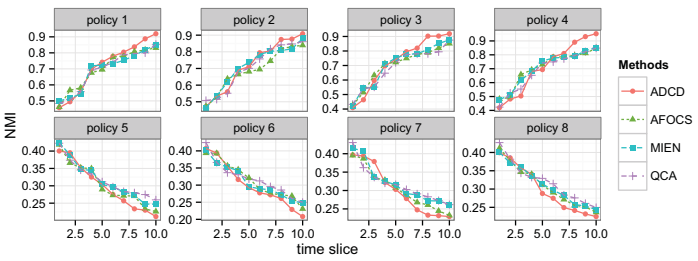

Fig. 3. The NMI comparison chart of QCA, AFOCS and MIEN

V. Conclusion

This paper designs a dynamic community detection method ADCD, which can dynamically adjust the community structure

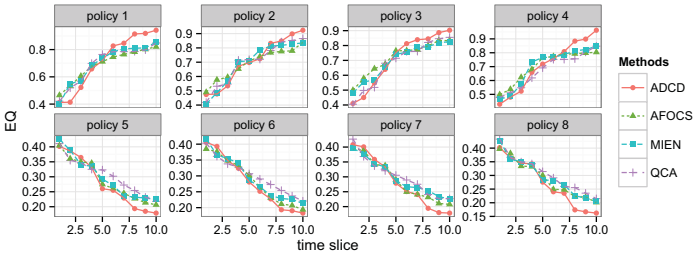

Fig. 4. The EQ comparison chart of QCA, AFOCS and MIEN

according to the dynamic events. The ADCD uses LDCW as the basic algorithm for initial community detection and adaptive adjustment, by which the community detection process is simplified. The innovation idea of this paper is that the LDCW is node-centered method, regardless of the network topology, which makes the LDCW suitable for dealing with dynamic community detection problem. The experimental analysis of this algorithm verifies that ADCD is more stable than other dynamic community detection methods.

REFERENCES

[1] W. Zhong, H. An, X. Gao, and X. Sun, "The evolution of communities in the international oil trade network," *Physica A Statistical Mechanics Its Applications*, vol. 413, no. 11, pp. 42–52, 2014.

[2] Y. Xin, Z. Q. Xie, and J. Yang, "The adaptive dynamic community detection algorithm based on the non-homogeneous random walking," *Physica A Statistical Mechanics and Its Applications*, vol. 450, pp. 241–252, 2016.

[3] D. Chakrabarti, R. Kumar, and A. Tomkins, "Evolutionary clustering," in *Twelfth ACM SIGKDD International Conference on Knowledge Discovery and Data Mining, Philadelphia, Pa, Usa, August*, 2011, pp. 554–560.

[4] Y. Chi, X. Song, D. Zhou, K. Hino, and B. L. Tseng, "Evolutionary spectral clustering by incorporating temporal smoothness," in *ACM SIGKDD International Conference on Knowledge Discovery and Data Mining*, 2007, pp. 153–162.

[5] Y. R. Lin, Y. Chi, S. Zhu, H. Sundaram, and B. L. Tseng, "Facetnet: A framework for analyzing communities and their evolutions in dynamic networks," in *International Conference on World Wide Web*, 2008, pp. 685–694.

[6] M. S. Kim and J. Han, "A particle-and-density based evolutionary clustering method for dynamic networks," *Proceedings of the Vldb Endowment*, vol. 2, no. 1, pp. 622–633, 2009.

[7] M. Girvan and M. Newman, "Community structure in social and biological networks." *Proceedings of the National Academy of Sciences of the United States of America*, vol. 99, no. 12, pp. 7821–6, 2001.

[8] N. P. Nguyen, T. N. Dinh, S. Tokala, and M. T. Thai, "Overlapping communities in dynamic networks:their detection and mobile applications," in *International Conference on Mobile Computing and Networking, MOBICOM 2011, Las Vegas, Nevada, Usa, September*, 2011, pp. 85–96.

[9] N. P. Nguyen, T. N. Dinh, Y. Xuan, and M. T. Thai, "Adaptive algorithms for detecting community structure in dynamic social networks." *Proceedings - IEEE INFOCOM*, vol. 28, no. 6, pp. 2282 – 2290, 2011.

[10] C. Guo, J. Wang, and Z. Zhang, "Evolutionary community structure discovery in dynamic weighted networks," *Physica A Statistical Mechanics and Its Applications*, vol. 413, no. 11, pp. 565–576, 2014.

[11] M. Takaffoli, F. Sangi, J. Fagnan, and O. R. Zaane, "Modec - modeling and detecting evolutions of communities." in *International Conference on Weblogs and Social Media, Barcelona, Catalonia, Spain, July*, 2010.

[12] D. Duan, Y. Li, R. Li, and Z. Lu, "Incremental k-clique clustering in dynamic social networks," *Artificial Intelligence Review*, vol. 38, no. 2, pp. 129–147, 2012.

[13] H. S. Ma and J. W. Huang, "Cut: community update and tracking in dynamic social networks," in *The Workshop on Social Network Mining and Analysis*, 2013, p. 6.

[14] M. Rosvall and C. T. Bergstrom, "Maps of random walks on complex networks reveal community structure," *Proceedings of the National Academy of Sciences of the United States of America*, vol. 105, no. 4, pp. 1118–1123, 2008.

[15] T. N. Dinh, Y. Xuan, and M. T. Thai, "Towards social-aware routing in dynamic communication networks," pp. 161–168, 2009.

[16] A. Lancichinetti, S. Fortunato, and F. Radicchi, "Benchmark graphs for testing community detection algorithms." *Physical Review E Statistical Nonlinear and Soft Matter Physics*, vol. 78, no. 2, p. 046110, 2008.

[17] A. Strehl and J. Ghosh, "Cluster ensembles — a knowledge reuse framework for combining multiple partitions," *Journal of Machine Learning Research*, vol. 3, no. 3, pp. 583–617, 2003.

[18] H. Shen, X. Cheng, K. Cai, and M. B. Hu, "Detect overlapping and hierarchical community structure in networks," *Physica A Statistical Mechanics and Its Applications*, vol. 388, no. 8, pp. 1706–1712, 2009.

A Priori Analysis of Reliability of Radio Engineering Systems with Recovery and Standby

Boris I. Filippov [1], Olga V. Sanina [2]
Novosibirsk State Technical University, Novosibirsk, Russia
[1] Associate professor of the Information Security Department, Ph.D.
[2] Student of the Information Security Department
[1] filippov–boris@rambler.ru, [2] lyalysa@gmail.com

Abstract—A priori reliability of radio engineering systems (RES) with recovery and standby is examined. To simplify analysis problem solution of a system reliability with recovery, limitations are introduced: flow of failures (or recoveries) is a stationary flow; flows of failures (or recoveries) is a flow without aftereffect. In terms of introduced limitations failure rate model for RES with recovery and standby is assumed. To estimate the states probability of RES with failures, recovery and standby, the algorithm of differential equations generation is shown. Calculation of availability index and unavailability index for RES with recovery and standby is presented.

***Index Terms*—a priori reliability; radio engineering system; differential equations; states graph; recovery; standby; flows of failures and recoveries**

I. INTRODUCTION

The radioelectronic industry development leads to rapid raising of product features and complication of radio engineering systems (RES) structure with increasing of requirements to their reliability at the same time. Models in use have several disadvantages, and the main is allowing getting accurate assessment of reliability indicators only in specific (particular) cases [1–6]. This assessment is suitable to verify specification requirements, but it does not allow comparing analysis of the various RES implementing options in level of reliability with recovery. Therefore, development of general RES reliability research methods, enable to consider different configuration and standby algorithms of systems with recovery, is a critical task.

II. PROBLEM STATEMENT AND SOLUTION

A. Reliability model of RES with recovery and standby

Mathematical apparatus of probability theory and queuing theory is applied to simulate RES with recovery reliability states [7]. RES with standby and recovery is studied as a queueing model with failures flow as input and recoveries flow as output.

Failures (or recoveries) are considered to be a discrete stochastic process. If we label failures amount on the interval $(0,t)$ as ν_t, then combined probability, that there can be k_i failures for the time moment t_i, can be written as:

$$P\left\{\bigcap_{i=1}^{n}\nu_t = k_i\right\} = P_{k_1,k_2,\ldots,k_n}(t_1,t_2,\ldots,t_n),$$

where $k_1 \le k_2 \le k_3 \le \ldots \le k_n$ and $t_1 \le t_2 \le \ldots \le t_n$. (1)

To simplify analysis problem solution of a system reliability with recovery, we will introduce limitations [6]:

1. Flow of failures (or recoveries) is a stationary flow, i.e. failure probability does not depend on the choice of the time reference point and probability measure is invariant with respect to the time axis shift:

$$P\{\nu_{t\,0+\tau} - \nu_{t\,0} = k\} = P_k(\tau), \quad (2)$$

2. Flow of failures (or recoveries) is a flow without aftereffect, i.e. failure amount for the current interval τ does not depend on failure amount for previous interval *t*.

3. Flow of failures (or recoveries) is an ordinary flow (only one event occurs on an infinitesimal interval $\tau > 0$).

Therefore, $P\{\nu_{t+\tau} - \nu_t > 1\} = P_{>1}(\tau,t) \approx 0(\tau)$ is a small quantity, i.e.

$$\lim_{\tau\to 0}\frac{0(\tau)}{\tau} = 0 \quad (3)$$

In terms of introduced limitations, we can make a differential equations system for failures (or recoveries) flow, which solution allows us to determine failures flow state in any time moment.

B. RES with standby and queue for recovery

States graph for a RES with standby and queue for recovery is given in the Fig. 1. The number of maintenance crews is *n*, and the standby blocks number is *m*. The interval τ is assumed 1.

In the Fig. 1, digits 0,1, …*i*..., *n* stand for system states (0 – all elements are working, 1 – failure of one element, 2 – failure of two elements, etc.), transition to the right means failure of one element fro, the standby, transition to the left means recovery of repairing element, P_0, P_1,...P_n –final probabilities of system states.

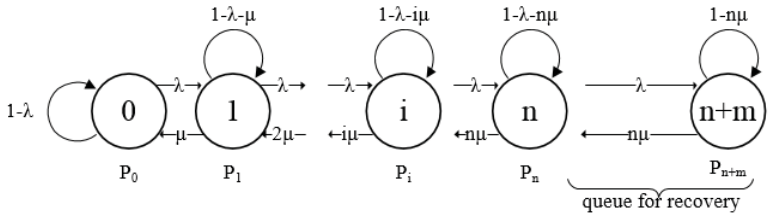

Fig. 1. RES states graph with queue for recovery (cold standby).

Differential equations for the system are following:

$$P_0'(t) = -\lambda P_0(t) + \mu P_1(t), i = 0;$$
$$P_i'(t) = -\lambda P_{i-1}(t) - (\lambda + i\mu)P_i(t) + (i+1)\mu P_{i+1}(t), i \neq 0, i \neq n;$$
$$P_n'(t) = \lambda P_{n-1}(t) - (\lambda + n\mu)P_n(t) + n\mu P_{n+1}(t), i = n;$$
$$P_i'(t) = \lambda P_{i-1}(t) - (\lambda + n\mu)P_i(t) + n\mu P_{i+1}(t), n < i < n+m;$$
$$P_{n+m}'(t) = \lambda P_{n+m-1}(t) - n\mu P_{n+m}(t), i = n+m. \quad (4)$$

Solution of the equations system (4) in a steady state $(t \to \infty)$ and $\sum_i P_i(t) = 1$, leads to system of linear equations solution:

$$-\lambda P_0 + \mu P_1 = 0, \quad i = 0,$$
$$\lambda P_{i-1} - (\lambda + i\mu)P_i + (i+1)\mu P_{i+1} = 0, \quad i \neq 0, i \neq n,$$
$$\lambda P_{n-1} - (\lambda + n\mu)P_n + n\mu P_{n+1} = 0, \quad i = n,$$
$$\lambda P_{i-1} - (\lambda + i\mu)P_i + n\mu P_{i+1} = 0, \quad n < i < n+m,$$
$$\lambda P_{n+m-1}(t) - m\mu P_{n+m} = 0, \quad i = n+m. \quad (5)$$

Solution of linear equations system (5) is following:

$$P_i = \frac{\frac{1}{i!}\left(\frac{\lambda}{\mu}\right)^i}{\sum_{i=0}^{n}\frac{1}{i!}\left(\frac{\lambda}{\mu}\right)^i + \sum_{i=1}^{m}\frac{1}{n!}\left(\frac{\lambda}{\mu}\right)^n\left(\frac{1}{n}\frac{\lambda}{\mu}\right)^i}, \quad 0 \le i \le n;$$
$$P_{i+1} = \frac{\frac{1}{n!}\left(\frac{\lambda}{\mu}\right)^n\left(\frac{1}{n}\frac{\lambda}{\mu}\right)^i}{\sum_{i=0}^{n}\frac{1}{i!}\left(\frac{\lambda}{\mu}\right)^i + \sum_{i=1}^{m}\frac{1}{n!}\left(\frac{\lambda}{\mu}\right)^n\left(\frac{1}{n}\frac{\lambda}{\mu}\right)^i}, \quad n \le i \le n+m \quad (6)$$

C. Sliding standby

Sliding standby is applied if blocks of the system are identical. Fixed standby can be economically unprofitable. The failed block is replaced by the block from the common reserve (Fig. 2).

In the Fig. 2, $n>1$ is the number of main working blocks, m stands for the number of reserve blocks; $p(t) = p$ is the probability of reliable work of each block.

We can find the probability of reliable work of RES consists of n working blocks (units) with multiple number m of sliding standby blocks $P_{mn}^{(c)}(t)$.

The system consists of $(n+m)$ units, and failure of the $(m+1)^{th}$ unit means failure of the whole system. Therefore, we can write

$$P_{mn}^{(c)}(t) = \sum_{k=n}^{n+m} C_{n+m}^k p^k(t)[1-p(t)]^{n+m-k}, \quad (8)$$

where k is the number of working blocks, $C^k_{n+m} = n!/[k!(n+m-k)!]$;

or $P_{mn}^{(c)}(t) = \sum_{k=n}^{n+m} C_{n+m}^k p^k (1-p)^{n+m-k}$, when p does not depend on time.

This standby can be expedient in, for example, multi-channel systems, including satellite systems of data transmission. Such systems except working trunks (transmission channels) have one or two reserve trunks, which take over the burden in the case of main trunk fail. Since separate trunk blocks (both main and reserve) are identical, applying all trunks as main and having some amount of different reserve blocks, turning them on instead of failed is economically profitable.

Equations system solution and state graph forming are examined for particular cases.

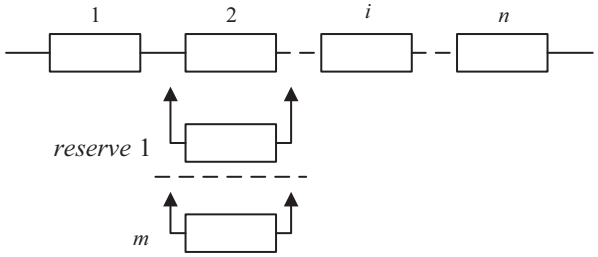

Fig. 2. Structure chart of reliability with sliding standby.

III. EXAMPLE

Consider communication system to have $m = 3$ standby blocks in hot mode, $n = 3$ standby blocks in cold mode and $k = 2$ maintenance crews, failure rate of operation block and block in hot standby λ; repair success rate of the system for one crew μ. Flows of failures and repair success are elementary.

The system can be operated in two modes of standby applying:

1) In the case of the operating system failure, hot standby blocks are operated; after failures of all hot standby blocks, cold standby blocks turn on consecutively.

2) In the case of the operating system failure, hot standby blocks are operated consecutively; simultaneously, one of the cold standby blocks is switched to the hot standby.

Fig. 3 presents system states graphs for the first (fig. 3a) and for the second (fig. 3b) operating mode.

The states matrix for the first mode:

$$\begin{bmatrix} 1-4\lambda & 4\lambda & 0 & 0 & 0 & 0 & 0 & 0 \\ \mu & 1-3\lambda-\mu & 3\lambda & 0 & 0 & 0 & 0 & 0 \\ 0 & 2\mu & 1-2\lambda-2\mu & 2\lambda & 0 & 0 & 0 & 0 \\ 0 & 0 & 2\mu & 1-\lambda-2\mu & \lambda & 0 & 0 & 0 \\ 0 & 0 & 0 & 2\mu & 1-\lambda-2\mu & \lambda & 0 & 0 \\ 0 & 0 & 0 & 0 & 2\mu & 1-\lambda-2\mu & \lambda & 0 \\ 0 & 0 & 0 & 0 & 0 & 2\mu & 1-\lambda-2\mu & \lambda \\ 0 & 0 & 0 & 0 & 0 & 0 & 2\mu & 1-2\mu \end{bmatrix}$$

Using matrix, we can pass on to a system of linear equations.

$$\begin{cases} -4\lambda P_0 + \mu P_1 = 0 \\ 4\lambda P_0 - (3\lambda+\mu)P_1 + 2\mu P_2 = 0 \\ 3\lambda P_1 - (2\lambda+2\mu)P_2 + 2\mu P_3 = 0 \\ 2\lambda P_2 - (\lambda+2\mu)P_3 + 2\mu P_4 = 0 \\ \lambda P_3 - (\lambda+2\mu)P_4 + 2\mu P_5 = 0 \\ \lambda P_4 - (\lambda+2\mu)P_5 + 2\mu P_6 = 0 \\ \lambda P_5 - (\lambda+2\mu)P_6 + 2\mu P_7 = 0 \\ \lambda P_6 - 2\mu P_7 = 0 \end{cases}$$

After that, we can express all variables by P_0 and make similar calculations for the second mode.

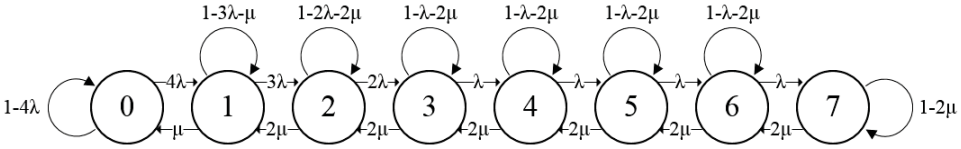

Fig. 3a. System states graph for the first operation mode.

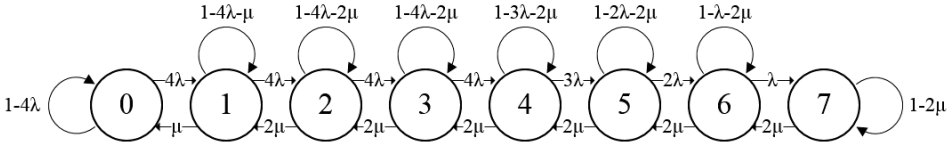

Fig. 3b. System states graph for the second operation mode.

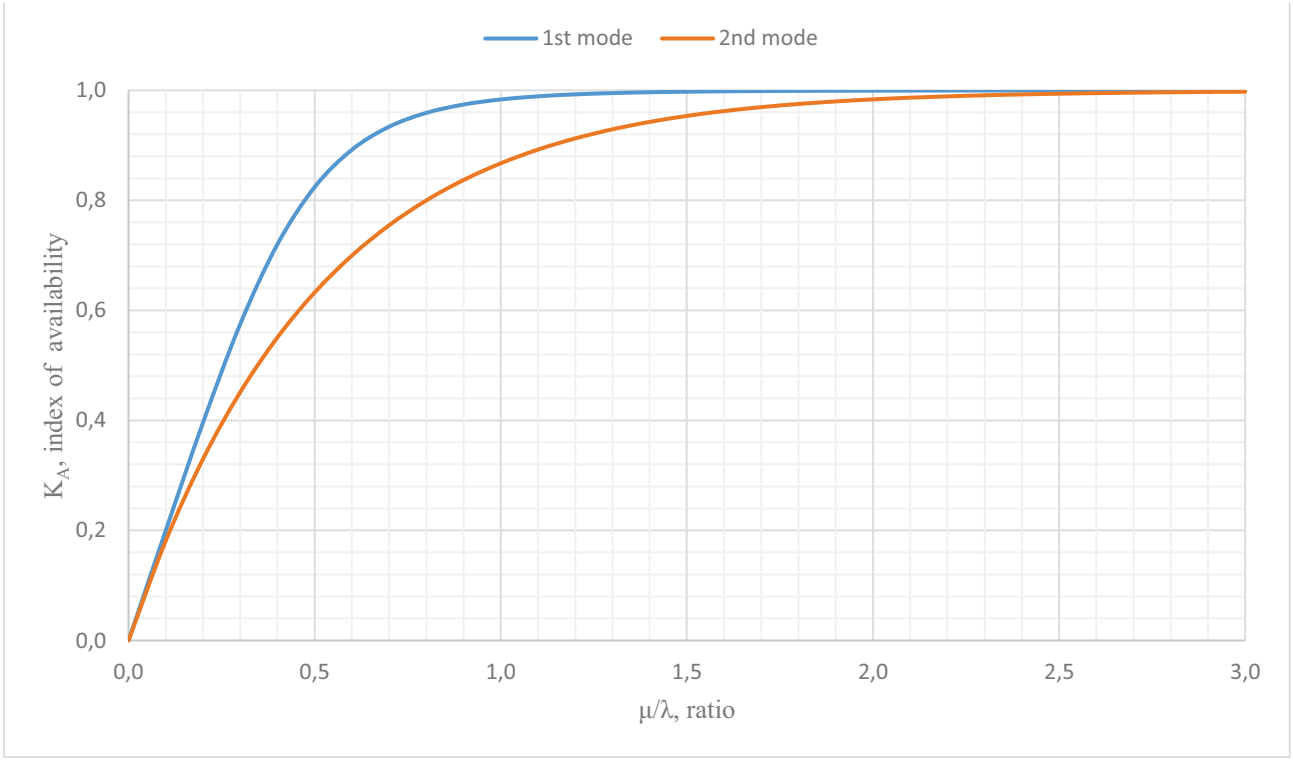

Fig. 4. Availability index versus μ/λ ratio graph for the first and the second modes.

System availability index is a probability to find it in a working state at any time t. System unavailability index is a probability to find it in a not working state. The seventh system state describes system disability, hence the probability of this state can considered as unavailability index.

We can express availability index by ratio μ/λ.

$$K_A = 1 - \frac{3(\frac{\mu}{\lambda})^7}{(8 + 32\frac{\mu}{\lambda} + 48(\frac{\mu}{\lambda})^2 + 48(\frac{\mu}{\lambda})^3 + 24(\frac{\mu}{\lambda})^4 + 12(\frac{\mu}{\lambda})^5 + 6(\frac{\mu}{\lambda})^6 + 3(\frac{\mu}{\lambda})^7)}$$

By the same way, we can analyze the second mode. Fig. 4 represents relation between availability index and ratio λ/μ for the two modes.

Fig. 4 provides the answer that using of the first mode is more preferably in terms of unavailability index reducing and availability index increasing.

This standby is possible in satellite system of data transmission. In this case, maintenance crew number *k* should be accepted as zero. Evidently, state graph will change in this case.

In additional, sliding standby can be applied for recovery of separate blocks, as it is suggested in [8].

IV. CONCLUSION

With given problem conditions the system operating in the first mode is definitely more reliable. It is possible that maintenance crew number increasing will raise reliability of the second mode, but this requires further analysis with related calculations.

REFERENCES

[1] *Zhadnov V. V., Polesskii S. N.* Design assessment of reliability of radio engineering systems. International symposium "Reliability & Quality". Vol. 1. PSU Publ., pp. 24–29, 2006.

[2] *Zhadnov V. V., Sarafanov A. V.* Quality management at design of the heatloaded radio-electronic means]. Moscow, SolonPress, 464 p., 2004.

[3] *Artiukhova M. A., Zhadnov V. V., Polesskii S. N.* Impact consideration method of dependability management system of the enterprise for estimated assessment of the electronic equipment reliability. Radio Electronics, Computer Science, Control. No. 2. pp. 48–53, 2013

[4] *Reliability of electro-radio units: Reference book*. Moscow, MO, 641 p. 2006

[5] *Filippov B. I.* A priori reliability analysis of radio systems without restoration. Izvestia VSTU. Vol. 12, No. 11 (176), pp. 97–103, 2015.

[6] Filippov B.I. Definition of characteristics of reliability of radio-electronic systems. Vestnik of ASTU, No. 2. – pp. 42-49, 2016.

[7] *Levin B. R.* Theory of reliability of radio engineering systems. Moscow, Sovetskoe radio Publ., 1978. 264 p.

[8] Tyurin S.F. Moving redundancy of tolerant elements. Dependability. No. 1 (17). – pp. 17-21, 2017.

A web-based application for data visualisation and non-linear regression analysis including error calculation for laboratory classes in natural and life sciences

Titus Keller and Danny Kowerko
Chemnitz University of Technology,
Endowed Professorship Media Computing,
D-09111 Chemnitz, Germany
Email: titus.keller@s2012.tu-chemnitz.de, danny.kowerko@informatik.tu-chemnitz.de

***Abstract*—In practical laboratory classes students traditionally receive data by reading from a measurement device (ruler, clock, voltmeter, etc.) or digitally as files in exchange formats such as CSV (comma separated value). In many cases these data have to be processed later using non-linear regression, here referred to as curve fitting. Therefore, analog data first have to be digitalised and imported to a data analysis and visualisation program, which is often commercial and requires installation. In this paper we present an alternative concept fusing open-source community tools into a single page web application facilitating data acquisition, visualisation, analysis via non-linear regression and further post processing usable for error calculations. We demonstrate the e-learning potential of this web application accessible at curvefit.tu-chemnitz.de in the context of acquired data as typically obtained in physical laboratory classes from undergraduate studies. A prototype workflow for the topic 'specific electric resistance determination' is presented along with a technical description of the basic web technology used behind. Restrictions, such as limited portability or cumbersome ways to share results electronically between student and supervisor as occurring in traditional software applications are overcome by enabling export via URL.**

The discussion is complemented by thorough comparison of curve fitting web applications with focus on their capability to be adaptable to user-specific models (equations) as faced by (undergraduate) students in the context of their education in laboratory classes in natural and life sciences, such as physics, biology and chemistry.

I. Introduction

The term regression analysis (also often referred as curve fitting) describes mathematical methods which determine the relationship between dependent and independent variables of a mathematical model (typically an explicit equation). The most commonly used approaches for this problem are based on the least squares problem. [1]

$$y = a \cdot x + b \tag{1}$$

As example, consider equation 1 as the model, with y as dependent and x as the independent variable. The least squares approach tries to determine the values for a and b which minimize the sum of squared distances between the function and the data points of the respective data set [2].

Curve fitting algorithms solving this problem can be generally separated in two categories:

1) Linear regression algorithms, which are only applicable to linear combinations, but produce a deterministic result.
2) Non-linear regression algorithms (for example the Levenberg-Marquardt algorithm), which are applicable to generic models, but use an iterative way to produce a non-deterministic result. [3]

The generic use case of curve fitting can be described as statistical analysis. Accordingly, it is used in a wide range of disciplines, such as natural, life, human, social and economic sciences or data mining [4], [5], [6], [7]. An explicit example of non-linear regression using equations with 6 or more parameters is thermal melting curve analysis, a widespread method used in biochemistry to study stability of DNA (deoxyribonucleic acid) and proteins [4], [8]. By means of the web application presented herein, it was recently demonstrated that such complex multi-parameter equations can be fitted to experimental RNA (ribonucleic acid) thermal melting curve data including the required post-processing calculations derived from the fit parameters [9].

In the context of the broad variability of use cases, this paper will discuss the practicability of this curve fitting web application as e-learning tool employed in practical lab classes which are part of basic studies e.g. in physics. This proof of concept will be exemplified using data and equations from a real lab class [10]. Existing open-source or open-access based computation methods are merged into a browser-based web application including data import, visualisation, regression analysis and URL-based data and results export, usable to quickly and systematically share results between supervisor and student/user. Using non-proprietary resources makes the application attractive to be offered by computing centers such as the 'Universitätsrechenzentrum' of the Chemnitz University

TABLE I
E-LEARNING RELEVANT CRITERIA AND THEIR DESCRIPTION USED TO COMPARE THE FUNCTIONALITY OF WEB-BASED CURVE FITTING APPLICATIONS.

Criteria	Description
1. Non-commercial	Is the application non-commercial?
2. Help	Are there further information about the use of the software?
3. Input options	Can the user define explicit equations and choose between regression algorithms?
4. Graphic output	Can the result and the data set be plotted as a graph?
5. Export	Are there options to export the results, for example as PDF?
6. Error measures	Are error measures displayed, which can help to determine the goodness of the fit?
7. Post-processing	Is it directly possible to perform further calculations using the regression results?

of Technology as university-wide services for students and academic staff.

II. ANALYSIS OF EXISTING CURVE FITTING WEB APPLICATIONS

Widely used programs for calculation and visualisation of results in practical lab classes are often commercial, such as MS Office/Excel (Microsoft Corporation), OriginPro (OriginLab) or Igor Pro (Wavemetrics) and require installation. In E-learning non-commercial and installation free applications are of relevance as both criteria save money, (i) for software licenses and (ii) for their maintenance (installation, upgrades, ...). Accordingly, we studied freely available existing web applications in a structured and systematic manner according to defined criteria summarised in Table I.

More than twenty functional curve fit web applications were identified. Even though there are eventually more, we focus only on four representatives fulfilling a maximum of relevant functionality from Table I), namely fitteia[1], WolframAlpha[2], mycurvefit[3] and statpages[4]. The respective analysis results are summarised in Table II.

It can be concluded that several regression web applications exist which have various limitations. Aside from these quantifiable results, it has to be noted that there are other important criteria which are not straightforward to measure, such as ease of use or GUI (graphical user interface) design. For example, WolframAlpha, as more generic mathematical software, requires syntax knowledge about the existence and use of functions. An approach to determine such aspects could be based on the use of software ergonomic standards, such as ISO 9241 [11].

[1]http://fitter.ist.utl.pt/, 17.03.2017
[2]https://www.wolframalpha.com/, 17.03.2017
[3]http://mycurvefit.com/, 17.03.2017
[4]http://statpages.info/nonlin.html, 17.03.2017

TABLE II
A COMPARISON OF REPRESENTATIVE WEBSITES, WHICH CAN BE USED TO SOLVE CURVE FITTING PROBLEMS, BASED ON THE CRITERIA DEFINED IN TABLE I.

Criteria	fitteia	WolframAlpha	mycurvefit	statpages
1.	✓	-	-	✓
2.	✓	✓	✓	✓
3.	partly	✓	partly	partly
4.	✓	✓	✓	-
5.	✓	partly	partly	-
6.	-	partly	✓	partly
7.	-	✓	-	-

III. RESULTS AND DISCUSSION

The web application developed by the authors (available at [5]) consists of two main components, a GUI to execute regular curve fitting functionality and a curve fit evaluation tool not discussed here in detail.

With regards to the contents of Table I, the web application presented in this paper fulfills all criteria at least on an elementary functional level. A special property of the software is the possibility to choose between various implementations of regression algorithms, such as solutions developed in MATLAB's curve fitting toolbox, Java[6] or GNU Octave (optim package available under [7]). Note that the latter two are open-source and access tools, thus free to use in education.

A. User interface for curve fitting

The graphical user interface covering the full curve fitting workflow is separated into five elements, as shown in Fig. 1. Thereby following concept is realised:

- (left, top) Definition of the data set and options for further processing and data import (for example of a CSV file).
- (left, middle) Input for the mathematical model via ASCII characters and the related rendered output formula.
- (left, bottom) Parameter of the function with their start values, results and confidences.
- (right, top) The result function and the data set plotted as exportable graph.
- (right, bottom) Post processing of curve fit and other parameters can be conducted through this element. Alternatively, the residuum, which plots the difference between the data set and the result function, can be displayed.

B. Technical background of the web application

The back end of the application is written in Java and based on Jetty as HTTP-server and servlet-container. Due to the lack of implementations of regression algorithms written in JavaScript the respective functionality is executed by the server (alternatively to-JavaScript-compiler, such as Emscripten could be utilised). Hence the application programming interface (API) for the necessary asynchronous calls is

[5]http://curvefit.tu-chemnitz.de/, 17.03.2017
[6]https://www.ee.ucl.ac.uk/~mflanaga/java/, 20.03.2017
[7]https://octave.sourceforge.io/optim/, 20.03.2017

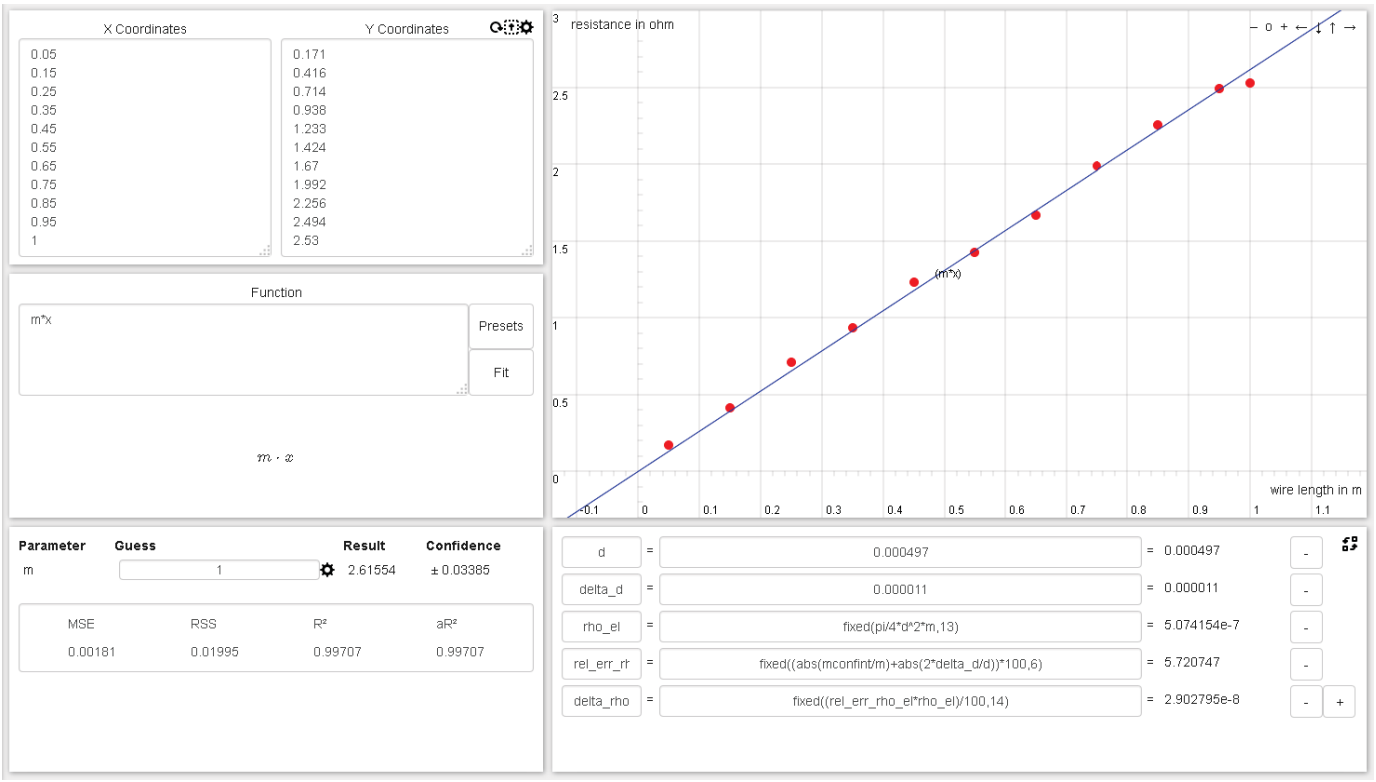

Fig. 1. Screenshot representing the graphical user interface for the curve fitting functionality of the developed application. Data taken from a template protocol of a lab class in physics at TU Chemnitz (available under https://www.tu-chemnitz.de/physik/PGP/allgemein.php, 20.03.2017). For further description, be referred to section III-C.

implemented based on REST (Representational State Transfer) using Jersey as a servlet. For the storage of permanent data on server-side (for example to share results by URL) a MongoDB database is connected to the back end.

The front end is using the regular web technologies HTML, CSS and JS. To simplify the work process the code is mainly written using the MVC-framework AngularJS. Advantages for this are for example the possibility to write reusable components or the use of data binding to connect HTML and JavaScript content [12].

Other important libraries which have been utilised are:

- JS Expression Evaluator to parse and evaluate mathematical functions in a secure manner.
- MathJAX as a way to render the formulas entered by the user.
- JSXGraph to plot the data set and regression results in a graph.
- Plotly to display the heatmap of the evaluation tool.

C. Determination of specific electrical resistance as model application used in laboratory classes

Among the multitude of potential applications for the presented curve fitting web tool is its use in education for example in laboratory classes where experiments are carried out producing data that have (i) to be visualised and (ii) to be evaluated using or testing the correctness of mathematical models. This background is well-known from physic or chemistry in secondary school or college/university courses. Especially at the higher levels of education the use of dedicated curve fitting software is indispensable [10].

Here, a typical use case of such an approach was chosen from a lab course in physics, namely the problem to determine the specific electrical resistance ρ of a wire from the correlation between its length and its resistance. A concrete workflow is describable as follows:

- Wires of different lengths L will be probed.
- An electric circuit is built to measure the current I and voltage U from respective devices.
- The electrical resistance is calculated using the measured current and voltage according to following the equation:

$$R = U/I \tag{2}$$

- The data set of wire lengths and respective resistances are entered into a data visualisation and analysis software.
- Regression analysis using a linear function is applied to the data to calculate an average ratio of resistance and length. This is the slope m of the fit equation $R = m \cdot l$.

$$m = dR/dl \tag{3}$$

- From regression analysis, the slope m is used to calculate the specific electrical resistance according to:

$$\rho = m \cdot A = m \cdot \frac{\pi}{4} \cdot d^2, \tag{4}$$

where A is the cross section of the wire defined by its diameter d in units of meters.

- Regression also provides the 95% confidence value of m which is here denoted Δm. Together with the error of diameter measurement, the relative error of the specific electrical resistance is calculated according to:

$$\left|\frac{\Delta\rho}{\rho}\right| = \left|\frac{\Delta m}{m}\right| + \left|\frac{2\Delta d}{d}\right|. \quad (5)$$

The experimentalist may use the post-processing module shown in the bottom, right of Fig. 1 to provide d and Δd as values, while equations (4) and (5) have to be typed to the GUI using their ASCII representations. Results are automatically generated and usable for the protocol. In the above-mentioned example, the specific electric resistance is directly at hand from Fig. 1 (bottom, right) giving $\rho_{el} = (0.51 \pm 0.03)\mu\Omega \cdot m$ yielding a relative error of 5.7%. Note, that values may be fixed to a user-defined number of digits using the command *fixed()*. The example provided in Fig. 1 is available under[8] and is usable as exchange format between supervisor and student, e.g. to evaluate the correctness of the equations and calculations entered by the students to a previously empty GUI.

IV. Conclusion

The web application available at curvefit.tu-chemnitz.de was presented in the context of its application in e-learning. We successfully exemplified how typical tasks which are part of laboratory classes are fully covered, i.e. the data import and visualisation as scatter plot, regression analysis using topic-specific functions and post-processing of user-defined (given) and parameters obtained from curve-fitting. The latter allow for mathematically reproducible error calculation. Compared to other web applications, we have overcome various limitations to provide a generic easy-to-use single page tool that can be widely used in laboratory classes.

V. Outlook

The presented curve fit tool offers also a comprehensive solution to evaluate regression algorithms utilising simulated data not discussed here in detail. However, as errors based on regression are rather determined numerically, it may be used in teaching to practically visualise the influence of measurement insecurities or statistical noise on data and their consequences for accuracy of regression-based parameter determination.

To increase the scope of the curve fit application a sustainable data and result storage management system is currently in preparation. The input for data sets is at present based on text boxes, which could benefit from a change to the familiar worksheet-like table structure well known from Excel, Google Spreadsheets or Apache OpenOffice Calc. More comprehensive data management also include multiple columns and multiple worksheets including cross-calculations, e.g. used for data pre-processing. In the example given in section III-C, the electrical resistance *R* could then be automatically calculated from the measured voltage *U* and current *I* data according to eq. 2. The common issue of outlier values could be solved by an assisted detection method or completely automatic support using methods such as random sample consensus [13].

As generic navigation structure for files and folders a tree view can be used to permanently save and organise data. In combination with user management it enables a possibility to offer a cross platform web storage, which could be used for collaborative working.

To systematically improve the application user evaluations in multiple iterations are in preparation using either example questionnaires or observation studies.

Acknowledgments.

This work was partially accomplished within the project *localizeIT* (funding code 03IPT608X) funded by the *Federal Ministry of Education and Research* (BMBF, Germany) in the program of *Entrepreneurial Regions InnoProfile-Transfer*.

[8] http://curvefit.tu-chemnitz.de/#?58d14390468c6a0adc2ee4c2, 20.03.2017

References

[1] K. Backhaus, *Multivariate Analysemethoden eine anwendungsorientierte Einführung*. Berlin: Springer, 2006. [Online]. Available: http://dx.doi.org/10.1007/3-540-29932-7

[2] H. Skala, "Will the real best fit curve please stand up?" *The College Mathematics Journal*, vol. 27, no. 3, pp. 220–223, 1996.

[3] M. I. Lourakis, "A brief description of the levenberg-marquardt algorithm implemented by levmar," *Foundation of Research and Technology*, vol. 4, no. 1, 2005.

[4] A. Böttcher, D. Kowerko, and R. K. Sigel, "Explicit analytic equations for multimolecular thermal melting curves," *Biophysical chemistry*, vol. 202, pp. 32–39, 2015. [Online]. Available: http://www.sciencedirect.com/science/article/pii/S0301462215000757

[5] D. G. Kleinbaum, L. L. Kupper, A. Nizam, and E. S. Rosenberg, *Applied regression analysis and other multivariable methods*, fifth edition ed. Boston, MA: Cengage Learning, 2013.

[6] R. Ramcharan, "Regressions: Why Are Economists Obessessed with Them?" *Finance Dev*, vol. 43, 2006. [Online]. Available: http://www.ecostat.unical.it/aiello/didattica/Econometria/Regressions_%20IMF.pdf

[7] D. J. Hand, H. Mannila, and P. Smyth, *Principles of data mining*. MIT press, 2001. [Online]. Available: https://books.google.de/books?hl=de&lr=&id=SdZ-bhVhZGYC&oi=fnd&pg=PR17&dq=Data-Mining++curve+fitting&ots=yxP8BjqumY&sig=ZRnkbwFJ2edTfds__6LrMPF9ZGg

[8] J.-L. Mergny and L. Lacroix, "Analysis of Thermal Melting Curves," *Oligonucleotides*, vol. 13, no. 6, pp. 515–537, Dec. 2003. [Online]. Available: http://www.liebertonline.com/doi/abs/10.1089/154545703322860825

[9] T. Keller, D. Kowerko, and M. Ritter, "Entwicklung eines webbasierten Curve-fitting Tools für komplexe Multiparameter-Funktionen," in *Studierendensymposium Informatik 2016 der TU Chemnitz*. Chemnitz: Univ.-Verl, May 2016, pp. 75–85. [Online]. Available: http://nbn-resolving.de/urn:nbn:de:bsz:ch1-qucosa-201104

[10] W. Schenk, F. Kremer, G. Beddies, T. Franke, P. Galvosas, and P. Rieger, *Physikalisches Praktikum*, W. Schenk and F. Kremer, Eds. Wiesbaden: Springer Fachmedien Wiesbaden, 2014. [Online]. Available: http://link.springer.com/10.1007/978-3-658-00666-2

[11] C.-C. E. de Normalisation, *Ergonomische Anforderungen für Bürotätigkeiten mit Bildschirmgeräten Teil 10: Grundsätze der Dialoggestaltung*. Februar, 1995.

[12] M. Heinrich and M. Gaedke, "Data binding for standard-based web applications," in *Proceedings of the 27th Annual ACM Symposium on Applied Computing*. ACM, 2012, pp. 652–657.

[13] M. A. Fischler and R. C. Bolles, "Random sample consensus: a paradigm for model fitting with applications to image analysis and automated cartography," *Communications of the ACM*, vol. 24, no. 6, pp. 381–395, 1981.

Analysis of Particle Size Distribution of Milk Fat Based on Image Processing

Siqi ZHANG, Zhen ZHOU, Xu YANG, Xiaotong Na
The Higher Educational Key Laboratory for Measuring & Control Technology and Instrumentations of Heilongjiang Province, Harbin University of Science & Technology
Harbin, China
e-mail: zhzh49@126.com

***Abstract*—When the concentration of the solution is detected by the light scattering method, the size of the particles in the solution is an important factor affecting the detection results. Most of the existing studies assumed that the size of the particles in the homogeneous solution was uniform. However, in the actual solution, the particles still have particle size distribution. In this paper, a method of grain size distribution analysis based on image processing technology was proposed. The pretreatment of milk fat solution with EDTA was carried out. The images of fat particles were processed by Matlab software, and finally the distribution curve of fat particles was obtained. This paper provides a basis for the further study of light scattering detection of milk fat.**

I. INTRODUCTION

With the continuous progress of optical theory, light scattering detection technology is also developing rapidly. In the light scattering technique for solution concentration detection, three important physical quantities are involved, namely the light source wavelength, the solution concentration and the particle size[1]. In the course of the study, the solution was usually homogenized to prevent measurement errors caused by uneven solution. In the existing studies, it was generally assumed that the particle size after homogenization was uniform[2,3,4]. But the particles in the actual solution still have particle size distribution[5]. And this distribution will lead to changes in the light scattering characteristics of the solution. Accurate analysis of the distribution of particle size is conducive to improving the accuracy of light scattering detection and in-depth study of light scattering detection theory.

The most common particle size distribution measurement method is to use the electron microscope to get the particle picture. The picture is processed by the relevant tool, and then the particle size of the particle is measured. The researchers use the manual method to draw the diameter of each particle one by one in the picture. After the statistics, the average diameter and distribution of droplets are obtained. But only by the eyes to manually measure a large number particles which have different sizes and ambiguous edges, a lot of work is needed, and the results are not accurate. Zhang Hongyan and others used image processing technology and prepared a program to measure the crude oil. They first determine the number of droplets by edge detection, and then calculate the average diameter of the droplets by calculating the total number of pixels in the droplet[6]. In this method, the subjective factors in the measurement are eliminated, and the defects measured manually in the particle size measurement are overcome. However, this method can only measure the average particle size of droplets. And it can not achieve the droplet size distribution of the measurement.

Based on the previous research, milk fat particles as the object of study, this paper presents a particle size distribution analysis method based on image processing technology to realize the analysis of particle distribution, which provides a basis for the further study of light scattering detection of milk fat.

II. SOLUTION PRETREATMENT AND IMAGE PROCESSING

A. Milk Fat Solution Pretreatment

When using the light scattering technique to detect milk fat components, first use EDTA reagent to dissolve the protein components in the milk solution, so that the macromolecules in the milk solution are only fat[7]. And then through the ultrasonic homogeneous, fat is refined into particles of about 2μm in diameter. The treated solution was placed under an optical microscope to capture the fat particle image. In this paper, we refer to the pictures of milk fat particles in document [8], as shown in Figure 1.

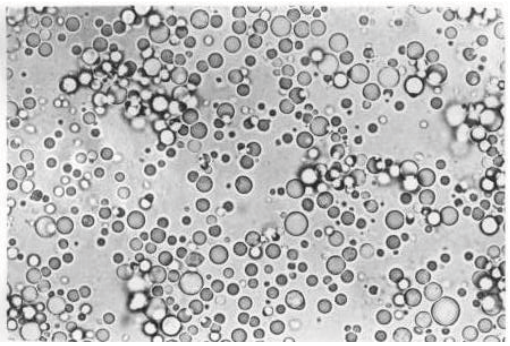

Figure 1. Milk fat particles photo under the microscope

B. Image Processing of Fat Particles

The original image is a three-dimensional matrix that contains brightness information and color information. But only two-dimensional matrices containing the luminance information are needed during the analysis of the image processing. Therefore, the original image should first be converted to a grayscale image to reduce the amount of data in the image. In Matlab, "rgb2gray" function can achieve gray image processing. After obtaining the grayscale image, the "graythresh" function is used to help us obtain the appropriate threshold for the image, which transforms the grayscale image into a binarized image, as shown in Figure 2.

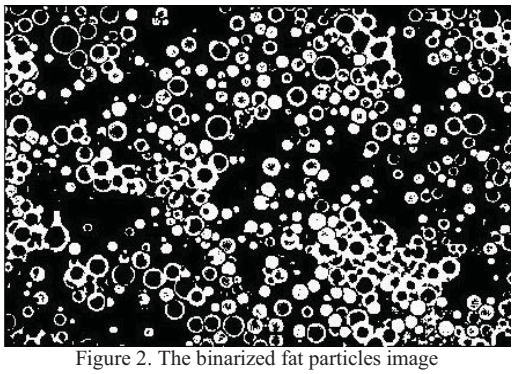

Figure 2. The binarized fat particles image

Image mask processing is used to extract fat particle regions. The processed image is masked with the selected image. The image values in the target area remain unchanged, and the area image values are both 0. The processed image is shown in Figure 3.

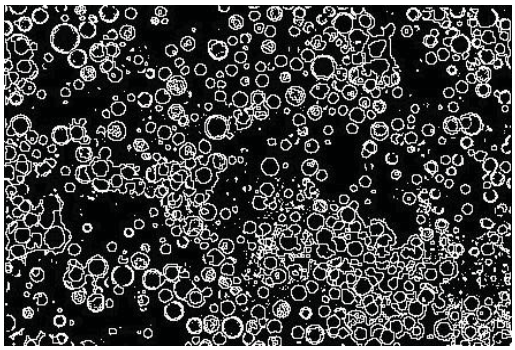

Figure 3. Masked processed fat particles image

There are various influencing factors in the image acquisition process, which leads to the existence of noise information in the image and affect the image quality. So the image noise reduction is very necessary. In this paper, we use the median filter method, which can not only suppress the interference pulse and point noise, but also can maintain a good image edge. The selected median filter function is "medfilt2". The processed image is shown in Figure 4.

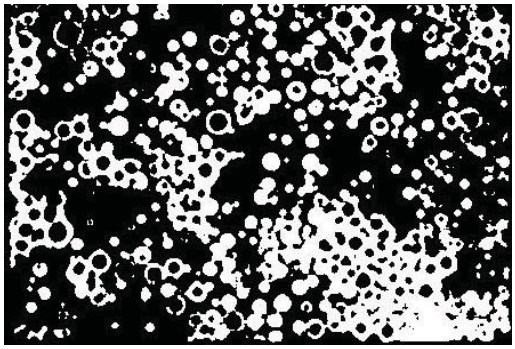

Figure 4. Median Filtering of Fat Particles Image

At the edge of fat particles, the gray value changes drastically. So the first-order differential and second-order differential can be used to extract the edge change detection operation.

(1) First order differential

The first order differential value of the gray level gradient at the coordinate point (x, y) can be represented by the G (x, y) = (f_x, f_y) vector, which has the size and direction. Where f_x represents the differential of the x direction and f_y represents the differential of the y direction. f_x, f_y are derived from Equation 1 and 2.

$$f_x = f(x+1, y) - f(x, y) \tag{1}$$

$$f_y = f(x, y+1) - f(x, y) \tag{2}$$

The intensity of the edge can be obtained from $\sqrt{f_x^2 + f_y^2}$, and the direction of the vector (f_x, f_y) is the direction of the edge.

(2) second order differential

The second order derivative L (x, y) is another derivative of the gradient, only for the intensity of the edge detection, and it is represented by Equation 3 in the digital image.

$$L(x, y) = 4f(x, y) - \begin{vmatrix} f(x, y-1) + f(x, y+1) \\ + f(x-1, y) + f(x+1, y) \end{vmatrix} \tag{3}$$

The image after exact edge detection is shown in Figure 5.

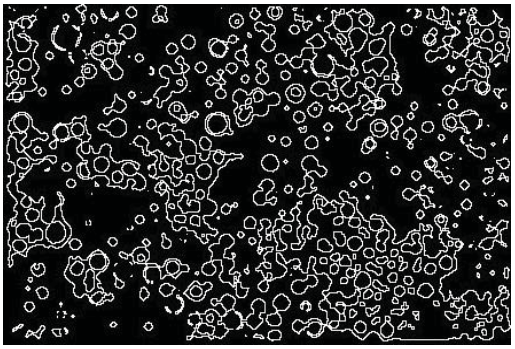

Figure 5. Image of precise edge detection

C. *Particle Size Distribution Analysis*

The particle size of the fat particles in the picture was statistically analyzed to obtain 432 particle size and the particle size distribution range is shown in Table 1.

Table 1 Effective particle diameter distribution range

Diameter(μm)	Number	Percent(%)	Amount
0.384~1.0	105	24.31	
1.0~2.0	132	30.56	
2.0~3.0	121	28.01	
3.0~4.0	43	9.95	432
4.0~5.0	9	2.08	
5.0~10.0	16	3.70	
＞10.0	6	1.39	

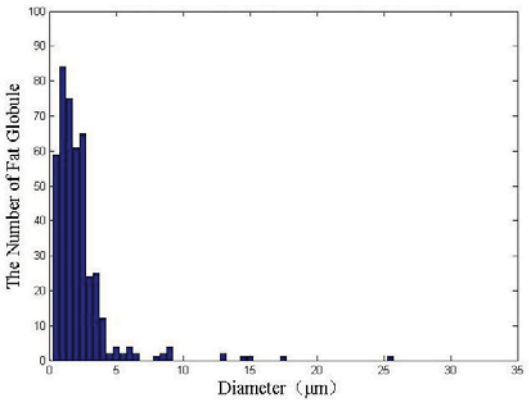

Figure 6. Histogram of Fat Globule Diameter Distribution

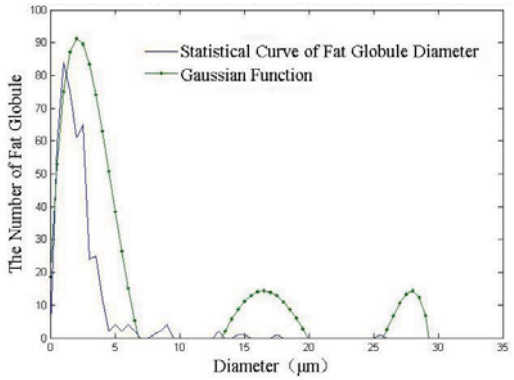

Figure 7. Statistical Curve of Fat Globule Diameter and Gaussian Function

According to Table 1, the homogeneous milk fat solution does exist in the particle size distribution, and the particle size is mainly distributed between 0.5μm and 3.0μm, accounting for 82.88% of the total number of fat globules. It is calculated that the particle size of the fat globules in the milk fat solution after homogenization is subject to the Gaussian distribution of the expected $\mu = 2$ and the standard deviation $\sigma = 0.0006$. Fat particle size distribution histogram and the comparison chart between the particle size statistical curve and the Gaussian curve are shown in Figure 6 and Figure 7, respectively.

III. CONCLUSION

The particle size and particle size distribution of the measured particles are important factors that affect the components detection of light scattering. In this paper, the milk fat particles were used as the research object. And a particle size distribution analysis method based on image processing technique was proposed to verify the fact that the particle size distribution still existed after homogenization. The mathematical expectations and variance of the particle size distribution of the fat particles were obtained. This paper has laid a theoretical foundation for the follow-up study of light scattering components, which is of great significance to improve the accuracy of light scattering detection.

ACKNOWLEDGMENTS

This work was supported by the National Natural Science Foundation of China (Grant No. 51206038) and the Scientific Research Fund of Heilongjiang Provincial Education Department (Grant No. 12521122). We gratefully acknowledge invaluable experimental help from The Higher Educational Key Laboratory for Measuring & Control Technology and Instrumentations of Heilongjiang Province (Harbin University of Science & Technology).

REFERENCES

[1] Jinying Yin, Siqi Zhang, et al. Theoretical Study of the Effect of Multi-Diameter Distribution on the Mie Scattering Characteristics of Milk Fat[J]. Journal of Harbin Institute of Technology (New Series), 2015, 22(6):115-120.

[2] Zhen Zhou, Jianjun Wen, et al. Factors Affecting light scattering technique to detect when milk protein[J]. Infrared, 2010, 31(1):36-40.

[3] Changlong Tan, Tao Shen, et al. Effects of temperature and pressure on the milk protein heterogeneity test[J]. Science and Technology Information, 2008, (30):7-8.

[4] Chenlong Chen, Zhiling Hou, et al. Experimental study on the impact of homogenization of milk fat test[J]. Harbin University of Science Report, 2002, 7(1):96-98.

[5] Cabassi G, Profaizer M, Marinoni L, et al. Estimation of fat globule size distribution in milk using an inverse light scattering model in the near infrared region[J]. Journal of Near Infrared Spectroscopy, 2013, 21(5): 359-373.

[6] Hongyan Zhang, Xiaoping Li, et al. Method for measuring the diameter of crude oil emulsion based on image processing[J]. Technology Supervision in Petroleum Industry, 2011, (12):44-46.

[7] Changlong Tan, Guangju Ji, et al. Research on milk fat test laser scattered through ratio[J]. Technological information, 2008, (31):11-11.

[8] Min Chang. Study on mechanism and influence factors of optical measurement of milk quality[D]. Tianjin: Tianjin University, 2006.

Noise Signal Analysis for Fault Detection

Yanjin Altankhuyag[1,2], Wolfram Hardt[2]
[1]Power Engineering School, Mongolian University of Science and Technology
[1]yanjin@must.edu.mn, yanjin.altankhuyag@s2014.tu-chemnitz.de
[2]Professorship Technische Informatik, Technishe Universität Chemnitz
[2]wolfram.hardt@informatik.tu-chemnitz.de

Abstrac: The fault detection of electric machinery is important necessity for stability of system. The noise signal of rotating machinery is utilized for early fault diagnostic. A measured noise signal is divided down by short time duration parts. Fault carrying frequencies are extracted from digitalized signal. Envelope detector and demodulation were utilized for identifying fault frequencies with their harmonics and sidebands. Automated noise analysis is dedicated to detect and report a machinery abnormal condition. Implementation was conducted with noise signals which were obtained from an electric motors, turbine generators and bearing fault motors.

***Index Terms*—noise signal, fault detection, mechanical fault detection, signal processing**

I. Introduction

Critical component or machinery of system and/or operating process is required doing maintenance through the operation without ceased. Machinery condition based monitoring (CBM) helps to reduce maintenance cost and increase machinery lifetime. CBM of electrical machinery prefers to detect malfunctions early before failures are growing up serious condition which influence system breakdown. Undesired break down of system especially in industry is excessive costly. According the monitoring system's benefit, any mechanical system have expected percentage of improvement due to utilizing CM. The improvement of CM system has been shown in a table 1 [1]. Therefore, condition monitoring (CM) has been developing from early maintenance techniques such as relay protection systems until a fault diagnostic system which is a smart fault tolerant sensor techniques based signal processing. In extant literature has been developing a CM with different techniques such as vibration signal, motor current signature analysis (MCSA), non-destructive techniques (NDT), laser based measurement and optical rotatory encoder etc. The implementation cost of CM system is increased due to a sensors, signal processing circuits, and control system. In addition, the power and nuclear plants, hydraulic chemical plants et., have a components which are complexity for structure. In many cases, these components like as turbines and electric machinery are a critical for fault diagnostic and are not permitted to access. Therefore, noise signal which is obtained through microphone is a noninvasive attempt for fault detecting system. This trend has been covered few researchers who were used microphones for fault detection system [2], [3], [4], [5]. All of research was conducted in laboratory or vacuum condition and some used microphone arrays and acoustic camera in order to increase the signal noise ratio (SNR) of recorded signals. A microphones are relatively cheap sensor compared to other specialized sensors, so these are can positioned freely, unlike other sensors. Noise signal of electric machinery can broadly classified that electromechanical, aerodynamic, and mechanical vibration and noise. A part of vibration energy within the audible range (20=f=16000Hz or even up to 20000Hz) is transmitted into sound energy. There is airborne noise radiating directly from vibration source and structure-borne noise transmitted to the surroundings via mechanical connections, couplings, base plates, and supports etc., [6]. Consequently, noise signal based fault detecting research is new development among rotating machinery condition monitoring. The target of paper is dedicated to propose a fault detection algorithm derived from a noise signal feature selection.

TABLE I: Improvements in reliability using a monitoring system .

Maintenance cost	Reduction of 50% − 80%
Equipment damages	Reduction of 50% − 60%
Extra hours expenses	Reduction of 20% − 50%
Machine life expectancy	Increase of 50% − 60%
Total productivity	Increase of 20% − 30%

II. Mechanical Faults and Fault Signature

Every mechanical components when they are failed produce a fault signature with harmonics. Therefore, fault detection purpose is identifying faulty frequencies. Before analyzing the noise signal, need to study on mechanical failures of electric machinery. The mechanical failures are represented in table2 regarding frequency ranges of malfunctions. There are the faults which are commonly occurred and influenced system efficiency, heating, and to increase vibration. These are bearing their defects, gearbox, rotor unbalance, journal ovality, bent shaft, and sliding contacts etc. All fault having characteristic frequencies. For instance, bearing and their defect are showed in table 3. Gearbox faults are also produce same different fault signatures such as $f_c = \frac{N_{rpm}}{60}$, $f_{gear} = \frac{N_1 T_1}{T_2}$, $f_{gearmesh} = N_1 T_1 = N_2 T_2$. All mechanical faults can divided frequency ranges regarding types of failures. Also, a mechanical malfunctions are related noises which generated from rotation of motors.

TABLE II: Frequency ranges for mechanical system

Frequency range	Fault types	Frequency selection calculation
Low frequency range	Low frequency domain defined as the frequency from below rotational speed up to the lower harmonics. It contain information about unbalance, misalignment, bent shaft, instability in journal bearings and mechanical looseness	2^{nd} harmonic : 2X rotational speed component for bent shaft, misalignment (40%-49%)x rotational speed derived from shaft with loaded high speed-self excited. $(0.5x1.5x2.5)$x rotational speed indicate inter harmonics and subharmonics components for mechanical looseness.
Medium frequency range	Medium frequency domain: information about fault in gearboxes. The degree of gear wear can be seen at the toothmeshing frequency and its harmonics.	$(n * rev/60)f$: Its harmonics can indicate an incipient fault. Toothmeshing frequency signal is weak signal high spectral energy.
High frequency range	High frequency range called blade spectral components which are usually low in amplitude. Typically, it is into the frequency range from a few hundred hertz to 10-20 kilohertz [11].	9.6-11.3kHz heap spectrum indicates the possibility of rolling element bearing faults and steam flow thrust forces.

TABLE III: Bearing fault characteristic frequencies

Shaft rotational frequency	$F = \frac{shaftspeedinrpm}{60}$
Ball pass frequency inner race	$BPFI = \frac{N}{2}F(1 + \frac{B}{P}\cos\alpha)$
Ball pass frequency outer race	$BPFO = \frac{N}{2}F(1 - \frac{B}{P}\cos\alpha)$
Fundamental train frequency	$FTF = \frac{F}{2}(1 - \frac{B}{P}\cos\alpha)$
Ball pass frequency	$BPF = \frac{P}{2B}F[1 - (\frac{B}{P}\cos\alpha)^2]$

III. PROPOSED NOISE PROCESSING TECHNIQUES

The condenser microphone and the audio sound data acquisition card were used for all sample creation. Sampling and quantization were made automatically by software based algorithm.

A. Noise signal preprocessing

Noise signal recognition system is splitting a noise signal track in to smaller pieces which helps to identifying a precise features. Software based data splitting with has a new wav header is represented in fig1 and fig2. Afterward the

Fig. 1: Sampled data track

new wav data was added to each chunk of data. The noise signal recognition system consists of pattern recognition. The fast Fourier transform (FFT) transformation is utilized for

Fig. 2: Sample after spitting

digitalized signal in frequency domain. This helps to extract fault frequency features. Then normalizing digitalized signal in both amplitude and frequency separately for each spectrum analysis. Fault features extracted selected from a frequencies which has peak amplitudes were detected. We create database from feature vectors for different cases because in power plant failures are impossible to predict and collecting structural and condition information is a time consuming.

IV. FREQUENCY SELECTION

The dominant noise frequency is related to malfunctions and their defects. A frequency selection is estimated by frequency spectrum. The state of electrical machinery is dependent on power and load variation. Also, it is depending on a construction of the electric motors.

A. Frequency analysis of some mechanical faults

The noise analysis is focused to address signal smearing and frequency beating during noise recording. In order to identify the fault carrying frequency, their harmonics and sidebands, this paper is proposing the demodulation techniques and signal envelope detector techniques for fault detection system which is used the noise signal. Generally, fault carrying frequency is derived from rotational speed and can indicate a characteristic frequency of early fault state. The structural scheme of noise analyzing is showed in a fig3.

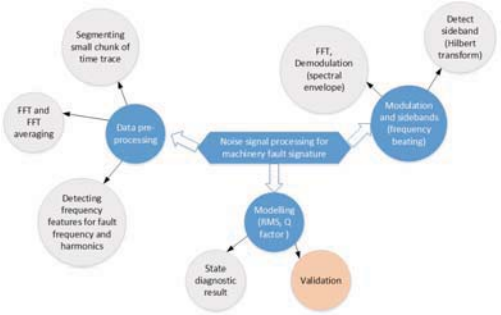

Fig. 3: Automated noise signal processing scheme

B. Hilbert Transform

Hilbert transform can helps to create analytic signal from original real valued signals.

$$z(t) = x(t) + j\hat{x}(t) \tag{1}$$

$\hat{x}(t)$ is the Hilbert transform. Hilbert transform of original signal $x(t)$ is an defined as following equation [7].

$$Hx(t) = \hat{x}(t) = p\upsilon\frac{1}{\pi}\int_{-\infty}^{\infty} x(\tau)\frac{1}{t-\tau}dt = \frac{1}{\pi}x(t)\frac{1}{t} \tag{2}$$

The Cauchy principle value is denoted pv [8]. Hilbert transform $Hx(t)$distribution of signal $x(t)$ enables an analytic signal[1] in following way:

$$z(t) = x(t) + jHx(t) = |Z(t)|e^{j\phi(t)} \tag{3}$$

where $x(t)$ is mono-component signal [2], $|z(t)|$ is an amplitude of analytic signal identifies an instantaneous amplitude or enveloping signal of phase $\phi(t)$ in instantaneous phase. The instantaneous frequency is referred as carrier frequency. Hilbert transform applies as demodulation techniques also.

C. Short Term Fourier Transform

Noise signals can contain lots of main information. Also, can detect faults in time and frequency domain or time-frequency domain. For instance, a misalignment fault can detecting by noise signal in time domain. The bearing faults are detecting in both time and frequency domain comprehensively. Common Fourier analysis decomposes signal into its frequency components and determines relative strengths. The Fourier transform formulated as:

$$\begin{cases} F(\omega) = \int_{-\infty}^{\infty} f(t)e^{-j\omega\tau}dt & \leftrightarrow \\ f(t) = \frac{1}{2\pi}\int_{-\infty}^{\infty} F(\omega)e^{j\omega\tau}d\omega \end{cases} \tag{4}$$

The difference between existing transformation is the term of computational complexity,simplicity, and unambiguity of the interpretation of signal output [12]. In this, a spectral analysis of noise signal is performed by STFT. A signal is dived into small sequential or overlapping data frames figure 4. The STFT is used windowed function $\psi(t)$ at τ on the time axis. Then the FFT implemented into a windowed signal is expressed by following equation.

$$F(\omega, \tau) = \int_{-\infty}^{\infty} f(t)\psi^*(t-\tau)e^{-j\omega\tau}dt \tag{5}$$

This transform is generated by modulation and transformation function $\psi(t)$. Where τ and ω are location of time axis and window function respectively [13]. Given signal $x(n)$ is

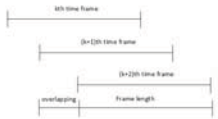

Fig. 4: Data Frame

described by STFT at the frequency band k and time n given by:

$$X_n(e^{j\omega_k}) = \sum_{m=-\infty}^{\infty} x(m)\omega(n-m)e^{-j\omega_k m} \tag{6}$$

$\omega_k = 2\pi k/N$ frequency in radians, N number of frequency band. $\omega(m)$ symmetric window of size L; $L \leq N$. Reconstructing using AM modulation into above that is equivalent to:

$$X_n(e^{j\omega_k}) = e^{-j\omega_k n}\bar{X}_n(\omega_k) \tag{7}$$

[1]Signal which satisfied Cauchy Riemann condition for complex is called analytic signal

[2]Monocomponent signal: Amplitude of signal of only one frequency component varies in a function of time.

where

$$\bar{X}_n(\omega_k)\sum x(n-m)\omega(m)e^{j\omega_k m} = x(n)h_k(n) \tag{8}$$

is result of k^{th} band pass filter, with impulse response $h_k(n)$, center frequency f_k.

$$\begin{cases} h_k(n) = \omega(n)e^{j\omega_k n} \\ f_k = \frac{f_s k}{N} \qquad \text{for} k = 0, 1, ..., N-1 \end{cases} \tag{9}$$

Considering $\omega_k = 2\pi k/N$ as above , plugging into AM modulation formula gives expression as follow:

$$X(n,k) = X_n(e^{j\omega_k}) = \sum_{m=-\infty}^{\infty} x(m)\omega(n-m)e^{-j2\pi km/N} \tag{10}$$

$X(n,k)$ is short term spectral amplitude of $x(n)$ signal.

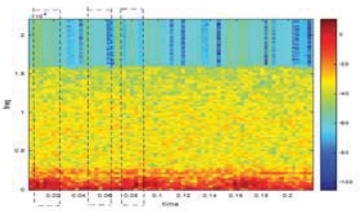

Fig. 5: Spectrogram of healthy motor from STFT distribution

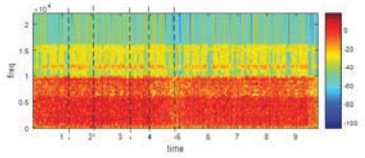

Fig. 6: Spectrogram of lubricant faulty motor from STFT distribution

The STFT distribution was calculated with window that in time domain resulting in wide frequency band. The STFT distribution simulation results are illustrated in figure5 and 6. In our case, the STFT is used a window functions such as Gaussian, β-splin , Hannning etc. These functions determine the size of the time frequency window. The window width at time scale is equal to the root mean square duration in window function multiplied by two. The height is estimated by the root mean square bandwidth of the window function is multiplied by two. The window function of Gaussion function:

$$g_a(n) = \frac{1}{2\sqrt{\pi\alpha}}e^{-\frac{n^2}{4\alpha}} \quad \alpha > 0 \tag{11}$$

The Gaussian function provide to optimize window function as possible as fixed time frequency window size that controlled by variable α.

V. Feature extraction for decision making stage

Every mechanical components which are detected failure produce significant fault characteristic signature in frequency

ranges. For example the bearing faults and their defect have fault carrying frequencies which are showed in table3 in mechanical vibration noise range. These will selected for bandpass filters for further diagnostic. The system's diagnostic section is introduced in figure 7. The fault detection algorithm

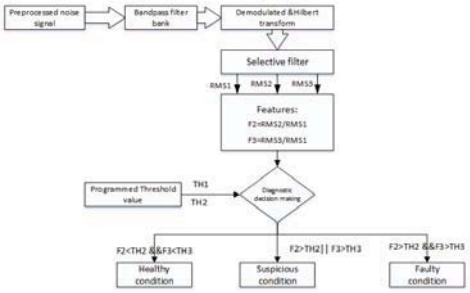

Fig. 7: Flowchart of decision making for fault detection

is consists of three sections that were illustrated in figure 3.

- Signal Pre-processing: In order to increase the efficiency of signal processing, the recorded noise signal was digitalized and pre-processed before the features can be extracted in a computer based system.
- Modulation and Envelope detector methods were associated with STFT transform.
- Fault detection algorithm is simulated for detecting and recording abnormal state of motors.

In study case as mentioned before, study on noise signal for bearing fault detection. Simulation is extract features for every single types of bearing failure utilizing the proposed noise signal processing algorithm. Before we having difference

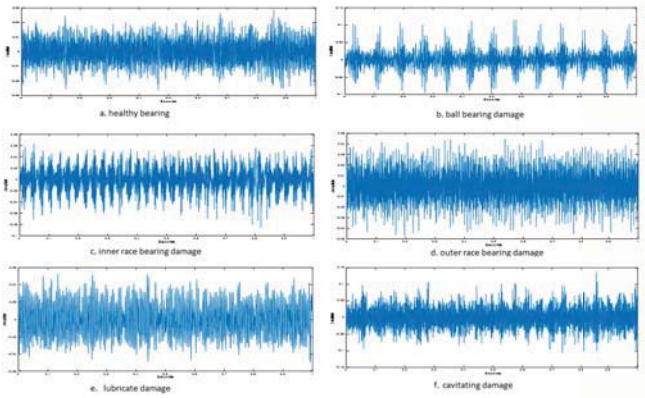

Fig. 8: Pre-processed noise signal in time domain

on noise signal context between normal and faulty, we will applied simulation result both two condition respectively. The pre-processing such as remove background noise is evaluated. The simulation results of segmenting in small chunk in time domain are in following figures 8. The recorded noise signals in time domain are filtered by averaging FFT. After increasing SNR for measured noise signal, the FFT was calculated for frequency feature selection. Carrying frequency feature selection was simulated after filtering. The implementation giving result for many investigating amplitudes of frequencies might cause

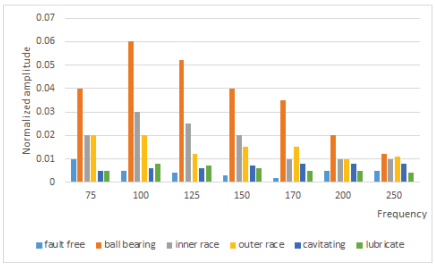

Fig. 9: Frequency spectrum of motors at frequency selection

numerical errors in calculation step. Thus extraction using threshold amplitude for common characteristic frequencies for all states of motor figure 9. The selection of a frequency

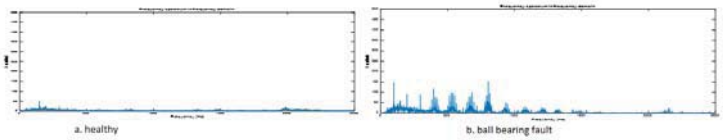

Fig. 10: FFT transformation result after preprocessing for a. healthy, b. ball bearing fault

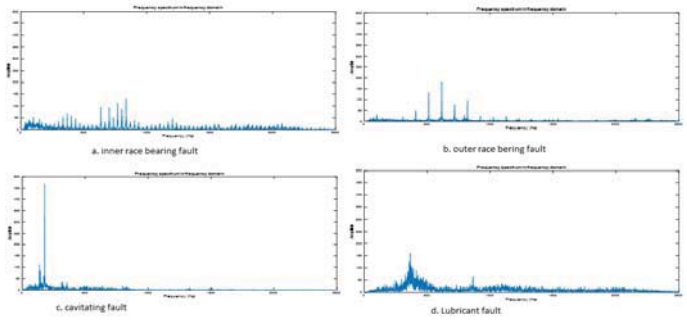

Fig. 11: FFT transformation result after preprocessing: a. inner race bearing fault, b. outer race bearing fault, c. cavitation fault, d. lubricant fault

with its amplitude potentially indicates the failure features in frequency domain. Due to utilizing noise signature ratio method for ambient noise may affect eliminate important information noise signal. More efficient way in this case was averaging FFT method. The low pass filtering was one attempt to reduce ambient noise content, however some mechanical faulty signature exists in low frequency range. In figure 10 and 11 are showing the FFT analysis in noise signal. The results of analysis, in the frequency plots are been having noise. In mechanical signal processing, the machine's rotating speed undergoes a change because of a power supply variation and load variation. These speed variation ($RPM \pm \Delta RPM$) is been influencing to signal smearing in noise signal. These clearly showed in band pass filtering after FFT transform.

VI. Fault detection system implementation and Result

Automated noise analysis (ANAS) for fault detection system used a statistical feature calculation method and signal processing techniques (fig7). In this algorithm, the noise signal is analyzed in selective band pass filter bank. The short term Fourier transform (STFT) is utilized to identify certain frequency bands for different failures. The RMS identifies the average of maximum and minimum amplitude. In digital noise signal, the maximum RMS allowed 0dB. In algorithm, the programmed threshold RMS is estimated equal as 0.6dB. This value indicates that a peaks were detected. In addition crest factor was utilized for increase algorithm result for fault detection. The RMS is calculated in each frequency band. Low

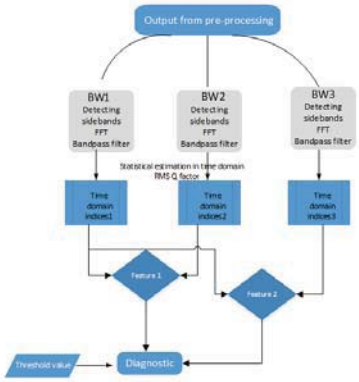

Fig. 12: Automated fault detection algorithm

frequency band RMS is used as reference value. Others mid and high frequency band RMS are used for feature calculation. In order to reducing complexity of analysis processing identifying spectrum content in time domain using STFT. In this algorithm determining signal processing in concrete frequency band that set of three band pass FIR filter. Band pass filtering designed as Matlab filter design tool. The filter design template utilizing bandpass FIR filter. The noise signal processing and fault detection algorithm which is illustrated in figure 12 are simulated in Matlab. Case study results are introduced in figure 13.

VII. Conclusion

Mechanical system complexity for fault detection is potentially diagnosed by a noise which is emitted from its mechanical vibration. The main goal of automated noise analysis system is to alarm against future failures whether no action is taken. All tests were done in order to clarify the possibilities to construct an automatic on-line condition monitoring for the rotating machinery. This system can pulled out in practical scenarios. Also this system has an advantage for implementation without complexity for a power and size increases of motor. The automated noise analysis system is implemented with high effective result for fault detection. However, experiment could not carried on speed and load dependence measurement.

№	Sample data	RMS model	Q factor model	result
1	bearing ball fault			
2	outer race fault			
3	inner race fault			
4	contaminate fault			
5	cavitating fault			
6	undamaged bearing			
7	turbine generator			
8	combussion engine			
9	ultrasonic/lackoflubric			
10	ultrasonic /brinelling			
11	ultrasonic/fatigure failure			
		Faulty		
		Suspectable		
		Healthy		

Fig. 13: Matlab simulation result from detection algorithm

References

[1] Henriquez, Patricia, et al. "Review of automatic fault diagnosis systems using audio and vibration signals." IEEE Transactions on Systems, Man, and Cybernetics: Systems 44.5 (2014): 642-652.

[2] Bjeli, Milo, et al. "Fault Detection in Induction Motors Using Microphone Arrays."

[3] Orman, Maciej, and Cajetan T. Pinto. "Acoustic analysis of electric motors in noisy industrial environment." 12th IMEKO TC10 Workshop on Technical Diagnostics New Perspectives in Measurements, Tools and Techniques for Industrial Applications. 2013.

[4] Shibata, Katsuhiko, Atsushi Takahashi, and Takuya Shirai. "Fault diagnosis of rotating machinery through visualisation of sound signals." Mechanical Systems and Signal Processing 14.2 (2000): 229-241.

[5] Germen, Emin, Murat Baaran, and Mehmet Fidan. "Sound based induction motor fault diagnosis using Kohonen self-organizing map." Mechanical Systems and Signal Processing 46.1 (2014): 45-58.

[6] Janda, Marcel, Ondrej Vitek, and Vitezslav Hajek. Noise of Induction Machines. INTECH Open Access Publisher, 2012.

[7] Boashash, Boualem. "Estimating and interpreting the instantaneous frequency of a signal. I. Fundamentals." Proceedings of the IEEE 80.4 (1992): 520-538.

[8] Hildebrand, Francis Begnaud. Advanced calculus for engineers. Prentice-Hall, 1949.

[9] Barber, Antony. Handbook of noise and vibration control. Elsevier advanced technology, 1992.

[10] Lipovszky, Gyrgy, Kroly Slyomvri, and Gbor Varga. Vibration testing of machines and their maintenance. Vol. 10. Elsevier Science Ltd, 1990.

[11] Gaka, Tomasz. Vibration-Based Diagnostics of Steam Turbines. INTECH Open Access Publisher, 2012.

[12] Kymk, M. Kemal, et al. "Comparison of STFT and wavelet transform methods in determining epileptic seizure activity in EEG signals for real-time application." Computers in biology and medicine 35.7 (2005): 603-616.

[13] Jurado, Francisco, and Jose R. Saenz. "Comparison between discrete STFT and wavelets for the analysis of

power quality events." Electric Power Systems Research 62.3 (2002): 183-190.
[14] Zurita Milln, Daniel. "Mechanical fault detection by means of AE analysis." (2013).
[15] Mohanty, Amiya Ranjan. Machinery condition monitoring: Principles and practices. CRC Press, 2014.

CCA based Dual Algorithm in a Zigbee transmission under WLAN interference

Narangerel Purevdorj*, Khishigjargal Gonchigsumlaa*, Uuganbayar Purevdorj* and Young-il Kim#
*Dept. Information Technology, Mongolian University of Science and Technology, Ulaanbaatar, Mongolia
#Electronics and Telecommunications Research Institute (ETRI), Daejeon, Korea
Email: *p.narangerel@must.edu.mn

***Abstract*—Wireless sensor networks (WSN) have rapidly gained a growing importance in many other research works. IEEE802.15.4 is designed for low rate Wireless Personal Area Networks (LR-WPAN) named Zigbee which allows small, power-efficient, inexpensive solutions to be implemented for wide range of devices. It's necessary to introduce real time monitoring technology for freight train of Mongolian Railway using Zigbee. Due to the freight train WSNs have long linear chain-like topology Zigbee-only network is not reliable to the collecting node in the locomotive. To solve these problems, we assume additional high speed technology the Wi-Fi. Spectrum shortage is main difficulty to allocate a wireless network capacity. Spectrum sharing is important approach in this case. Spectrum sharing within the devices of same network is not problem.**

Keywords— Wireless Sensor Network; Interference; Coexistence

I. INTRODUCTION

ZigBee is IEEE 802.15.4-based specification for the suite of high-level communication protocols used to create personal area networks with small, low-power digital radios and the wireless language that everyday devices use to connect to one another. The name "ZigBee" is derived from the erratic zigging patterns many bees make between flowers when collecting pollen. This is evocative of the invisible webs of connections existing in a fully wireless environment. The standard itself is regulated by a group known as the ZigBee Alliance [7]. The mission of the ZigBee Alliance is to enable reliable, cost-effective, low-power, wirelessly networked, monitoring and control products based on an open global standard, and the goal is to provide consumers with ultimate flexibility, mobility, and ease of use by building wireless intelligence and capabilities into everyday devices [1].

II. CONVENTIONAL ALGORITHMS

A. Time Agility (TA)

An interference avoidance scheme, called Time Agility (TA), where TA enables spectrum coexistence between short-range IEEE 802.11 (Wi-Fi). The basic idea is to allow 802.15.4 and 802.11 devices to adapt to each other's traffic pattern and the time varying channel conditions. To avoid transmissions (and thus potential re-transmissions) during poor channel conditions, the transmit probability is decreased when interference power increases, thus avoiding severe interference scenarios [2].

B. Dynamic Frequency Selection (DFS)

There is another typical interference avoidance scheme called dynamic frequency selection. Normally, a wireless system operates on a frequency band, which is divided into multiple channels [3]. The wireless system may dynamically select an operational channel so as to dynamically avoid harmful interference from other wireless systems sharing the same frequency band. This scheme for dynamically selecting one of the possible channels within the band is referred to as Dynamic Frequency Selection (DFS). Sometimes we called Frequency Agility (FA) algorithm. The scheme uses three mechanisms: Interference Detection, Group Formation, and Demolition. Each 802.15.4 node checks for interference on the current channel using the Interference Detection (ID) [4]. It can be called periodically or on demand. In case of interference, the node enters into Group Formation (GF).

C. Transmit Power Control (TPC)

Traditional approaches for the coexistence of wireless devices focus on transmit power control (TPC). The idea of TPC is that each device transmits only the minimum power necessary to maintain communications [6]. This would help in minimizing interference into other existing services and facilitate frequency reuse between devices [2]. This is especially useful to enable spectrum sharing between systems with different levels of regulatory status, e.g., primary and secondary users, but does not fit the coexistence situation of systems with equal regulatory status, e.g., IEEE 802.15.4 WSNs and IEEE 802.11b/g WLANs. This approach fits coexisting systems which have comparable adjustable transmit power scopes, rather than the coexisting IEEE 802.15.4 WSNs and IEEE 802.11b/g WLANs, whose adjustable transmit power scopes are substantially different. Hence, it is not a good solution for the scenarios we are considering.

D. Transmit Interval Control (TIC)

Another category of solutions focuses on Transmit Interval Control (TIC). The hub, i.e., a special Zigbee coordinator which integrates both functions of IEEE 802.11 and Zigbee is designed [5]. It is capable of controlling the transmit interval of 802.11b interferer by generating periodic "fake IEEE 802.11 CTS (Clear to Send)" frames to silence 802.11 traffic and thus reserve the channel for Zigbee transmission. This approach is useful in some cases, but it may degrade the IEEE 802.11 performance dramatically even in case of no pending Zigbee transmission. Besides, fake CTS frames sent by the hub need to be able to cover all the potential IEEE 802.11 interferers,

which may, on the one hand, not be guaranteed and on the other hand, make the exposed node problem more serious for the coexisting IEEE 802.11 and Zigbee networks [3]. Hence, it is not a good solution for the scenarios we are considering. In the following section, we will present a decentralized approach to help IEEE 802.15.4 nodes mitigate interference. The approach is robust, responsive and easy to be implemented at a low cost.

E. CSMA/CA

Similar to the IEEE 802.11 family, IEEE 802.15.4 standard defines the CSMA/CA as its medium access mechanism at MAC sub layer. The CSMA/CA protocol aims at enabling two or more wireless devices to access the same frequency channel resource reducing data collisions and, ultimately, performance loss due to interference. The CCA is a PHY layer function. It is used to sense the power and/or carrier in the operating channel and determines whether a certain channel is active or not. CCA is an essential ingredient of CSMA/CA based MAC protocols.

III. PROPOSED ALGORITHM

The one of key ideas proposed to implement interference avoidance process is to make the system more flexible with dynamic channel allocation. The general aim is to make sure that there is no collision caused by multiple systems using exact same frequency range at the same time. This approach described in [7]. The other one is dynamic channel selection approach to implement interference avoidance and in this case, the victim network must change current channel to new channel. These two approaches based on Carrier sense multiple access with collision avoidance (CSMA/CA).

A. Method

Our proposed algorithm consists of two sections such as interference avoidance and interference mitigation. Figure 1 shows a proposed algorithm. In the first section of algorithm, proposed algorithm checks carrier signal on current WSN channel. If carrier signal strength is lower than threshold strength (-77dBm), transmission will continue. Otherwise, algorithm checks a carrier signal strength of other channels. If algorithm can find any available channel, current channel will be changed to new channel and transmission will continue.

However, algorithm couldn't find any available channel, algorithm will switch to the second section of algorithm. The second section of algorithm transmits to make sure that there is no collision caused by multiple systems using exact same frequency range at the same time. This sub algorithm find the gaps called back-off time between the packets and transmit their packets on gaps. To find back-off time, we use CCA algorithm.

The following renewed procedure is used to initiate a transmission. The procedure is complete when the frame is transmitted successfully or a collision is detected during transmission (Figure 1).

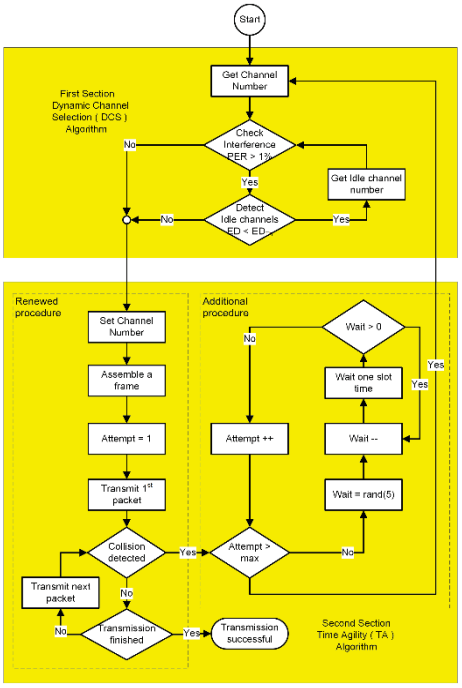

Fig 1. Simplified flowchart of Proposed CCA based dual Algorithm

- Is frame ready for transmission? If yes, it goes to the next point.
- Is medium idle? If not, algorithm waits until it becomes ready.
- Start transmitting and monitoring process for collision during transmission.
- Did a collision occur? If so, go to collision detected procedure.
- Reset retransmission counters and end packet transmission.

The end of procedure, we can find back-off time and transmit packet. In addition, algorithm can detect the collision for wireless networks during the transmission. Therefore, we considered about additional procedure when collision is detected.

The additional procedure is used to resolve a detected collision. The procedure is complete when retransmission is initiated or the retransmission is aborted due to numerous collisions (Figure 1).

- Continue transmission (with a jam signal instead of frame header/data/CRC) until minimum packet time is reached to ensure that all receivers detect the collision.
- Increment retransmission counter.
- Was the maximum number of transmission attempts reached? If so, abort transmission and run algorithm 1.
- Calculate and wait random back-off period based on number of collisions.

- Re-enter main procedure at stage 1.

IV. Simulation Result

Figure 2 shows simulation result for throughput performance using proposed standard algorithm and dual algorithm. Interference is generated randomly a packet to packet time wireless networks.

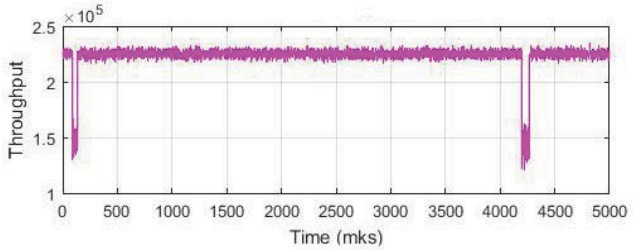

Fig 2. Throughput performance using standard CSMA/CA algorithm

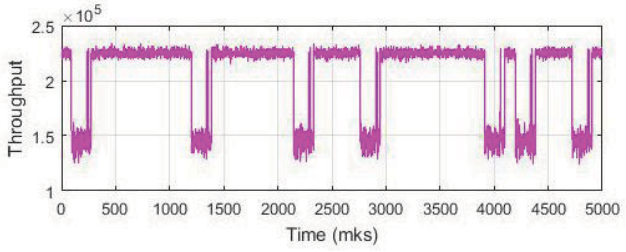

Fig 3. Throughput performance using proposed dual algorithm

Figure 2 shows simulation throughput performance using standard CSMA/CA algorithm. This result shows much collision occurs.

Figure 3 shows throughput performance using proposed dual algorithm and it shows lesser collision detected than standard CSMA/CA algorithm.

V. Conclusion

This paper dealt with the interference problem of coexistence between Zigbee and Wi-Fi for real time monitoring system in Mongolian railway. We presented a dual algorithm with dynamic channel selection (DCS) algorithm and time agility (TA). Using the dual algorithm, analytical result shows the proposed algorithm is more reliable data than traditional algorithms when working together. However, second section algorithm is working alone, transmission rate is decreases and bit error rate is enough to transmit.

References

[1] IEEE Standard for Information Technology- Telecommunications and Information Exchange Between Systems- Local and Metropolitan Area Networks- Specific Requirements Part 15.4: Wireless Medium Access Control (MAC) and Physical Layer (PHY) Specifications for Low-Rate Wireless Personal Area Networks (WPANs), IEEE Standard, 2006.HUO H et al, "Coexistence of 2.4 GHz sensor networks in home environment" The Journal of China Universities of Posts and Telecommunications 2010; 17(1) :9-18.

[2] S. Kang et al, "Adaptive Interference-Aware Multi-Channel Clustering Algorithm in a ZigBee Network in the Presence of WLAN Interference," in 2nd International Symposium on Wireless Pervasive Computing, 2007 (ISWPC '07), February 2007.

[3] G. Zhou et al, "RID: Radio interference detection in wireless sensor networks," in 24th Annual Joint Conference of the IEEE Computer and Communications Societies (INFOCOM 2005), pp. 891-901, 2005.

[4] Antoine BB et al, "Experimental Evaluation of Interference Mitigation on The 2.4 GHz ISM band Using Channel Hopping" Proceedings of the IEEE Wireless Days' October 2010; Venice: Italy: 1-5.

[5] Lin Zhu et al, "Implementation of the Adaptive CSMA-CA algorithm based on traffic load" in vol 7 IJFGCN, on July 2014.

[6] L.Angrisani et al, "Modeling the Performance of CSMA-CA Based Wireless Networks Versus Interference Level," IEEE Instrumentation and Measurement Technology Conference, pp.376-381, 2008.

[7] J. Yun et al, "A Channel switching scheme for avoiding interference of between IEEE 802.15.4 and other networks". in 2008 International Multi-symposiums on Computer and Computational Sciences (IMSCCS'08), Oct. 2008, pp. 136-139.

Design of a Laboratory for Audio and Video Based Object Localization and Tracking

Hussein Hussein*, Robert Manthey*, Abul Hasan*, Manuel Heinzig*,
Marc Ritter†, Danny Kowerko* and Maximilian Eibl‡
*Junior Professorship Media Computing, Chemnitz University of Technology, D-09107 Chemnitz, Germany
†Professorship Media Informatics, University of Applied Sciences Mittweida, D-09648 Mittweida, Germany
‡Chair Media Informatics, Chemnitz University of Technology, D-09107 Chemnitz, Germany
Email: {hussein.hussein, robert.manthey}@informatik.tu-chemnitz.de

***Abstract*—This paper presents the design of a laboratory for object localization and tracking using acoustic and visual information. The audio-video laboratory of the junior professorship media computing at the Chemnitz university of technology is planned to use a number of passive sensors (including acoustic and optical sensors) which will be installed inside the tracking area. Multiple microphone arrays with a total number of 64 microphones will be used to receive audio signals emitted from objects which will be simulated by loudspeakers with a total number of 16 loudspeakers. The optical sensors with a total number of 10 will be distributed at different positions, directions and heights.**

I. Introduction

Object localization is the estimation of the object positions using acoustic, visual or both acoustic and visual information. The object localization and tracking is an important task in many applications such as mobile robots, surveillance systems and human-computer interaction. Acoustic source localization (ASL) is based on the time delay estimation of received acoustic signals by a set of microphones in a specific configuration (microphone array). In a similar way, the visual localization is processed. Cameras capture the light of their field of view and subsequent image processing operations realize the identification and tracking salient objects. To develop, verify and improve algorithms which represent real world events, a laboratory is needed to set up and reproduce them under controlled conditions, for instance to capture motions of people without disturbing environment [1].

Smart homes are the typical domestic environments, which use multitude of sensors (microphones and cameras). For example, 20 condenser microphones are distributed on the walls and the ceiling, 6 Micro-Electro-Mechanical System (MEMS) microphones and 2 close-talk microphones as well as one Kinect camera are used in a two room smart home [2]. A laboratory for cognitive systems is established. The main component is a 3D microphone array consisting of 64 microphones with two layouts of 32 microphones in each layout. The 64 microphones are connected to eight 8-channel pre-amplifiers. In addition, one video camera and one Kinect camera are used for the detection of gestures [3].

The paper is organized as follows: Section II gives an overview on the project *localizeIT* for object localization and tracking using acoustic and visual information. The design of audio and video systems are described in Sections III and IV, respectively. Finally, conclusions and future work are presented in Section V.

II. LocalizeIT

The aim of the project *localizeIT* (http://www.localize-it.de) is the localization and tracking of objects as well as the analysis of object behavior by using acoustic and visual information. Figure 1 shows the sketch of the audio-video laboratory. The laboratory consists of two rooms. The first one (L x W x H = 7.2 x 6 x 4 meter) is for the installation of acoustic and optical sensors in order to locate and track objects in this room. It will be equipped with sound insulation materials to dam the acoustic reflections. The second room is for the mounting of audio interfaces in a cooled server room. Passive sensors, including acoustic as well as optical sensors (cameras with stereo optics) here referred to as smart sensor, will be installed inside the tracking area. The optical sensors can be hindered due to different physical properties. In this case, the acoustic sensors can be used instead. The fusion of audio and visual based object tracking can be used to improve the tracking task. The five-year project is funded by the Federal Ministry of Education and Research in the program of Entrepreneurial Regions.

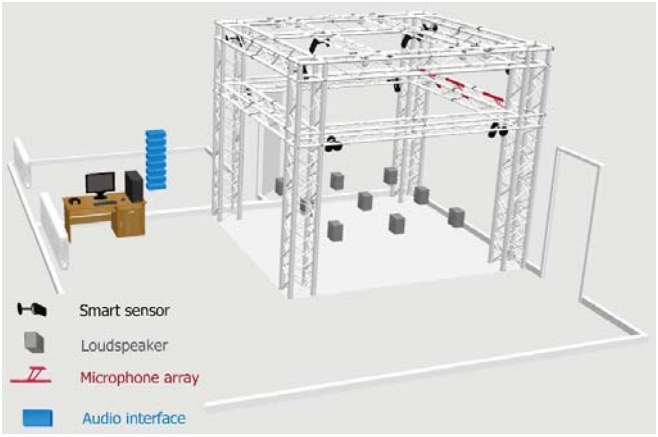

Fig. 1. Sketch of the audio-video laboratory showing the positions of acoustic and optical sensors.

III. Design of Audio System

Figure 2 shows the system design for audio components. The acoustic signals received by microphones must be preamplified and digitalized by an audio interface. Each 8 microphones can be connected to an audio interface (there are 8 audio interfaces for 64 microphones). Every audio interface has an Alesis Digital Audio Tape (ADAT) output which will be used to transmitted the audio data using optical cables to a multi-channel interface. The multi-channel interface offers format conversion from Multichannel Audio Digital Interface (MADI) [4] to ADAT and vice-versa. The maximal number of channels can be used with MADI is 64 channels by 24 bit audio and up to 48 kHz sampling rate. The 8 ADAT optical inputs in the multi-channel interface are transferred to MADI digital audio stream as output. The audio data can be transmitted with MADI cable (coaxial or optic) with a cable length of more than 100 meters to the MADICard in the computer. A software will be used to record the audio data from 64 microphones in 64 mono audio files. On the other side, the audio data can be transmitted from the computer using the MADI cable, whereas the input MADI channels are transferred to 8 ADAT optical outputs in the multi-channel interface (we need only two ADAT optical outputs for 16 loudspeakers) to the loudspeakers. An audio master clock system is essential to make every audio interface a slave to the centralized master clock unit using Bayonet Neill–Concelman (BNC) cables. Different types of microphones including small (lavalier) and big (measurement) microphones will be tested in each microphone array to detect its effects on the localization results. In addition, different geometries of microphone arrays with different number of microphones will be investigated.

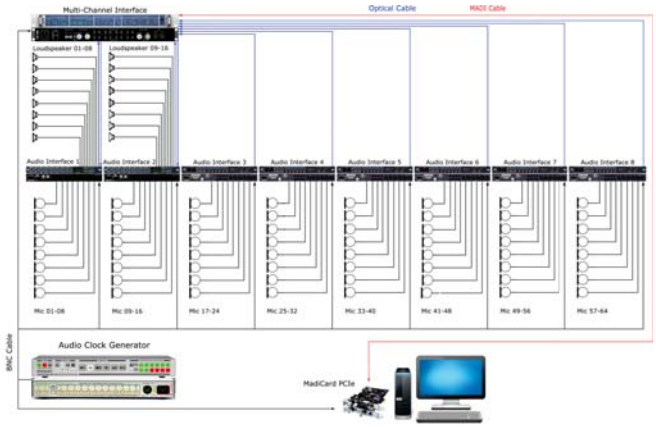

Fig. 2. Schematic diagram of audio components in the audio-video laboratory.

IV. Design of Video System

Multiple optical sensors will be distributed inside the tracking area at different positions, several directions and heights to focus on different tasks and optimize theirs effectivity. The optical sensors are used to detect the objects of interest from different points of view. As a result, an applicable view can be used to trigger an identification process as well as a tracking operation to follow that object. The most suitable view can be used for a comparison with a list of known objects. In a similar way, the tracking is processed by using all suitable views to follow the object and to temper the masking of the object by the environment with the use of another optical sensor as shown in Figure 3. Based on the tracking of persons and there arms for instance, an analysis of the behavior can be detected. In our environment, a total number of 10 ethernet attached optical sensors will be used to track objects.

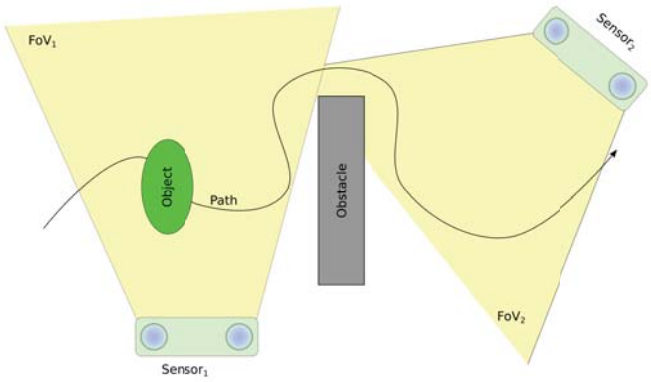

Fig. 3. Exemplary scene with an object moving on a path and optical sensors with their field of view.

V. Conclusion and Future Work

This paper described the design of the laboratory for object localization and tracking by using acoustic (microphones) and optical sensors (cameras) in order to improve the tracking of objects in the room when obstacles such as masking are occur, by combining cameras and microphones or by fusion both sensor technologies. In the audio system, 64 microphones and 16 loudspeakers will be used. The optical sensors with a total number of 10 will be used. As the result of this setting any scene can be captured simultaneously from different positions allowing complex analysis and the development of algorithms and systems. The next steps are to realize the laboratory as well as to develop algorithms for audio and visual object localization and tracking.

Acknowledgment

This work is funded by the program of Entrepreneurial Regions InnoProfile-Transfer in the project group *localizeIT* (funding code 03IP608).

References

[1] Mocapdata, *Mocapdata*, Available on http://mocapdata.com/, 2017, Last accessed at 20. March 2017.

[2] A. Tsiami, I. Rodomagoulakis, P. Giannoulis, A. Katsamanis, G. Potamianos and P. Maragos. *ATHENA: a Greek Multi-Sensory Database for Home Automation Control*, In Proc. of 15th Conference Interspeech 2014, pp. 1608–1612, Singapore, September 2014.

[3] C. Richter, J. Lindemann, R. Römer and M. Wolff, *Das Labor für kognitive Systeme an der BTU Cottbus-Senftenberg*, In Proc. of the 26st Conference ESSV 2015, pp. 240-247, Eichstätt-Ingolstadt, Germany, March 2015 (in German).

[4] P. Wilton, *MADI (Multichannel Audio Digital Interface)*, In Audio Engineering Society Conference: UK 3rd Conference: AES/EBU Interface, http://www.aes.org/e-lib/browse.cfm?elib=5340, September 1989.

Designing a Heart Sound Sensor Matrix Structure and Data Processing Platform Using FPGA

*Wang, Tian +Shi, Yunbo #Wolfram Hardt

*+The Higher Educational Key Laboratory for
Measurement and Contrl Technology and Instrumentation of Heilongjiang Province,
Institute of Measurement - Control Technology and Communications Engineering,
Harbin University of Science and Technology,
No. 52 Xuefu Road, Nangang Dist, Harbin, China
#Fakultät für Informatik, Technische Universität Chemnitz, Straße der Nationen 62, D-09111 Chemnitz, Germany
Email: *wt1988114@outlook.com +shiyunbo@126.com #wolfram.hardt@informatik.tu-chemnitz.de

***Abstract*—Currently, heart sound sensors are usually large in size, expensive in cost, and therefore unable to be embedded in cloth or mattress to record heart sound for home and continuous use. For solving these problems, a new heart sound sensor matrix structure using low-cost ECM sensor, Electret Condenser Microphone, is proposed, also a testing platform of matrix data processing and recording with FPGA and MCU is implemented. After testing the sensor matrix and platform by using additive noise suppression method, good results have been obtained. The noise level of the sensor matrix is 2dB lower than single sensor noise. The result also proves that the sensor matrix and testing platform function well, so that a series of deeper research can be done in the future.**

I. Introduction

Heart sound signal is an important clinical medical signal. Auscultation is still a widely-used way for doctors to check heart diseases because of several advantages e.g. vitro examination, non-invasiveness, convenience and economy. Despite a variety of electronic stethoscopes have been developed, they still use the traditional sensing method, that is, the head of stethoscope directly contact the surface of the patient's chest. This method gets good quality on heart sound, yet it causes bad comfort and privacy to patient, moreover it is hard to achieve a continuous heart sound monitoring.

For improving the traditional sensing method, new ways are discovered, one of which is to embed the heart sound sensor in cloth or mattress. By using this way, heart sound can be automatically sensed when users just wear a shirt or lay on bed. Because of a strong attenuation, the monitoring system must be highly sensitive, meanwhile, the sensor must be thin and soft.

In heart sound sensing applications, specific heart sound sensors are commonly used for accuracy. General heart sound sensors usually contains a resonant cylinder, by which the sensor amplitude may increase. This leads to a big size. Some PVDF thin-film[1] and optical fiber[2] are also used to make heart sound sensors. Those heart sound sensors are thin enough, but not massive produced, so the high cost keeps them away from home use.

ECM, the Electret Condenser Microphone, can respond well to low frequency sound, and can be very small in size. Some general heart sound sensors are just made by putting the ECM sensor into resonant cylinder[3]. It outputs analog voltage signal, so analog circuit and AD converter are necessary, which makes it more complicated to connect to digital system compared with MEMS acoustic sensors.

Most mass-productive MEMS acoustic sensors are designed for space-limited acoustic applications e.g. cell phone. It has a bad response to low frequency sound because it is optimized for improving speech signal and suppressing wind noise. So it is not suitable for sensing heart sound signal even though it has a significant advantage in size.

Figure 1 shows the frequency response curve between Knowles SPH0641LM4H-1 MEMS acoustic sensor[4] and Panasonic WM-62C ECM sensor[5]. ECM sensor gets a flat frequency response, yet MEMS sensor starts decreasing response from 100Hz.

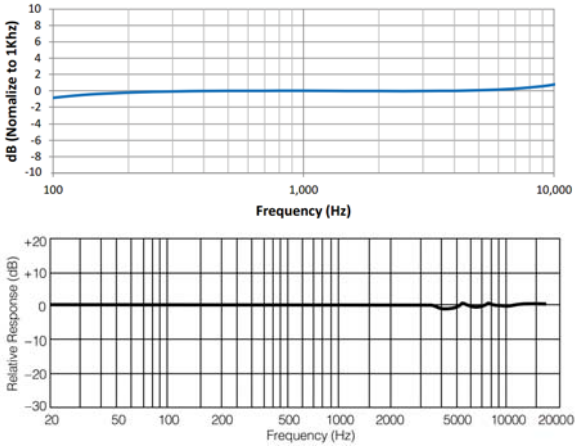

Figure 1 - Frequency Response Curve Comparison

Considering the points above, ECM sensor is capable for a embedded heart sound sensing application, as it may achieve good quality while keeping small.

In this paper, a heart sound sensor structure is proposed, that is, arranging several ECM sensors into a matrix. This makes

the sensing area larger than single sensor, so that the sensitivity and SNR could increase. Also, for verifying the sensor matrix, an FPGA-MCU combination platform is designed to drive the sensor matrix and process multi-channel sensor data. An additive noise suppression method is implemented in FPGA to reduce noise and outputs one channel sound signal. MCU stores the sound signal in standard wave file format for further analysis.

II. Matrix Data Processing Algorithm

Each sensor in the matrix gives a linear output which is proportional to the Sound Pressure Level it senses, so the sensor output signal represents the sound information. The noise which is acquired by system can be recognized as two parts, that are addictive noise and multiplicative noise. Addictive noise comprises the components background noise, and the noise influenced by the environment. It adds up with useful signal. If useful signal stops, noise still exists. Multiplicative noise is caused by an non-ideal signal transmission channel, for example the non-linearity or time-variation of the device model. It disappears when useful signal stops.

The result sampled by system contains noise which caused by the power supply, sensor itself, digital circuit, ADC quantization noise, etc. Because those different noise sources exists permanently, this noise can be treated as Poisson-distributed addictive noise[6].

Assume that the output signal of each sensor is $f(p,t)$, which contains useful part $S(p,t)$ and addictive noise part $N(p,t)$. The argument p represents different sensors, its domain is $[1,n]$, which n is the count of all sensors in the matrix. At a time t_0, by adding up all sensor outputs together, the sensor matrix output signal is shown as formula (1) and (2):

$$g(p,t_0) = \frac{1}{n}\sum_{i=1}^{n} f(i,t_0) \quad (1)$$

$$= \frac{1}{n}\sum_{i=1}^{n} S(i,t_0) + \frac{1}{n}\sum_{i=1}^{n} N(i,t_0) \quad (2)$$

If the sensor matrix area is small enough, we can treat the different signals from sensors as equal, that is assumed as formula (3):

$$S(1,t_0) = S(2,t_0) = \cdots = S(n,t_0) \quad (3)$$

So the output can be written as formula (4):

$$g(p,t_0) = S(a,t_0) + \frac{1}{n}\sum_{i=1}^{n} N(i,t_0) \quad (4)$$

in which $a = 1,2,3,\cdots,n$.

From formula (4) we can see that, the useful signal is kept as original, and the term

$$\frac{1}{n}\sum_{i=1}^{n} N(i,t_0)$$

is the noise part. A Poisson noise can be treated as a stationary process which is ergodic, so the noise part decreases after processing[7].

This is the theoretical basis of the sensor matrix and its processing algorithm using FPGA.

III. Platform Design

The sensor matrix consists out of 16 ECM sensors which are arranged as 4x4. Every two sensors outputs are connected to a stereo audio ADC for sampling. So there are totally 8 ADC chips to sample 16 sensor outputs. The structure of the sensor matrix is shown in Figure 2.

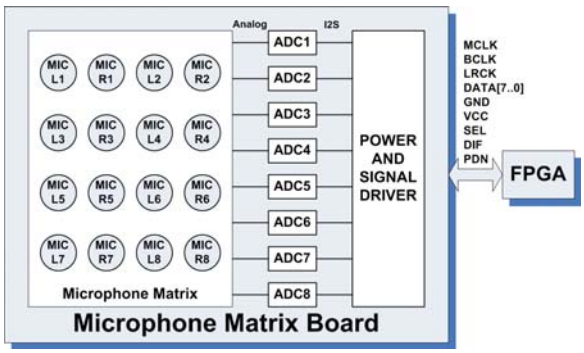

Figure 2 - Structure of Sensor Matrix

Figure 3 is one circuit part of 8 ADC chips and 16 sensors. By biasing the ECM sensor using a resister connected to the analog power supply, sensors gives response to sound and output signal. After a capacitor, the DC part of the signal is eliminated and AC part is sampled by ADC.

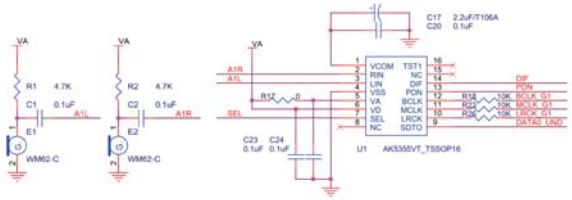

Figure 3 - Two Sensors and ADC Circuit

The ADC chip uses I2S port to interface with digital system. There should be an I2S Master device and an I2S Slave device exists in a general I2S system. Because there are totally 8 I2S ADC chips in the matrix circuit, external signal drivers are needed to extent bus driving capability. Here the general 74HC04 CMOS hex-inverter chips are used as I2S bus drivers, as shown in Figure 4.

In Figure 4, the sensor matrix signal port is also illustrated. In this port, three I2S clock signals, eight serial data lines from ADC chips, power supply and ground lines, also three ADC configuration signals are shown.

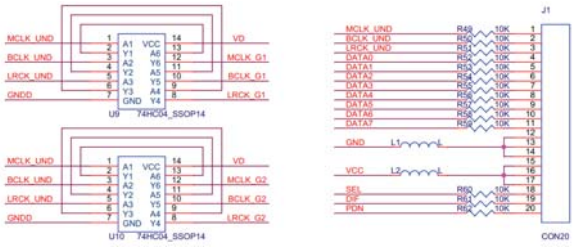

Figure 4 - Bus Drivers and Matrix Port

In most mass-productive MCU chips, there are one or two I2S bus modules for audio signal input/output, but seldom MCU chip has eight I2S modules to drive matrix ADC chips. So an FPGA chip should be used to implement several modules needed to drive the matrix, do data processing job, and send the mixed audio signal to external MCU for recording[8]. Also a control module and a control interface module are needed so that external MCU could control FPGA and get FPGA status. The FPGA logic structure is shown in Figure 5.

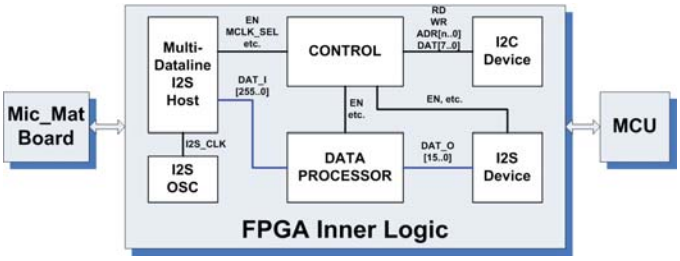

Figure 5 - FPGA Logic Structure

The MULTI-DATALINE I2S HOST module in FPGA is used to generate MCLK, BCLK and LRCK clock signals to drive ADC chips by dividing I2S Oscillator clock-out signal, receive multiple serial data to parallel out for data processing logic. The DATA PROCESSOR module implements addictive noise suppression algorithm, fuses the multi-channel signals to one-channel signal, and parallels the data out. I2S DEVICE module receives the external MCU I2S clock, and serializes the one-channel signal data out to external MCU. CONTROL and I2C DEVICE module is used to monitor and control other inner modules and communicate with external MCU for command and status.

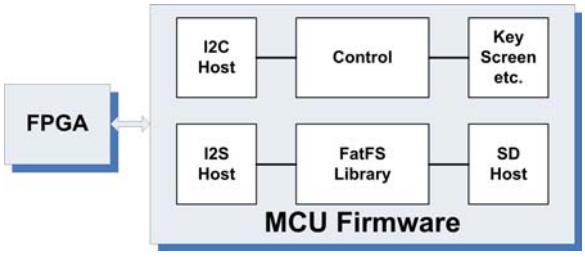

Figure 6 - MCU Firmware Function

Figure 6 shows the MCU firmware function and structure. MCU reads FPGA signal data through its I2S module, and stores the data as standard WAV file using file system driver and SDIO driver. The platform structure and photo are shown in Figure 7.

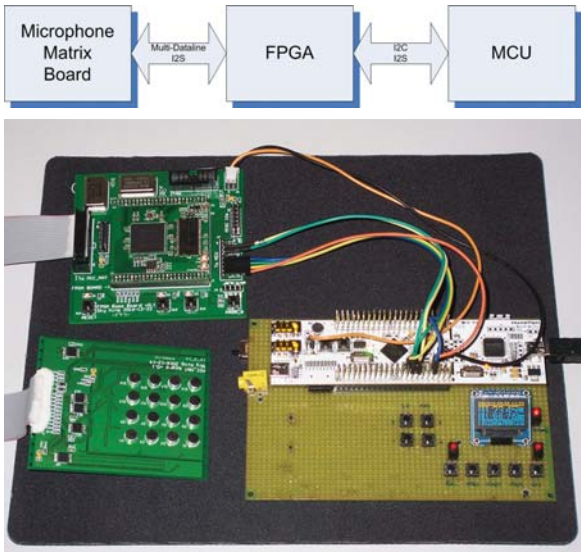

Figure 7 - Platform Structure and Photo

There are two important parameters in digital audio system, which are Sample Rate and Sample Depth. In general digital audio standard, sample rate is usually including 8kHz or 11.025kHz, and their multiples up to 44.1kHz and 48kHz. The sample depth is usually 8bit, 16bit, and 24bit.

The power of heart sound is usually distributed in the frequency band between 10Hz and 500Hz. A 8kHz sample rate of ADC is fine to record heart sound signal, while compatible to digital audio standards. FPGA inner logic can run up to tens mega-hertz which is thousands times faster than 8kHz sample rate, so FPGA processing is fast enough to apply additive noise suppression method on all sensor channels. If using higher sample rate to sample the input signals, the power of quantization noise spreads more widely on the frequency domain. By using a low-pass filter in digital domain, output signal may have less noise ideally. This is the way called Over-sampling, which will be considered in further research. Now in prototype period, 8kHz sample rate is used for fast platform verification.

The sample depth is 16bit which is commonly used in most audio situations. It gives the maximum value of 65536, which means that the ideal largest dynamic range is 96dB. Considering the sampling error of the ADC, actual dynamic ranges may be smaller. When analog signal is too small, it may be hard to sample. In further research, a higher sample depth can be used to achieve higher accuracy.

Considering the issues above, the main components of the prototype platform are chosen. Sensors are WM-62C ECM from Panasonic, ADCs are AK4355 chips from Asahi Kasei, FPGA is Spartan-6 Series XC6SLX16 chip from Xilinx, MCU is Cortex-M4F series NUC505 from Nuvoton. The FPGA inner logic is programmed using Verilog HDL, and MCU firmware is developed in the C language. The file system library is migrated from the open source FatFS project written and maintained by ChaN.

IV. Test and Analysis

After building the platform, tests are done in a quiet laboratory. The acquired signals in quiet environment can be treated as the summary of the environment noise and the sampling noise. In the first test, FPGA data processor module is disabled, MCU directly drives any one of the sensors in the matrix to sample the signal for 10s. In the second test, FPGA data processor module is enabled, all sensor signals in the matrix is acquired and proceeded by FPGA, MCU just records the output data from FPGA for 10s. Two WAV audio files are stored after test.

The audio editing and analyzing jobs are done using Audition, a professional audio software from Adobe. The two audio signals in corresponding WAV files are first 45dB gained in digital domain, so that the waveforms can be easily observed. Figure 8 shows the two audio signals.

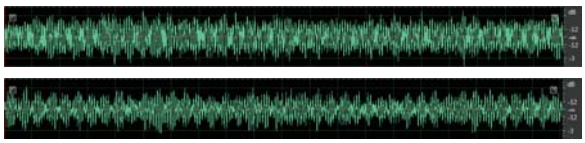

Figure 8 - Two Audio Signals

The first picture is the gained signal from one sensor, and the second picture is the gained signal which is processed by FPGA. The horizontal axis represents time, from 0 to 10 seconds. The vertical axis represents the amplitude of the signal. Because audio is AC signal, the middle position of vertical axis represents the smallest amplitude, and the amplitude enlarges on the positive and negative direction of the vertical axis. The after-FPGA signal has a smaller amplitude than the single-sensor signal from the pictures above.

Figure 9 shows the frequency spectrums of these two signals.

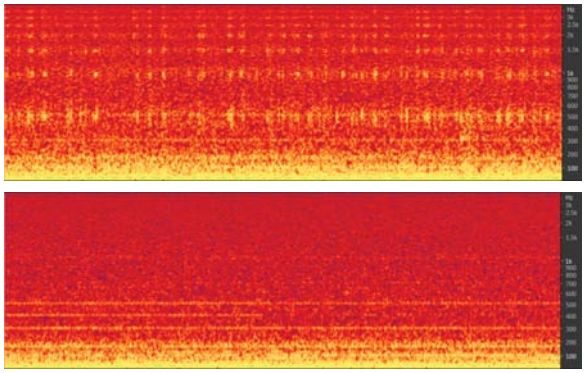

Figure 9 - Frequency Spectrums of the Two Audio Signals

The first picture shows the frequency spectrum of the signal from one sensor, and the second picture shows the frequency spectrum of the FPGA output signal. The horizontal axis respects time, and the vertical axis represents frequency. The brightness represents the amplitude of one frequency component at a time point. High brightness means high amplitude, and low brightness means low amplitude. There are much more brighter points in spectrum 1 than in spectrum 2, which means that the signal from one sensor is much noisier than the signal from FPGA outputted. Comparing the two WAV files when playing, a direct feeling that the FPGA outputted audio is quieter than one sensor audio can be heard.

By using Amplitude Statistics tool in Audition, the quantized parameters can be seen in Table 1 below.

Test File	Single Sensor	Sensor Matrix
Peak Amplitude	-0.06 dB	-1.85 dB
Max. RMS Amplitude	-5.10 dB	-6.32 dB
Min. RMS Amplitude	-16.46 dB	-23.54 dB
Aver. RMS Amplitude	-10.37 dB	-12.48 dB
Loudness	-7.89 dB	-9.61 dB

Table 1 - Amplitude Statistics

From the table we can see that, every parameter has decreased for several decibels. The Average RMS Amplitude decreases more than 2dB. Because the test files are noise signals, this result indicates that the average noise level has decreases more than 2dB, which meets our designing expectations that, after using sensor matrix and under the process of FPGA, the noise level will decrease comparing with single sensor signal. Loudness also decreases for almost 2dB, which means the noise strength a person can hear also decreases. So noise is suppressed by using sensor matrix and FPGA processing.

V. Conclusion

From the results and the comparisons, we can see that, the whole system, including the sensor matrix and the prototype platform, is running normally, and it has an effect on noise suppression by using a simple addictive noise suppression method.

Currently, the noise level is still high. More jobs on hardware and algorithm optimization need to be done in the future to achieve lower noise level, higher dynamic range so that the clearer heart sound can be recorded. Also, the designing and fabricating of heart sound specific MEMS sensor may also be considered if necessary, so that the optimization to the sensor may make the sensor have better frequency response and sensitivity, while keep smaller and thinner size.

References

[1] Yi-Yuan Chiu and Wan-Ying Lin and Hsin-Yao Wang and Song-Bin Huang and Min-Hsien Wu, *Development of a piezoelectric polyvinylidene fluoride (PVDF) polymer-based sensor patch for simultaneous heartbeat and respiration monitoring*, Sensors and Actuators A: Physical, Vol.189, 2013

[2] Zazula, DAMJAN and Donlagić, DENIS and Šprager, SEBASTIJAN, *Fibre-optic interferometry as a means for the first heart sound detection*, Advances in Applied Information Science, 2012

[3] ADINSTRUMENTS *MLT201-DCW-15A Cardio Microphone Datasheet*

[4] Knowles Electronics *SPH0641LM4H-1 Datasheet, Revision A*, 2014

[5] Panasonic Corporation *Omnidirectional Back Electret Condenser Microphone Cartridge Series: WM-62A/62C/62CC/62K, WM-62B(pin type) Datasheet*

[6] XU Mei-fang, HAN Yan, *Linear Filter methods for Image Denoising in Digital Radiography*, Nondestructive Testing, Vol.5, 2005

[7] K. C. Zangi, *A New Two-Sensor Active Noise Cancellation Algorithm*, 1993 IEEE International Conference on Acoustics, Speech, and Signal Processing, 351-354 vol.2

[8] René Schmidt, Stephan Blokzyl, Wolfram Hardt, *A Highly Scaleable FPGA Implementation for Cross-Correlation with Up-Sampling Support*, International Workshop on Impedance Spectroscopy : abstract book, September 2016, ISBN 978-3-9817630-2-7

Device-Independent testsets for inspection of virtual reality devices

Robert Manthey and Danny Kowerko
Chemnitz University of Technology,
Endowed Professorship Media Computing,
D-09111 Chemnitz, Deutschland
Email: firstname.lastname@informatik.tu-chemnitz.de

***Abstract*—Multimedia devices like HTC Vive and Zeiss Cinemizer OLED offer augmented, virtual and mixed reality. The determination of the visual correctness or quality measured by common testsets like Fig. 1 is incommensurate to them. We developed a system to create artificial device-independent testsets in a automatic way.**

I. Introduction

The capabilities of current multimedia systems increase from ancient standard video with stereo sound to well-known Full HD and UHD with 5.1 surround sound and introduce augmented, virtual and mixed reality likewise. The resolution and display refresh rate grows as well as the complexity of their combinations. On the other side, measuring the correctness, performance and quality is frequently performed by ancient samples as shown in Fig. 1. Often captured from real world to obtain audiovisual intrinsic properties and features, but also artifcial structures to evoke potential errors. Nevertheless, their adaptability to the new application fields is limited regarding small resolution and artefacts in the case of upscaling or other adjustments.

To overcome these shortcomings *Manthey et al.* [1] developed a flexible system to produce artificial testsets in a device-independent way as much as possible. Using abstract mathematically descriptions of the elements of the testcases like rectangles, circles etc. as well as their properties like colors, lights, reflections and movements, the scenes are constructed in an artificial way. To realize the tests, subsequent transformations construct the device-dependent versions with specified resolutions and frame rates for instance, and realize automatic evaluations of the designated multimedia systems. Some results of the visual testdata produces the artefacts indicated in Fig. 2.

(a) Frame of the Flower test video.[1]

(b) Lena test image.[2]

Fig. 1. Common visual test data to determine visual correctness or quality.

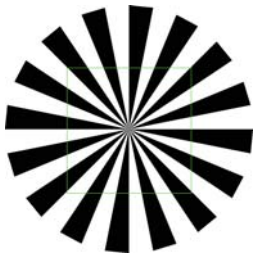

(a) Original unrotating Siemens star pattern with green cutout marking.

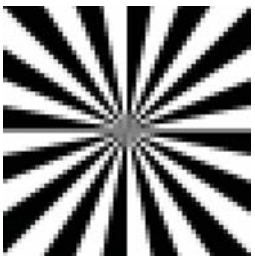

(b) Cutout from result frame 1.

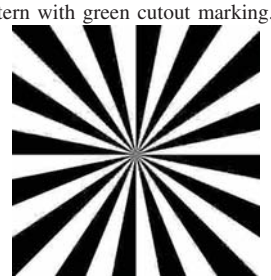

(c) Cutout from result frame 7.

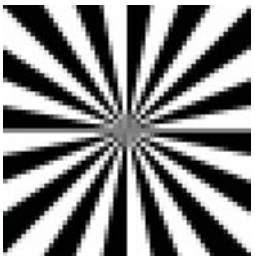

(d) Cutout from result frame 15.

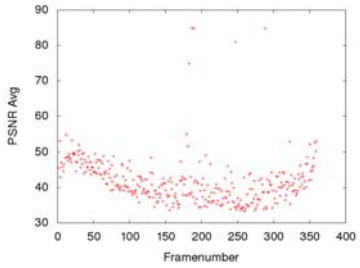

(e) Curve of the PSNR quality measure confirming the previous images and showing the variance of the degeneration.

Fig. 2. A motionless test video in Fig. 2a compressed with FFmpeg[3]results in a sequence of frames with visual artefacts of different intensity and a curve showing the progession.

[1]http://media.xiph.org/video/derf/y4m/flower_cif.y4m
[2]http://sipi.usc.edu/database/download.php?vol=misc&img=4.2.04
[3]https://ffmpeg.org/

II. Testset Architecture and Implementation

In view of that results a adaption to the field of virtual reality systems with multiple displays [2] is performed to analyse the visual properties of the available devices *HTC Vivee*[4] and *Zeiss Cinemizer OLED*[5].

With the build-in Blender/Python API[6] we realize the mathematical descriptions of the testcases with their geometric elements like Siemens-Stars and Sierpinski-Triangles shown in Fig. 3. To view the different aspects of the elements, their perspective correctness and to inspect the behavior of the motion we append different pathways to each of the visual objects of a testcase.

The Zeiss Cinemizer can take the testset data directly from Blender so that the device-dependent settings being configured their. To bring the testset data to the HTC Vive the cross-platform game-engine Unity[7] is used, realize the final settings and control the device.

III. Device Inspection

We deploy the generated testset to both devices and present them to our inspection group of technical skilled persons each. All visible artefacts perceived being registered and captured by a digital camera taking up the position of the eyes of the member of the group. Some salient artefacts be shown in Fig. 4.

```
def SierpinskiDreieck(Koordinaten, Kantenlänge, Ebene, Elementnummer):
    x = Koordinaten[0]
    y = Koordinaten[1]
    z = Koordinaten[2]
    if (Ebene >= 1):
        Kantenlänge /= 2.0
        Ebene -= 1
        # Koordinaten berechnen (LU,RU,MO)
        SierpinskiDreieck((x,y,z), Kantenlänge, Ebene, 0)
        SierpinskiDreieck((x+Kantenlänge,y,z), Kantenlänge, Ebene, 1)
        SierpinskiDreieck((x+Kantenlänge/2.0,y+
          DreieckGleichseitigHöhe*Kantenlänge,z), Kantenlänge, Ebene, 2)
    elif (Ebene == 0):
        # Zeichnen
        if Elementnummer==0:
            DreieckGleichseitig(Koordinaten, 2*Kantenlänge, matRot)
        elif Elementnummer==1:
            DreieckGleichseitig(Koordinaten, 2*Kantenlänge, matGelb)
        elif Elementnummer==2:
            DreieckGleichseitig(Koordinaten, 2*Kantenlänge, matBlau)
```

(a) Code sample of the descriptions to create the Sierpinski-Triangles.

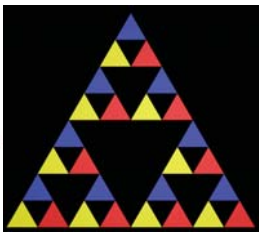

(b) 2D sample of a Sierpinski-Triangle.

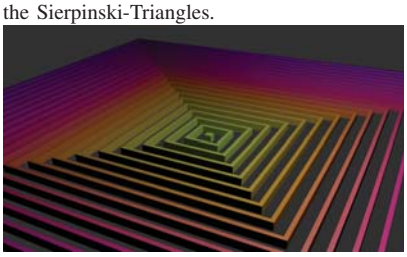

(c) Pattern with multiple beams with single colors and different extent each. Grouped to form a grid.

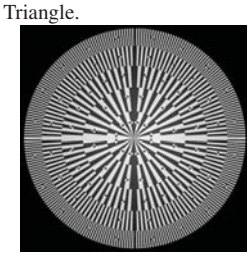

(d) The Siemens-Star test element based on black and white stripes stacked like a pyramid.

Fig. 3. Some testcases used to analyse the visual properties and the quality of the virtual reality devices.

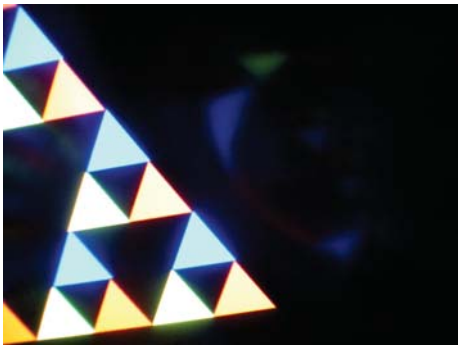

(a) Artefacts caused by Sierpinski-Triangle.

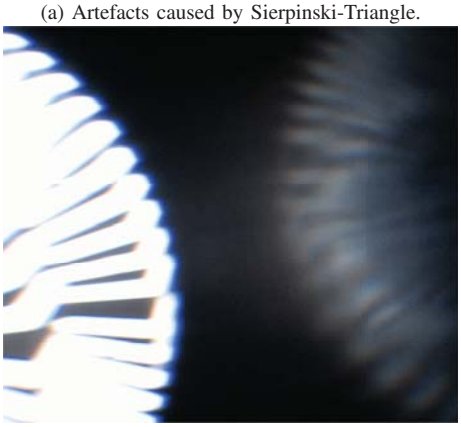

(b) Artefacts caused by Siemens-Star.

Fig. 4. Caused by moving along a predefined pathway the reflection artefacts become clearly visible.

IV. Conclusion & Future Work

As result, the usefulness of a device-independent testset for virtual reality devices is demonstrated and show some salient artefacts caused. Future work introducing camera based automatic image capturing can simplify the process and provide automatic systems to inspect virtual reality systems.

Acknowledgment

This work was partially accomplished within the project localizeIT (funding code 03IPT608X) funded by the Federal Ministry of Educa- tion and Research (BMBF, Germany) in the program of Entrepreneurial Regions InnoProfile-Transfer.

References

[1] R. Manthey, S. Conrad, and M. Ritter, "A Framework for Generation of Testsets for Recent Multimedia Workflows," in *Universal Access in Human-Computer Interaction, HCI International*. Springer, 2016, pp. 460–467, http://dx.doi.org/10.1007/978-3-319-40238-3_44.

[2] G. Westheimer, "Three-dimensional displays and stereo vision," *Proceedings of the Royal Society*, vol. 278, pp. 2241–2248, August 2011, http://escholarship.org/uc/item/1r81b987.

[4] https://www.vive.com/

[5] https://www.oculus.com

[6] https://docs.blender.org/api/blender_python_api_2_78a_release/

[7] https://unity3d.com/

Digital Learning, Culture and Delivery Mode on E-learning in Mongolia

Ariunaa Khashkhuu,
Department of Business Administration
School of Business Administration and Humanities
Mongolian University of Science and Technology
Ulaanbaatar, Mongolia
E-mail: ariunaa@csms.edu.mn

***Abstract*— The primary purpose of this research paper is to understand the role of national cultural dimensions on e-learning practices in Mongolia. Adaptation to customer needs is a key component of competitiveness in any service industry. In e-learning on HE (higher education), which is increasingly worldwide, students with different learning styles prefer different learning formats, so the issue is critical for competitiveness. Students preferring particular learning styles are unlikely to choose modes which do not fit their styles well and are likely to prefer learning modes that fit their learning styles. This conceptual paper uses Hofstede's national cultural dimensions and Hall's high- and low- context culture. This research proposes that national cultural dimensions of power distance, uncertainty-avoidance, individualism, short term orientation and high-context communication style influence e-learning practices. This study provides e-learning strategies, which suggested strategies can be implemented by universities in other countries with similar national cultural dimensions as well.**

Keywords*— *Digital, cultural dimensions, delivery mode, e-courses, e-learning

I. INTRODUCTION (*HEADING 1*)

The generation of young people, who were born around 1990s, may be called "digital natives", since they were born together with Internet and mobile technologies. [1] Typical knowledge practices for this generation are claimed to be multi-tasking, that is, carrying out several activities side-by-side. [2] They are also reading comfortably from screens, are fond of computer games, and are using social media extensively. Young people outsource many cognitive functions to different technological tools.

The concept of "digital native" is, however, a controversial idea. [3] Regardless, we can claim that the knowledge practices of young people-students have drastically changed during the last decade although the educational practices have largely remained the same. Marc Prensky (2012) pointed out that "today's students are no longer the people our educational system was designed to teach" (p. 68). Further, there is no reason to assume that new technologies would automatically have a beneficial impact on learning and development.

Electronically supported learning is said to offer a wide range of opportunities to create, store, manipulate, access and distribute information, and provide new channels and tools to facilitate learning and knowledge building through meaningful actions and interaction [4, 5]. The influence and impact of these technologies can be seen through academia and industry as more and more institutions of higher education and corporations offer, or plan to offer, e-learning courses and programs [6].

Accordingly, a majority of higher education institutions across the globe have found this mode of offering instruction and learning (e-learning) to be economical and have adopted ICT-based initiatives either as single mode (i.e. providing fully online programs/courses) or as a complementary mode (i.e. blended learning) for delivering and enhancing their educational services [7].

There is a substantial market for higher education in Mongolia. In the 2014 to 2015 academic year, 13,360 lecturers and administrators provided service to 178,295 students out of which 19,065 were master's students and 3,391 were PhD students at 101 higher educational institutions (Ministry of Education and Science, 2015). Mongolia ranks seventh internationally in the share of GDP (9.0%) allocated to education, and its education law guarantees that at least 20% of the government budget is spent on education (Government of Mongolia, 2006). However Mongolian higher education receives only 12% of that amount (Asian Development Bank Institute, 2010). [8]

Likewise, E-learning initiatives can be a cost-effective method of delivering higher education in Mongolia with its vast territory and sparse population. There were numerous e-learning materials developed over the last couple of years. However, there is a limited research on e-learning in Mongolia. [8]

Mongolia has adequate infrastructure to develop e-learning. This achievement is a result of the E-Mongolia National Program 2005–2012 which aimed to become one of the most Information and Communications Technology (ICT) developed 10 countries in the Asia pacific region. Out of 144 nations, Mongolia ranked 73st in ICT use, 40rd in higher education and training, and 62th in Internet access in schools in the 2014–2015 Global Competitiveness Report (World Economic Forum, 2015). A study by the International Trade Union (ITU) and the United Nations Educational, Scientific, and Cultural Organization (UNESCO; 2016) indicates that in Mongolia, 49.5% of population use internet and 29% of households have an Internet connection . In 2016, Mongolia ranked per 100 inhabitants, 67th of 182 counties in fixed broadband

penetration, 47st of 184 countries in mobile broadband penetration (ITU & NESCO, 2016). Furthermore, Mongolia ranked 90nd out of 175 economies worldwide in the information development index in 2016 (ITU, 2016).

The Mongolian University of Science and Technology (MUST) is a multidisciplinary and multileveled university for education, training and scientific research. It is also one of the largest centers for scientific and cultural exchanges in Mongolia. MUST is one of primary university of Mongolia where started implementing e-learning into to higher education.

The MUST is key university of e-learning in country. There are many activities running parallel for develop and successful implement e-learning for education. One of main mission of MUST is to become First E and Open University of Mongolia. With this target MUST implementing several phase of master plan. [9]

In 2010, the Information Technology Centre and ICT Teaching Methodological Centre were joined on the basis of Order No.183 of Minister of Education, Culture and Science and according to Order No. 28 of the Rector, E-Open School was founded to administrate distance-learning activities of the University and it has been working with below structure since January, 2010 (E and Open University Story, 2012)

- Training & Teaching Methodological Team
- Information Technology & Software Team
- Internet & Hardware Team
- Online Testing room
- U-CLASS distanced-learning room
- Online & Video Conference hall
- Multimedia Studio with full equipment

From 2007 start release master plan of e-learning into life. In 2007 MUST had only 62 e-students which selected 19 different e-courses. In this year 648 students selected 106 different e-courses. (Total e-courses 400, including 247 undergraduate courses, 153 graduate courses).

This study was motivated by cultural dimensions of e-learning in higher education in Mongolia. The paper consists of four parts. The first part provides e-learning classifications briefly. The second part represents an investigation into the classification of Mongolian culture, using the four dimensional model of Geert Hofstede: Power Distance, Uncertainty Avoidance, Individualism-Collectivism and Masculinity-Femininity. Furthermore, the part investigates the Hall's high/low context cultural characteristics for Mongolia. The third part investigates the literature in the e-learning field that focuses on cultural issues. An overview of the cultural dimensions in educational settings in general and in e-learning course in particular is presented. The fourth part investigates Mongolian national cultural dimensions of power distance, uncertainty-avoidance, individualism, short term orientation, high-context communication style influence e-learning practices.

Finally, this study concludes that the application of the synchronous e-learning methods is appropriate in context of Mongolia, because the country has high power distance and high context culture.

II. E-LEARNING CLASSIFICATIONS (*HEADING 1*)

ICT-supported learning is flooded with a number of terms and concepts, which are used either interchangeably or with small difference to address the use of ICT in education: for example, E-learning, Distributed Learning, Virtual Education, Internet-Based Education, Online Learning, Flexible Learning, Synchronous Learning, Web Based Training, and so on. Negash, S., & Wilcox, M. V. (2008) proposes six types of e-learning classifications. The six classifications are outlined in Table I. [4]

TABLE I. E-LEARNING SYSTEMS CLASSIFICATIONS

Classification	Presence	eCommunication
Type I: Face-to-face	Physical	– post lecture notes – schedule assignments – discussion and e-mail outside classroom
Type II: Self-learner	None	None
Type III: Asynchronous	None	– includes all listed for Type I – audio/video lecture recordings
Type IV: Synchronous	Virtual	– includes all listed for Type III – "live" audio – "live" video – synchronous chat
Type V: Blended/Hybrid-Asynchronous	Physical	includes all listed for Type III
Type VI: Blended/Hybrid-Synchronous	Physical and Virtual	includes all listed for Type IV

III. AN INVESTIGATION OF MONGOLIAN CULTURAL VALUES

Even though Hofstede did not study any of the six cultural dimensions there, a Mongolian researcher Tuvshinzaya (2008) studied the first 5 dimensions and conducted surveys using VSM-94 model (the Values Survey Model) and Hall's (1976) models to compare Mongolia and China. Her findings suggested that Mongolians and Chinese people have three statistically same cultural dimensions (collectivism, power distance, and uncertainty avoidance). Moreover, Purdue University faculty members completed a research project titled "Mongolia: A Cultural Portrait using the Hofstede 5-D Model." "The results of this study suggested that Mongolian culture is low in power distance, high in individualism, very high in masculinity, high in uncertainty avoidance, and short-term oriented culture" (Rarick, Winter, Barczyk, Pruett, Nickerson, and Angriawan 2014). Most recently study of Mongolian cultural values was "An Investigation of Mongolian Cultural Values", Kh. Ariunaa, 2015.

Studies on Mongolian Cultural Values:

1. Tuvshinzaya Sunduijav (2008), "Cross Cultural Aspects of Advertising-Cultural Analysis of Mongolian and Chinese Web Sites"[8]

2. Siyeona Chang (2012), "Study of the Cultural Map of the World Today Through the Lens of Korean Television Program Exports and Their Determinants"

3. David R. Borker (2013), "Economic Growth and Cultural Value Analysis In Six Emerging Economies"

4. Charles Rarick (2014), "Mongolia: A Cultural Portrait using the Hofstede 5-D Model"

5. Ariunaa Khashkhuu (2015), "An Investigation of Mongolian Cultural Values" [7]

TABLE II. RESULT OF PREVIOUS STUDIES

Method	Researcher	PDI	IDV	MAS	UAI	LTO	IVR
Six dimensions	Ariunaa Kh	85	57	70	28	36	59
Four dimensions	Siyena Chang	75	30	44	78		
Five dimensions	Charles Rarick	18	71	103	92	41	
VSM94	Tuvshinzaya S	12	19	53	76	43	
	David R. Borker	Low	Low	Low	Low		

These studies results are different. Thus there is a lack of empirically based research on the cultural classification of Mongolian. This is related to the following items differences.

1. number of respondents
2. nature of respondents
3. month and year of data collection
4. languages of questionnaire used
5. VSM version

The results of this study (Ariunaa, 2015) indicate that Mongolia is a masculine, individualist culture that is relatively low in uncertainty avoidance and high in power distance, whose people have a short-term orientation towards time.

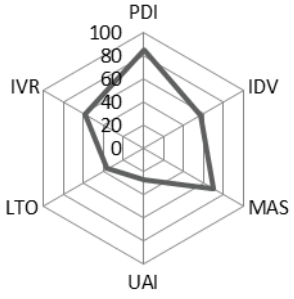

Fig. 1. Plot of the six cultural value dimensions in Mongolia

A. Power distance

At 85 Mongolia sits in the higher rankings of PDI – i.e. a society that believes that inequalities amongst people are acceptable. The subordinate-superior relationship tends to be polarized and there is no defense against power abuse by superiors. Individuals are influenced by formal authority and sanctions and are in general optimistic about people's capacity for leadership and initiative. People should not have aspirations beyond their rank.

B. Individualism

Mongolia, with a score of 57 is an Individualistic society. This means there is a high preference for a loosely-knit social framework in which individuals are expected to take care of themselves and their immediate families only. In individualistic societies offence causes guilt and a loss of self-esteem, the employer/employee relationship is a contract based on mutual advantage, hiring and promotion decisions are supposed to be based on merit only, management is the management of individuals.

C. Masculinity

Mongolia scores 70 on this dimension and is thus a masculine society. In masculine countries people "live in order to work", managers are expected to be decisive and assertive, the emphasis is on equity, competition and performance and conflicts are resolved by fighting them out.

D. Uncertainty avoidance

At 28 Mongolia has a low score on uncertainty avoidance. Uncertainty accepting cultures, are more tolerant of opinions different from what they are used to; they try to have fewer rules, and on the philosophical and religious level they are empiricist, relativist and allow different currents to flow side by side. People within these cultures are more phlegmatic and contemplative, and not expected by their environment to express emotions.

E. Long Term Orientation

Mongolia scores 36 in this dimension, marking it as a normative society. People in such societies have a strong concern with establishing the absolute Truth; they are normative in their thinking. They exhibit great respect for traditions, a relatively small propensity to save for the future, and a focus on achieving quick results.

Also Tuvshinzaya have conducted another survey among 164 Mongolians and 159 Chinese in order to compare the context level in their communication. The survey-II reveals that the context level of communication of these Chinese and Mongolian people are equal from the statistical point of view. The survey result (2008) show that it is "traditionally" a high context culture.

Additional, according to Hall (1959), perceptions of time in different cultures are either polychronic or monochronic. Polychronic time is characterized as simultaneous and concurrent, while monochronic time is characterized as being sequential and linear. Mongolian people has polychronic culture.

IV. CULTURAL IN E-LEARNING

There are a number of schemas for categorizing culture, but many cross-cultural researchers note that researchers should focus on cultural elements appropriate to the specific problem

and context. Here, we follow Hofstede (1991; 2009) and Hall (1976). Hofstede (1991; 2009) originally applied his cultural dimensions to management, but his schema is widely used in many fields, including education. For example, Swierczek and Bechter (2010) used it to examine cultural features of e-learning. Hofstede's schema consisted of four dimensions originally.

Hall's schema categorizes into high- and low- context cultures, based on the extent to which communication is carried by words or is embedded in the context in which people use the words.

Much of the message in high-context cultures is carried in how the words relate to the implicit background. Communication depends heavily on contextual and social cues for meaning. Thus, non-verbal language, such as voice, posture, gesture, body language, facial expression and periods of silence, play an important role, as do non-verbal variables, such as status, values and associations. Clearly, some kind of relationship would provide a richer context in which better communication could take place and high-context cultures have a focus on relationship building, similarly to collectivist and/or feminine cultures in some cultural schema. For example, the "sage on the stage" traditional style of teaching is likely to be more broadly accepted in high power distance cultures; uncertainty avoiding cultures are likely to prefer more structure to classes and learning tasks and collectivist cultures are more oriented towards various forms of group work and interpersonal interaction.

High context-cultures in Hall's schema are generally classified as collectivist in Hofstede's (1991; 2009). The extensive overlap seems to be good, because good communication in these cultures depends substantially on extensive shared knowledge and interpersonal relationships developed in group context facilitate discussion.

Communication in high-context cultures has difficulty in overcoming the lack of f2f (face-to-face) contact in DE modes which rely mainly on the written word. F2f provides contextual and social cues for meaning, as well as allows rich non-verbal language, such as voice, posture, gesture, body language, facial expression and periods of silence. This need for context and relationships in many cultures is a critical issue in online education, but often online education is particularly oriented toward individualistic and low-context cultures. There may be little opportunity for social interaction, which reduces communication for students from collectivist and/or high-context cultures.

V. Results

This paper will identify four national cultural dimensions and high- and low- context cultures that have demonstrated sufficient impact on learning and knowledge construction. Specifically, the dimensions of power-distance, uncertainty-avoidance, individualistic and short term orientation will be discussed. Scholars suggest the division of power (power-distance), the concept of structure (uncertainty-avoidance), the individualist and planning ahead (short term orientation) have considerable impact on learning practices. Scores for Mongolia on these cultural dimensions are briefly summarized in the previous section. This section will discuss these dimensions' relevance to e-learning for Mongolia.

At 85 Mongolia sits in the higher rankings of PDI – i.e. a society that believes that inequalities amongst people are acceptable. E-learning requires considerable autonomy and responsibility for one's own learning which high power distance cultures do not prefer. Classroom or passive methods of presentations seem to satisfy the concept of identifying levels, which is very important in high power distance cultures. In an e-learning environment, the students will prefer synchronous e-learning methods. Therefore, it would be right to argue that high power distance cultures would more likely adopt synchronous e-learning methods to those of asynchronous as it allows them to make power and status distinctions.

E-Open School of MUST refers to a form distance learning in which e-course content is delivered by various methods such as course management application, multimedia resources and video contents. The accepted e-course included asynchronous learning activities. The e-open school has synchronous learning technologies, but their usage in e-learning is low and irregular.

Mongolian people have high- context culture, so that communication in high context-culture has difficulty in overcoming the lack of face-to face contact in distance learning.

Some technologies can facilitate more interpersonal interaction at a distance. Synchronous modes, particularly those with audio-visual capabilities, may offer a way to gain more of the feel in f2f interaction. Some synchronous distance modes, in fact, are widely used in Asian cultures. Satellite and TV-based DE Networks seem to fit the traditional "group-based, teacher-dominated and centrally organized pedagogical culture".

Synchronous capabilities on the class Website seem better oriented towards student-student interaction than the older synchronous technologies represented by satellite. Negash, Wilcox and Emerson (2007), for example, argued that synchronous internet classes can overcome problems that some see in asynchronous courses, such as feelings of isolation and feelings of being overwhelmed by the responsibility inherent in the high autonomy of an asynchronous course.

Students who want synchronous interaction will come up with their own additional communications methods (including synchronous telephone and Facebook), if the capabilities are not provided in the Website. Thus, it is better to build synchronous audio-visual modes into the class site so that they can become a planned part of the class. Clearly, such modes allow for much more of the non-verbal content and context upon which communication in high-context cultures depends.

Educators that facilitate online, blended, or face-to-face instruction can initiate improved interest and engagement by students through using a platform that includes Facebook.

Facebook can be used as a learning tool to help students reach their academic goals by improving cognitive skills. The social network can facilitate an increase in a student's concentration, perception, long term memory, and logical

thinking by providing an inlet for new information. In a recent study conducted by the University of Queensland and Griffith University (2012), researchers found that college students believe adding Facebook to their courses will enhance their learning experiences.

Facebook can be used to enhance face-to-face, blended, or online courses; however, there are some risks associated with this type of social media in the classroom.

As of March 7 of 2015, Facebook had 1.86 billion (40%) monthly active users. The number of Mongolian Facebook users is 1.2 million as of 2015 . In terms of the age, the composition of the majority of Facebook users in Mongolia is dominated by age 18 -27 years with the number of users is 624 thousand (52%) of total users, where this age is the age of the students in the college. While the percentage of students who use Facebook is high, it is important to justify why, how much and how the students use Facebook as well as Facebook usage in an educational environment.

VI. Conclusions

This research was complemented by other related studies and concludes that the application of the synchronous e-learning methods is appropriate in context of Mongolia, because it has high power distance and high context culture. And then you will see why these methods work so well. While discussing the research findings combination of synchronous e-learning methods with Facebook usage was highly recommended.

We have argued here that purely asynchronous online modes, with interaction based on written discussion board, is a format attractive mainly to students from low-context cultures. Such interaction lacks the context necessary for relationship establishment among high-context students, and therefore inhibits real communication. Some research shows that high-context students are more likely to feel dissatisfied with the lack of social relationships in purely asynchronous discussion board interaction. Careful course design and skillful instructor participation can somewhat reduce this problem. However, synchronous audio-visual technologies can provide much more intimate interaction, similar to f2f, for high-context students. When integrated into a class site based on asynchronous discussion board, multiple technologies offer interaction modes which appeal to students from either high- or low- context cultures.

The use of multiple technologies to offer several interaction modes seems to overcome a problem that specific modes may be more attractive to students from particular cultures.

The most Facebook activities by students are commenting on status, photo or video that was shared by others user, viewing the photo posts by their friends and use the chat Facebook facilities as a tool online communication.

Facebook has significant potential in education. The advantages might include getting information about homework, information, material, final project, ideas and resources. In addition, sharing homework, ideas and resources also to be a positive benefit of Facebook in teaching and learning processes. Students feel comfortable learning through Facebook because Facebook has become part and parcel of their everyday life and Facebook can promote collaboration and social interchange between participants. Share text and multimedia content with the entire class and send reminders, announcements, upcoming due date or any other classroom news also is another reason why students use Facebook in education.

Mongolia is high in power distance and high context-culture, so that DE lecturer should use synchronous online teaching. Facebook has been used as a replacement or supplement to traditional learning management systems due to many LMSs lacking tools for social interactions and personal profile spaces found on Facebook. Facebook has significant potential in education as a learning management system and learning tool.

VII. References

[1].Prensky, M. (2005), Listen to the natives. Learning in the digital age, Educational Leadership, 63 (4), 8-13.

[2].Prensky, M. (2012), From digital natives to digital wisdom. Hopeful essays for 21st century learning, Thousand Oaks, CA: SAGE.

[3].Bennett, S., Maton, K., & Kervin, L. (2008), The 'digital natives' debate: A critical review of the evidence, British Journal of Educational Technology, 39, 775–786.

[4].Negash, S., & Wilcox, M. V. (2008). E-learning classifications: Differences and similarities. In S. Negash, M. E. Whitman, A. B. Woszczynski, K. Hoganson & H. Mattord (Eds.), Handbook of distance learning for real-time and asynchronous information technology education (pp. 1-23). London: Information Science Reference

[5].Suvdmaa Tuul, Otgontugs Banzragch, and Tsogzolmaa Saizmaa, 2016, " E-learning in Mongolian Higher Education", "International Review of Research in Open and Distributed Learning".

[6].Uranchimeg Tudevdagva *, Wolfram Hardt, 2013, "Distance learning from Asia to the Europe", International Summer Workshop Computer Science 2013

[7].Ariunaa Khashkhuu, 2015, "An Investigation of Mongolian Cultural Values", ICIED 2015, The International Conference on Innovation and Entrepreneurship Development, 131-136p

[8].Tuvshinzaya Sunduijav, 2008, "Cross Cultural Aspects of Advertising-Cultural Analysis of Mongolian and Chinese Web Sites"

[9].Davoud Masoumi, 2010, Quality in E-learning Within a Cultural Context: The case of Iran

[10].Rentsenkhand Enkh-Amgalan, 2016, The Indulgence and Restraint Cultural Dimension: A Cross-Cultural Study of Mongolia and the United States

[11].Mark Speece, 2012, Learning Style, Culture and Delivery Mode in Online Distance Education, US-China Education Review A 1 (2012) 1-12

[12].Gobbo, L. D., Nieckoski, M., Rodman, R., & Sheppard, K. (2004). Virtual limits: Multicultural dimensions of online education. International Educator, 13(3), 30-39.

[13].Hrastinski, S. (2008). Asynchronous and Synchronous E-Learning. Educause Quarterly, 31, 4, 17-23.

[14].Nathan, E (2008). Global Organizations and E-Learning: Leveraging about learning in different cultures. Performance Improvement, 47 (6), 18-24.

[15].Vaughn, N. (2007). Perspectives on blended learning in higher education. International Journal on E-Learning, 6(1), 81-94.

[16].Negash, S., Wilcox, M. V., & Emerson, M. (2007). Synchronous hybrid e-learning: Teaching complex information systems classes online. International Journal of Information and Communication Technology Education, 3(3), 1-13.

[17].Hofstede, G. (2009). Hofstede™ cultural dimensions. Retrieved from http://www.geert-hofstede.com/

[18].Holtbrügge, D., & Mohr, A. T. (2010). Cultural determinants of learning style preferences. Academy of Management Learning &Education, 9(4), 622-637.

FPGA-based Straight Line Detection

Ammad Ali Syed and Stephan Blokzyl and Wolfram Hardt
Chemnitz University of Technology
Faculty of Computer Science
Professorship Computer Engineering
D-09107 Chemnitz, Germany
{amsy; sblo; hardt}@hrz.tu-chemnitz.de

***Abstract*—This paper introduces a novel realisation of Hough transform for reconfigurable integrated circuits. As the Hough transform is computational expensive, the proposed strategy reduces its complexity while obtaining the required accuracy. The solution is implemented on a standard Field Programmable Gate Array (FPGA), a platform which has become an eminent alternative for high-performance digital signal processing (DSP). The Approximated Hough transform, also called Incremental Hough transform, is realised on a Xilinx Virtex-6 LX series FPGA. The device provides advanced on-board storage capabilities as well as specific DSP-blocks and logic for computational extensive DSP applications, which require considerable memory resources and high computing power.**
The novel approach addresses advanced computer vision applications, offers real-time behaviour, and utilises extensive parallelism as one of the most significant advantages of FPGA technology. The implementation is fully pipelined and able to detect five straight lines in grey scale or colour images.

***Index Terms*—Image processing; Feature extraction; Image analysis; Image segmentation; Field programmable gate arrays; Fast Fourier transforms**

I. Introduction

Nowadays, an increasing number of digital signal processing (DSP) applications apply reconfigurable integrated circuits for powerful data exploitation. Especially Field Programmable Gate Arrays (FPGAs) combine flexibility, efficient parallelisation, and solid acceleration capabilities for computational demanding DSP processes. Single high-performance DSP chips are replacing several systems and sub-systems [1][2]. FPGA technology is mainly used for prototyping and validation of complex integrated circuit designs. It provides an efficient and flexible framework to validate system functionality with respect to the specification [3]. Despite these advantages, FPGA developers have to face challenges like design partitioning, design efforts, and difficult debugging. This leads to a higher design costs and times, but compared to performance advantages, FPGAs are more and more used in consumer and industrial products for accelerated computation of demanding algorithms [4]. Applications like Fast Fourier transform [5] or the Vitebri decoder [2] illustrate the variability of FPGA technology and its contribution to standard embedded processors and computing architectures.
An FPGA consists of a matrix of logic blocks, which are connected by a switch network. The hardware is configured by programming both logic blocks and switch network. The logic block is used to implement either sequential or combinational logic, which realises a specific operation at a separate hardware region. This allows the development of highly parallel computing architectures and enables the application of task and data parallelisation strategies [6]. This results in the acceleration of algorithms and a rise of computing performance while retaining the reprogrammable flexibility of software-based solutions. E.g. computer vision applications benefit from the parallelisation qualities of FPGA technology. FPGA-based image processors are able to exploit spatially different partitions of an image by applying data parallelisation as described in [6]. The input image is forwarded to multiple, parallel processing units computing independent image slices at the same point of time. This data parallelisation is restricted only to the available logic resources on the FPGA.

This paper is structured as follows. Section II introduces related work and validates the proposed approaches according to straight line detection. Section III gives a review of standard Hough transform (HT), its parameter space, the approximation of HT, and describes the hardware realisation. Finally, sections IV and V conclude the experimental results and resource utilisation of the proposed algorithm.

II. Related Work

In this paper, we propose an embedded algorithm for real-time detection of straight lines in grey scale and colour images. By literature survey, HT was found to be one of the most powerful straight line detectors in terms of accuracy and robustness for digital imagery [7]. Although high memory consumption and computational cost, the algorithm was initially developed to identify lines, but can be extended to recognise arbitrary pattern like circles, ellipses, triangles, and others.
Various FPGA-based hardware implementations of HT for line detection have been presented. X. Zhou *et al.* exploited the application of coordinate rotation digital computer algorithm for HT (CORDIC), which requires many iterations for accurate parameter calculation [8]. F. Zhou *et al.* proposed for efficient multiplication the use of DSP-blocks that are available in specific DSP-FPGAs, like in e.g. the Xilinx Virtex-6 LX FPGA family [9]. Both sine and cosine values from $(0 \leq \theta < \pi/2)$ are pre-loaded in DSP-blocks and their experimental results show that the implementation runs at 247.52 MHz for a

binary image of 512×512 pixel resolution. Tagzout *et al.* presented a method to implement HT without the need of any multiplication and trigonometric functions [10]. He applied the Incremental Hough transform technique (IHT), developed by Koshimizu [11]. Lu *et al.* proposed a parallel HT-based straight line detection for an FPGA-based implementation for embedded vision [12]. This implementation uses IHT with an angle resolution of approximately 0.895° and detects single straight lines in images with 1,024×768 pixel resolution. It operates at a frequency of 200 MHz when mapped on an Altera Cyclone series FPGA. Ahmed *et al.* suggested a memory efficient FPGA implementation of HT for line and circle detection [13]. In this paper, he proposed an 11.25° angle resolution and presented a strategy for efficient memory occupation. However, different image resolutions affect the detection rate significantly.

The literature review depicts the suitability of FPGA-based HT implementation for straight line detection. The proposed hardware realisations are limited in resolution, accuracy, and their runtime is significantly affected by the detection rate. The novel approach, which is presented in this paper, uses the improved IHT proposed by Djekoune *et al.* [14], does not require specific DSP-blocks, and allows the highly accurate, parallel detection of non-parallel straight lines with an angle resolution less than one degree.

III. Hough Transform Methodology

The standard HT converts binary edge images from Cartesian coordinate space $(x, y)^T$ into parameter coordinate space $(\rho, \theta)^T$. The transformation from Cartesian to parameter coordinate is done by using the following equation:

$$\rho = x \cdot \cos\theta + y \cdot \sin\theta \qquad \text{with} \qquad 0 \leq \theta < \pi \tag{1}$$

Cartesian coordinate to parameter space transformation maps a single edge point to all lines which pass through that point in image space. This yields a sine-like line representation in the Hough space (compare Fig. 1, right). A typical edge map includes many points and each edge point is transformed to a sine-like representation in Hough space. The locations in Hough space, where most of the lines intersect, are interpreted as true line in the (source) edge image. To determine these locations, an accumulator covering the Hough space is used. For each edge point transformation, bins in the accumulator are incremented for all lines passing through that particular point. The size of image and the angle resolution determine the accumulator dimension. The Fig. 1 illustrates two points in Cartesian coordinate space and their Hough space representation. Their Hough space intersection indicates the line which passes through both points. The block diagram depicted in Fig. 2 concludes all necessary steps for HT-method-based line detection.

The colour input image is initially converted to grey scale and passed to an Edge Detector, which generates the edges as input of the Line Parameter Estimator. All edge point coordinates, representing a potential line, are the base for the calculation of the Hough distribution, that is evaluated and accumulated in memory. Finally, the Maximum Detection identifies the line parameters of the five most significant straight lines in the source image by tracking the best Hough space intersection candidates.

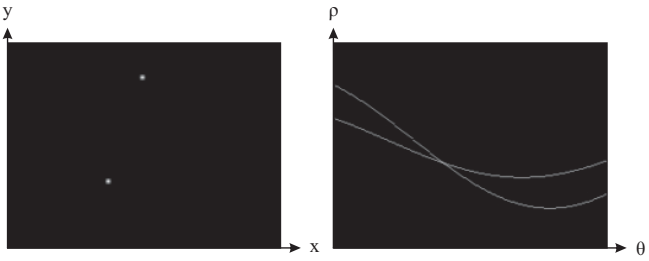

Fig. 1: Two points and their Hough space representation

This paper considers the implementation of HT for straight line detection only. Hence, the description of the hardware realisation focuses the two last blocks in the Fig. 2 (Line Parameter Estimation, Maximum Detection).

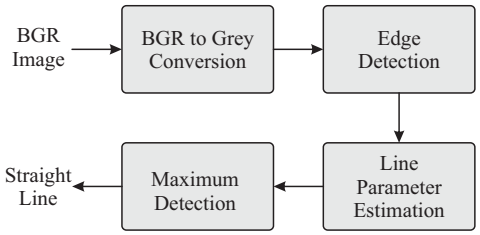

Fig. 2: Straight line detection process steps

A. Advanced Incremental Hough Transform

The complexity of HT is reduced by the approach proposed by Koshimizu [11]. His method substitutes the trigonometric functions in the Hough parametric equation (1) with *shift* and *add* operations. The proposed algorithm reduces the complexity of HT, but does not acquire full parallelism advantages of FPGAs due to the dependency in equations. This dependency was removed by Tagzout by proposing independent equations as follows [10]:

$$\rho_{n+1} = \rho_n + \epsilon \cdot \rho_{\frac{k}{2}+n} \tag{2}$$

$$\rho_{\frac{k}{2}+n+1} = \rho_{\frac{k}{2}+n} - \epsilon \cdot \rho_n \tag{3}$$

$$\text{with} \quad 0 \leq n \leq \frac{k}{2}$$

$$\text{and} \quad \epsilon = \frac{\pi}{k} \tag{4}$$

The parameters n, ϵ, and k represent index, resolution and number of quantisation of θ respectively, while $\rho_0 = x$ and $\rho_{\frac{k}{2}} = y$. The algorithms (2) to (3) compute iteratively and concurrently the Hough distribution for the first ($0 \leq \theta < \pi/2$) and second half ($\pi/2 \leq \theta < \pi$) of θ-interval ($0 \leq \theta < \pi$). Since this method is the approximation of sine and cosine functions, the error rises with increasing iterations to complete the whole interval for θ. To address this problem,

the θ-interval is separated into four subsets, which keeps the error comparatively low. The new expression of IHT becomes as follows:

$$\rho_{n+1} = \rho_n + \epsilon \cdot \rho_{\frac{k}{2}+n} \quad (5)$$

$$\rho_{\frac{k}{4}+n+1} = \frac{-\epsilon \cdot \sqrt{2}}{2}\rho_n + \frac{\epsilon \cdot \sqrt{2}}{2}\rho_{\frac{k}{2}+n} + \rho_{\frac{k}{4}+n} \quad (6)$$

$$\rho_{\frac{k}{2}+n+1} = -\epsilon \cdot \rho_n + \rho_{\frac{k}{2}+n} \quad (7)$$

$$\rho_{\frac{3}{4}+n+1} = \frac{-\epsilon \cdot \sqrt{2}}{2}\rho_n - \frac{\epsilon \cdot \sqrt{2}}{2}\rho_{\frac{k}{2}+n} + \rho_{\frac{3}{4}+n} \quad (8)$$

$$\text{with} \quad 0 \leq n < \frac{k}{4} \quad \text{and}$$

$$\rho_0 = x, \quad \rho_{\frac{k}{4}} = \frac{\sqrt{2}x}{2} + \frac{\sqrt{2}y}{2}$$

$$\rho_{\frac{k}{2}} = y, \quad \rho_{\frac{3}{4}} = \frac{\sqrt{2}y}{2} - \frac{\sqrt{2}x}{2}$$

B. Hardware Realisation

The most important feature of FPGA technology is its parallelisation capability. In order to exploit this parallelism, the equations (5) to (8) are realised concurrently, without the usage of DSP-blocks. Each equation calculates one quarter of the separated angle interval for θ and iterates independently from the others. The number of iterations is determined by the value ϵ which shall be defined in a way that keeps the Hough distribution error to a marginal level of acceptance. Furthermore, it shall be in power of two, so that simple shift operators can be used to supersede the multiplications. With $\epsilon = 2^{-6}$ and the equation (4), 50 iterations are needed to compute the Hough distribution of a single edge point. The angle resolution results in $\Delta \approx 0.895°$. With $k = 200$, parameters 0, $k/4$, $k/2$, $3k/4$ represent the angles 0°, 45°, 90°, and 135° respectively.

Both, performance and throughput of the architecture increase by pipelining the design in a way that each clock cycle one edge point is transformed into Hough distribution. This strategy increases the cost of pipelining registers, but takes the advantages of implicit parallelism. Introducing 50 pipeline stages, each stage is accountable for a single angle step. All stage units serve their output as input to the next one, as depicted in Fig. 3. In total, 51 units are instantiated and the first unit (Stage 0) calculates the initial values for subsequent iterations.

The HT algorithm uses a two-dimensional array (accumulator) to detect the existence of straight lines described by equation 1. The proposed HT implementation uses local instead of a global accumulators due to the pipelined, parallel processing architecture. Every step votes to four local small-sized accumulators, which results in a 51×4 accumulator memory configuration. The size of the accumulator space and the required memory resources are determined by:

$$D_{max} = \sqrt{(r-1)^2 + (c-1)^2} \quad (9)$$

With r and c as number of rows and columns of the input image, an image of 270×480 pixel resolution leads to $\rho_{max} = 530$, $\rho_{min} = -480$ (refer to equation (1)), and $D_{max} = 549$ (see equation (9)). The total range of ρ is $|\rho_{max}| + |\rho_{min}| = 1010$.

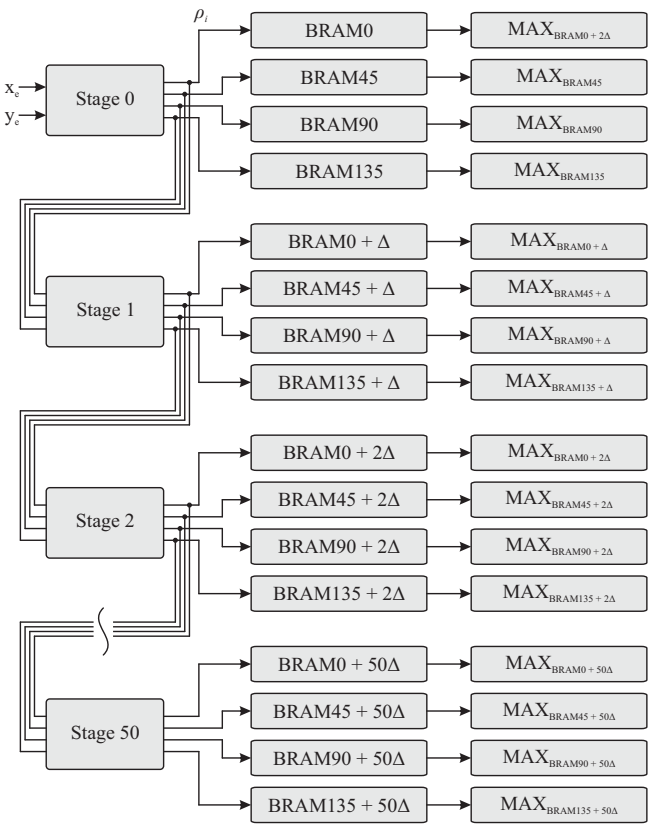

Fig. 3: Pipelining of IHT with $\Delta \approx 0.895°$

The hardware implementation is done on a Xilinx Virtex-6 LX240T FPGA with Block-RAM modules (BRAM) providing up to 36 Kb of memory. The BRAM can be configured by combining 18 Kb or 36 Kb BRAM elements. Each 18 and 36 Kb BRAM supports user-configurable write and read widths as well as a configurable storage depth. Furthermore, the BRAM components allow single- and dual-port access for simultaneous reading and writing.

With the given image dimension of 270×480 pixel, the accumulator BRAM is configured with 1Kb storage depth (1024 bit for the total range of ρ) and 10 bit write width (10 bit for $D_{max} = 549$). For each angle, a separate accumulator BRAM is used, which consumes $4 \times 51 \times 10 \times 1024$ Kb $= 2,088.96$ Kb BRAM (see Fig. 3).

The ρ_i, resulting from the pipeline stages, are forwarded to the accumulator voting circuitry and connected to the address pin of the subsequent BRAM. This port (ADDRA) serves the read address for the (read) output port DOUTA. The DOUTA port drives the BIN[ADDRA] bus with every rising clock edge. This BIN[ADDRA] data is incremented and connected to the BRAM input pin DINA (write port). As two ports are synchronously reading and writing content from/to a single

BRAM, the BRAM content will get inconsistent if an equal BIN shall be incremented in two adjacent clock cycles. In this case, read and write addresses are equal. To avoid this collision case, the incremented value BIN[ADDRA]+1 is stored in a register R_{BIN} after each incrementation step. If subsequent values of ρ_i are equal to the previous one, a multiplexer will switch to the register R_{BIN} instead of reading the output port DOUTA. This strategy keeps the BRAM data consistent.
The maximum detection for each BRAM is done simultaneously with the accumulator voting. A single register R_{MAX} is used to keep track of the maximum voted BIN for each BRAM. The register is arranged inside a feedback loop, as shown in Fig. 4. The incremented BIN[ADDRA]+1 is compared against the register R_{MAX} and if the value is greater, the register R_{MAX} is updated. Since 204 BRAMs are utilised, the circuit shown in Fig. 4 is instantiated 204 times.

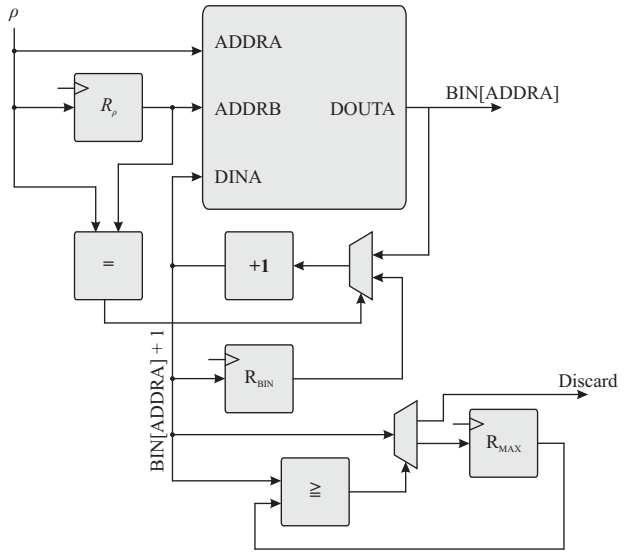

Fig. 4: Voting process and local accumulator peak detector

After the completion of the local accumulator voting, the Maximum Detection is computed. Considering 204 local maxima of the BRAMs, five global maxima are determined by register-wise comparison. The global maximum values are available after 203 clock cycles. The resulting global maxima indicate the maximum peaks of the global Hough space and represent the five most significant, non-parallel straight lines in the Cartesian coordinate space (source image space).
The data representation of input, intermediate, and result data depends strongly on the addressed application and required accuracy. If high precision with less quantisation error is required, the data representation has to be adapted. Hence, the trade-off between precision, operation frequency, and resource consumption has to be considered. The proposed design applies fixed-point representation with 9 bit for edge pixel coordinates, 10 bit for the axis of ordinates of the Hough space (Hough line distance), and 8 bit for the Hough line angle ranges from 0 (0°) to π (180°). To evaluate Hough distribution, Q11.17 representation is used.

IV. Experimental Results

The proposed architecture for hardware-accelerated HT is implemented on a Xilinx Virtex-6 LX240T FPGA. The design performance is evaluated with Xilinx ISE 14.5. The Table I shows the FPGA resource utilisation. The design is fully pipelined with 51 pipeline stages. Each stage has a latency of six clock cycles. The total latency of the HT architecture is 300 clock cycles. Each edge point takes a single clock cycle for the evaluation of the Hough distribution. The local maximum within each BRAM circuitry is computed concurrently with the voting process. The detection of the global maximum is running in parallel and initiates either after the last edge point passed the first pipeline stage, or each BRAM finished the local voting process. This Maximum Detection needs a single clock cycle for each BRAM and is done by comparing the local (BRAM) maximum with the five global maxima retrieved from the previous BRAMs.

TABLE I: FPGA utilisation for the HT system architecture

Logic Resources	Utilisation 6VLX240T
18Kb BRAM	203 (24.4%)
Slice Registers	31,338 (10.0%)
DSP48E1 Blocks	0 (0.0%)
Occupied Slices	10,084 (26.0%)

The circuitry determines five straight lines represented by polar coordinates $(\rho, \theta)^T$ in $N + 300$ cycles with 170.736 MHz. Considering the worst case scenario with $N = 270 \cdot 480 = 129,600$ edge points (all points in image represent an edge), the HT architecture computes five non-parallel Hough lines in maximum $\frac{129,600+300}{170.736 \cdot 10^6 Hz} = 735\mu s$. This deterministic worst case runtime guarantees real-time behaviour of the proposed solution.
The functional behaviour of the proposed solution is simulated with the Xilinx ISE 14.5 ISim simulator. The edge points (see Fig. 5a and 5c), which are pre-calculated with MathWorks MATLAB canny edge detector, are provided to the circuit. The circuit detects five robust non-parallel lines, which are plotted in blue colour with MATLAB in Fig. 5b and 5d.
While the processing of test image A produces correct results, the result of test image B (see Fig. 5d) shows a second (falsely) detected line for the horizontal bottom edge line. This false detection is caused by approximation errors occurring in the hardware implementation. Furthermore, the limitation of the current implementation to detect maximum five non-parallel, straight Hough lines leads to a detection miss of the diagonal most right edge line in test image B. Incrementing the number of acceptable maximum Hough peak detections will provide more straight line results in the source image space.

V. Conclusion

The paper introduces an efficient, powerful hardware realisation for Hough transform applying independent, pipelined voting stages. The proposed implementation provides real-time behaviour and uses standard logic resources only, which are available on every common FPGA device. No specific DSP-blocks, hard macros for mathematical operations, or lookup

tables for sine and cosine estimation are required.
The solution is able to detect five non-parallel, good-quality lines simultaneously, runs with 170.736 MHz operation frequency, and processes 270×480 pixel images with minimum 1,360 frames per second or faster. Images with higher resolution can be processed accordingly, which reduces the frame rate due to longer processing duration (e.g. high-definition 1080p imagery is exploited with a rate of minimum 340 frames per second or faster).

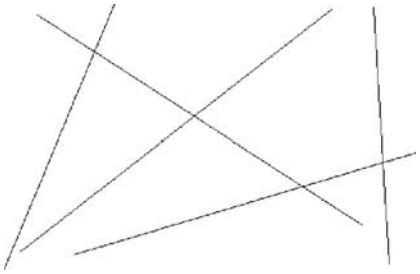

(a) Test image A

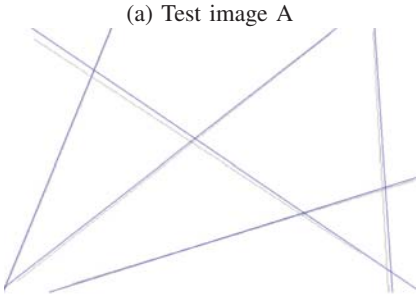

(b) Result of test image A

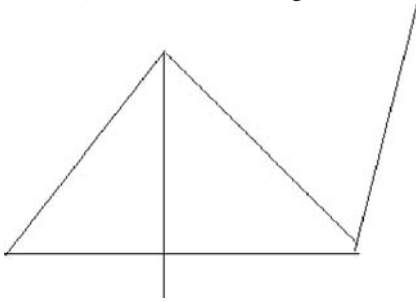

(c) Test image B

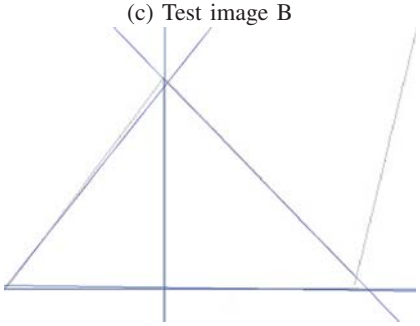

(d) Result of test image B

Fig. 5: Test results of hardware-accelerated HT

ACKNOWLEDGMENT

The results have been supported by the program Open Innovation for Remotely Piloted Aircraft Systems (RPAS), funded by the Federal Ministry for Economic Affairs and Energy, Germany. The collaboration of AIRBUS Defence & Space, German universities, and research institutes intends to develop holistic solutions to increase air traffic safety and the operation of RPAS for civil applications.

The authors gratefully acknowledge the cooperation of our project partners and the financial support of the DFG (Deutsche Forschungsgemeinschaft) within the Federal Cluster of Excellence EXC 1075 ”MERGE”.

REFERENCES

[1] K. Chapman, “Constant coefficient multipliers,” in *Proceedings of the 1995 International Conference on Signal Processing Application and Technology*, Boston, MA, USA, 1995, pp. 905-908.

[2] G. R. Goslin, “Using FPGAs in digital signal processing application,” in *Proceedings of the 1995 International Conference on Signal Processing Application and Technology*, Boston, MA, USA, 1995, pp. 145-149.

[3] M. Chene, “FPGA-Based Prototyping: Big Design - Small Budget?,” in *Getting the Most Out of FPGA Prototyping*, EETimes, USA, 2014, pp. 10-14.

[4] J. L. Bordim, Y. Ito, K. Nakano, “Accelerating the CKY parsing using FPGAs,” in *IEICE Transactions on Information and Systems*, vol. E86-D, no. 5, pp. 803-810, May, 2003.

[5] D. Ghosh, D. Debnath, A. Chakrabarti, “FPGA Based Implementation of FFT Processor Using Different Architectures,” in *International Journal of Advanced Information Technology*, vol. 1, 2012.

[6] S. Blokzyl, M. Vodel, W. Hardt, “A Hardware Accelerated Real-Time Image Processing Concept for High-Resolution EO Sensors,” in *Proceedings of the 61. Deutscher Luft- und Raumfahrtkongress*, Berlin, Germany, 2012.

[7] R. Duda, P. Hart, “Use of Hough transform to detect lines and curves in picture,” in *Communications of the ACM Magazin*, vol. 15, no. 1, pp. 11-15, January, 1972.

[8] F. Zhou, P. Kornerup “A High Speed Hough Transform Using CORDIC,” in *Proceedings of the 1995 International Conference on Digital Signal Processing*, Cyprus, Greece, 1995, pp. 27-39.

[9] X. Zhou, Y. Ito, K. Nakano, “An Efficient Implementation of the Hough Transform using DSP slices and Block RAMs on the FPGA,” in *Proceedings of the 2013 IEEE 7th International Symposium on Embedded Multicore Socs*, Tokyo, Japan, 2013, pp. 85-90.

[10] S. Tagzout, K. Achour, O. Djekoune, “Hough transform algorithm for FPGA implementation,” in *Signal Processing*, vol. 81, no. 6, pp. 1295-1301, June, 2001.

[11] H. Koshimizu, M. Numada, “FIHT2 Algorithm: A Fast Incremental Hough Transform,” in *Proce of the IAPR Workshop on Machine Vision Application*, Tokyo, Japan, 1990, pp. 233-236.

[12] X. Lu *et al.*, “Parallel Hough Transform-Based Straight Line Detection and Its FPGA Implementation in Embedded Vision,” in *Sensors*, vol. 13, no. 7, pp. 9223-9247, July, 2013.

[13] A. Elhossini, M. Moussa, “A Memory Efficient FPGA Implementation of Hough Transform for Line and Circle Detection,” in *Proceedings of the 2012 25th Canadian Conference on Electrical and Computer Engineering*, Montreal, QC, Canada, April, 2012.

[14] O. Djekoune *et al.*, “Incremental Hough Transform: An Improvement Algorithm for Digital Devices Implementation,” in *Real-Time Imaging*, vol. 10, no. 6, pp. 351-363, December, 2004.

Generation of Images with Hexagonal Tessellation using Common Digital Cameras

Robert Manthey and Tobias Schlosser and Danny Kowerko
Chemnitz University of Technology,
Endowed Professorship Media Computing,
D-09111 Chemnitz, Deutschland
Email: firstname.lastname@informatik.tu-chemnitz.de

***Abstract*—Nowadays, image and video capture devices and displays use a tessellation with sample points of nearly rectangle or square shape to form a full representation of the scene. However, the amount of information represented by each point can be improved by selecting other structures of tessellation. For instance, hexagonal grids increase the visual quality and reduce the amount of data needed to store the content. We investigate the useability and the constraints of common digital cameras to produce images based on this pixel shape to obtain the most of that increment.**

I. Introduction

In principle the light from a scene of the continuous real world is focused and projected on the surface of a sensor or an eye [1]. In technical applications, the surface of capture sensors like digital cameras are subdivided into smaller regions to measure and represent the local visual information, respectively. Displays are constructed in a similar fashion and both use the well-known rectangle or square shapes of the small picture elements. In contrast to that, biological capture systems like compound eyes of insects [2] or lens eyes of mammals use nearly hexagonal shaped cells as shown in Fig. 1.

The repercussions of that projection being shown in Fig. 2. The continuous structures of Fig. 2a being transformed by the used tessellation into small homogenous regions represented by single sensor elements. The size and shape of them define the resolution limit of structures being depictable [4]. The sample of Fig. 2b show that concurrence at the bars in the upper left as well as the star and the circle in the center. Strong stairway like artefacts being visible at the bar in the lower right. The hexagons in Fig. 2c being also effected but to a lower extent, especially at round and skew edges of the star or the bar in the lower right.

Effects like this caused early researches and comparisons of tessellations by Deutsch [5] which show significant advantages of hexagonal image structures in the field of algorithm design,

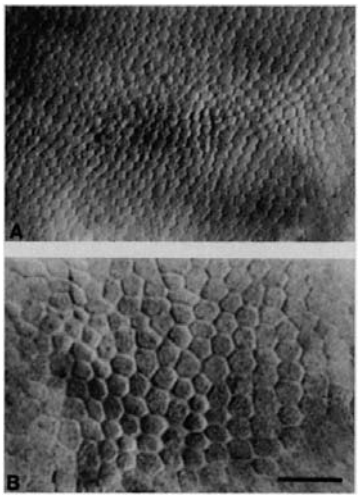

Fig. 1. Picture of a human retina showing a nearly hexagonal structure.[3]

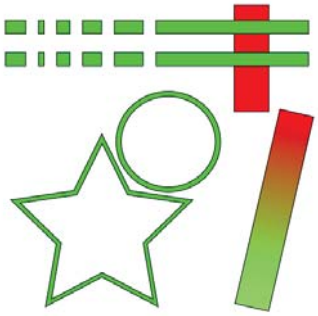

(a) Exemplary continuous scene with two fragmented green bars at the top, a partly covert red bar at the top right, a skewed bar at the right and a circle as well as a star in the center and the buttom left.

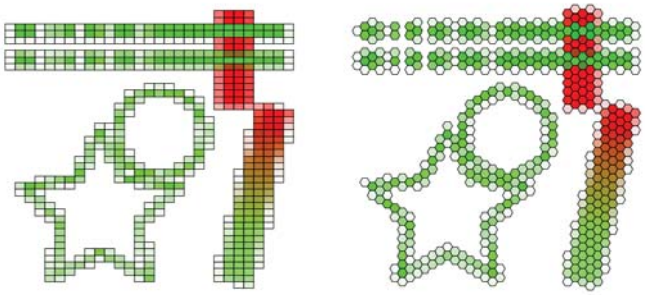

(b) Exemplary tessellation of scene showing the affected rectangle pixels.

(c) Exemplary tessellation of scene showing the affected hexagon pixels.

Fig. 2. Samples of equal size rectangle and hexagon tessellation of a exemplary scene.

complexity and time of execution. Mersereau analysed the projection of informations from real world to 2D sensors from theoretical principles and reveal an increase of the amount of informations by 13.4 percent compared to square tessellation [6]. Luczak and Rosenfeld [7] and [8] focused on distances and skeletonizing to retieve and use this information increment. Their results show more rotation insensitive and robustness as the square version of the algorithms [9]. The research of Staunton [10] compare the sobel edge detection algorithm and show the advantages of the hexagonal version, but request again suitable capture and display devices to receive images with hexagonal tessellation.

The most common traditional approach of resampling a rectangle based image to a hexagonal one creates intrinsic artefacts, blurring and information loss as well-known from most image transformations and results in researches of more advanced transformations as described by Ville [11], [12] to improve that process. Others like Staunton [10] modify analogous hardware components of capture as well as display devices to achieve hexagon related images. Our approach attempts to reduce the aforementioned drawbacks by combining the resampling with hardware-near access taking the raw informations from the capture sensor of digital cameras like the *Canon EOS 5DS R*[1].

II. Structure and properties of tessellation and addressing

A tessellation of a 2D plane is being achieved in a regular, periodic, gapless and simple way by only three types of geometric elements respectively – triangles, rectangles and hexagons [5]. Each type generates characteristic properties and constraints depicted for rectangles and hexagons in Fig. 3. The rectangles permit simple and well-known mathematical operations, easy measuring of distances in horizontal and vertical direction and well-known addressing of points in the grid. In contrast to that, hexagon require a somewhat more complex mathematic cause by the non-orthogonal axes and a more complex addressing of points, but are at the same time more consistent in algorithmic definitions and distance measuring. [8]

As a consequence of the shape, the dimensions are different. With an equal area of one, a square has a side length of one, but a horizontal hexagon has a width of 1.241 and a height of 1.0746 as shown in Fig. 3. This results in a shift of half a hexagonal in every odd line and adaptions in the addressing. Other selections of lengths cause the cases of Fig. 4.

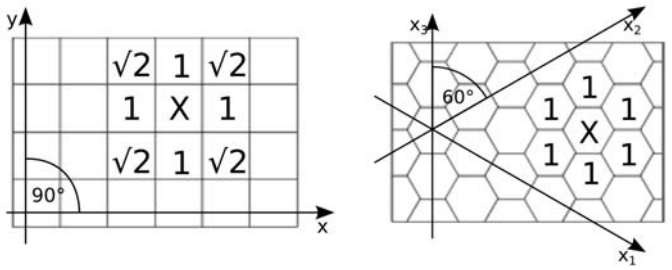

(a) Square tessellation with two orthogonal axes, but different distances to the straight neighbours and the diagonals.

(b) Hexagonal tessellation with three non-orthogonal axes, but equal distances to all neighbours.

Fig. 3. Principle structure of a square and a hexagonal tessellation with the exemplary point at $(x, y) = (3, 2)$ in 3a and $(x_1, x_2) = (2, 2)$ or $(x_1, x_3) = (4, 2)$ or $(x_2, x_3) = (2, -2)$ in 3b.

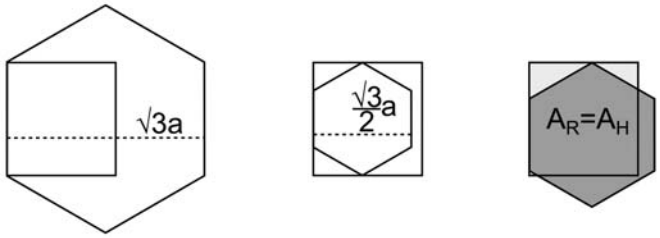

Fig. 4. Various relations of square and hexagon. Equal lengths of the edges cause a significantly bigger hexagon and a similar total length cause a slightly smaller hexagon. Equality of the area result in a slightly bigger hexagon with shorter length of the edges.

The location of a point of the grid is given by its distance from the zero point measured along each axes. Because of its three axes the most suitable combination can be selected in the hexagonal grid at any addressing operation. Another common addressing scheme uses a single index as presented in Fig. 5 allowing lossless translation and rotation operations. [13], [14]

III. Workflow

As described before most image transformations entail some loss of information and the generation of images with hexagonal grids needs at least two of them in a common case as shown in Fig. 6. The unmodified data from the camera sensor of our Canon EOS 5DS R is stored in a raw file and transformed to a normal image file using the tool *dcraw*[2]. We modify that tool (later termed *dcrawHMod*) to rearrange the data from the raw file being suitable in a hexagonal grid with shifted odd lines and an adjustment of the width and height. The result is saved as image file with single index addressing and also as 2D image for better visualisation.

[1] http://www.canon.de/for_home/product_finder/cameras/digital_slr/eos_5ds_r/

[2] http://www.cybercom.net/~dcoffin/dcraw/

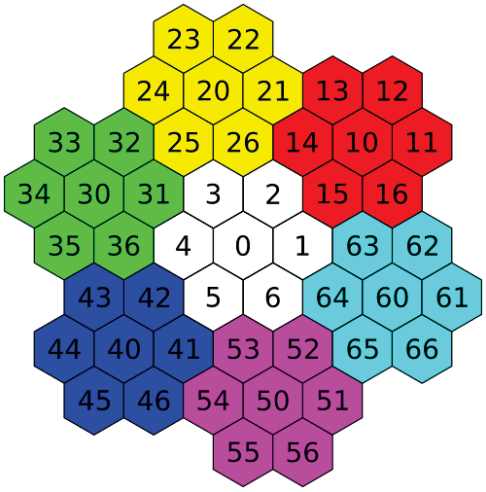

Fig. 5. Structure of the single index hexagonal addressing of pixels (cf. to [14]). Starting with 0 at the center of each group surrounded by its six neighbours of the same level of hierarchy. The next level elements surrounds this center again and obtain one prefixed digit.

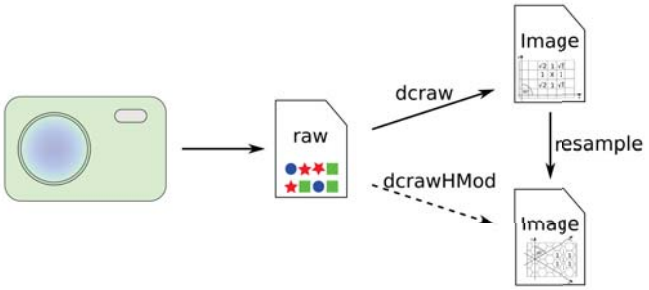

Fig. 6. Workflow of generation of images with hexagonal tessellation. A digital camera captures the scene and produces a raw-file specific to that camera. Tools like *dcraw* transform this file into a common image file format with rectangle pixels and another resampling tool transform it to a file with hexagon pixels finally. Our approach shortened the workflow and transform the hexagons from the *raw*-file directly.

IV. Results

Choosing the Fig. 7 as reference we process the workflow and achieve the samples of Fig. 8 and 9. Every raw data sample depict the device-depending distribution of red, green and blue corresponding to the structure of the capture sensor. The results from *dcraw* and from resampling show significant uniform distributed noise, spots of false colors and an overall color shift. Blurring of some degree is perceptible, especially at the borders of black areas. In contrast to that, *dcrawHMod* produces much lesser noise and the blurring is significantly reduced as shown at the border of the 16 especially. Only the color feature some shortcomings.

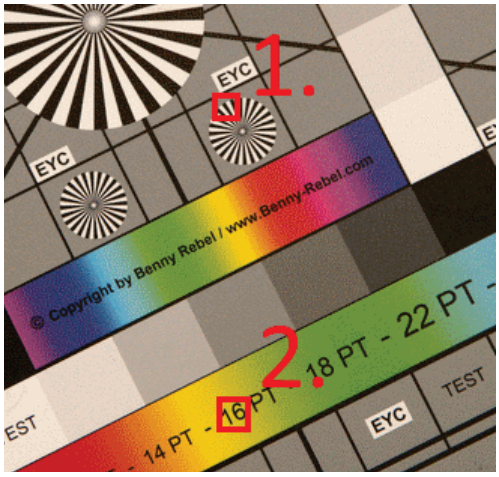

Fig. 7. Original image with the red cutout markings of region 1 and 2.

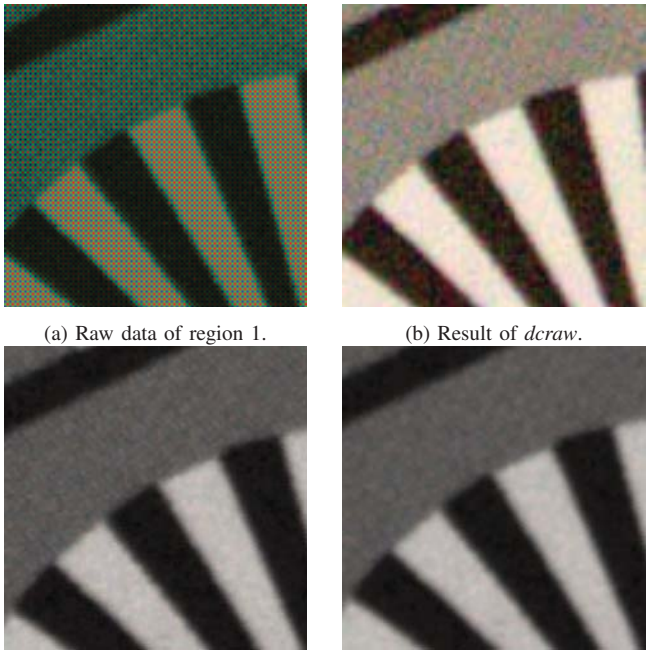

(a) Raw data of region 1. (b) Result of *dcraw*.

(c) Hexagons resampled from *dcraw*. (d) Result of *dcrawHMod*.

Fig. 8. Raw data and results of *dcraw*, resampled hexagons and *dcrawHMod* of region 1.

V. Conclusion & Future Work

Our approach of the generation of images with hexagonal tessellation by a modified tool is demonstrated and show useful results. Future adaptions to other camera systems and more advanced transformation algorithms with improved color mapping can outperform the traditional rectangle tessellation finally.

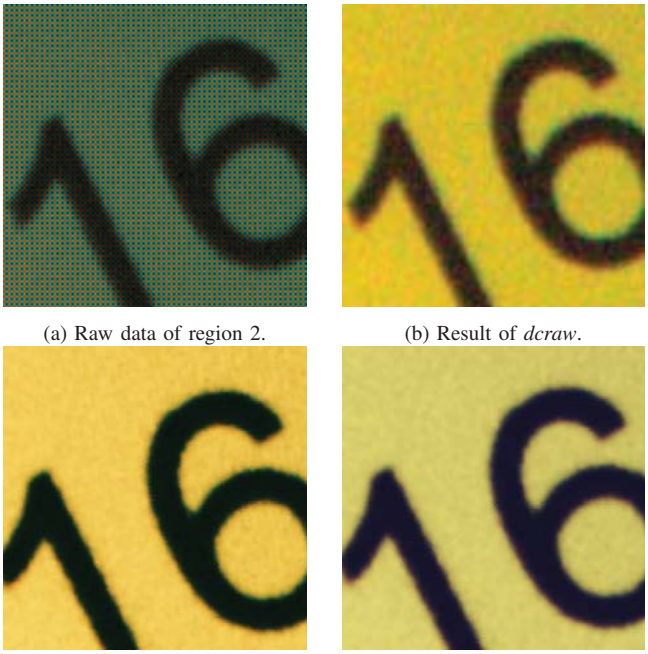

(a) Raw data of region 2. (b) Result of *dcraw*.

(c) Hexagons resampled from *dcraw*. (d) Result of *dcrawHMod*.

Fig. 9. Raw data and results of *dcraw*, resampled hexagons and *dcrawHMod* of region 2.

ACKNOWLEDGMENT

This work was partially accomplished within the project localizeIT (funding code 03IPT608X) funded by the Federal Ministry of Education and Research (BMBF, Germany) in the program of Entrepreneurial Regions InnoProfile-Transfer.

REFERENCES

[1] C. Wthrich and P. Stucki, "An algorithmic comparison between square- and hexagonal-based grids," *Graphical Models and Image Processing*, vol. 53, no. 4, pp. 324–339, July 1991.

[2] M. F. Land, "Visual acuity in insects," *Annual Review of Entomology*, vol. 42, no. 1, pp. 147–177, January 1997, pMID: 15012311. [Online]. Available: http://dx.doi.org/10.1146/annurev.ento.42.1.147

[3] C. A. Curcio, J. Kenneth R. Sloan, O. Packer, A. E. Hendrickson, and R. E. Kalina, "Distribution of cones in human and monkey retina: individual variability and radial asymmetry." *Science*, vol. 236, no. 4801, pp. 579–582, May 1987. [Online]. Available: http://www.jstor.org/stable/1699166

[4] R. C. Gonzalez and R. E. Woods, *Digital Image Processing*, 3rd ed. Pearson, 2008.

[5] E. Deutsch, "Thinning algorithms on rectangular, hexagonal, and triangular arrays," *Communications of the ACM*, vol. 15, no. 9, pp. 827–837, September 1972. [Online]. Available: http://doi.acm.org/10.1145/361573.361583

[6] R. Mersereau, "The processing of hexagonally sampled two-dimensional signals," *Proceedings of the IEEE*, vol. 67, no. 6, pp. 930–949, June 1979.

[7] E. Luczak and A. Rosenfeld, "Distance on a hexagonal grid," *Transactions on Computers*, vol. C-25, no. 5, pp. 532–533, May 1976.

[8] G. Borgefors, "Distance transformations in hexagonal grids," *Pattern Recognition Letters*, vol. 9, no. 2, pp. 97 – 105, February 1989. [Online]. Available: http://www.sciencedirect.com/science/article/pii/0167865589900421

[9] I. Her, "Geometric transformations on the hexagonal grid," *Transactions on Image Processing*, vol. 4, no. 9, pp. 1213–1222, September 1995.

[10] R. C. Staunton, "Hexagonal image sampling: A practical proposition," in *Proceedings of SPIE*, D. P. Casasent, E. L. Hall, and K. J. Stout, Eds., vol. 1008. SPIE, February 1989, pp. 23–27. [Online]. Available: http://dx.doi.org/10.1117/12.949123

[11] D. V. D. Ville, W. Philips, and I. Lemahieu, "Least-squares spline resampling to a hexagonal lattice," *Signal Processing: Image Communication*, vol. 17, no. 5, pp. 393–408, May 2002. [Online]. Available: http://www.sciencedirect.com/science/article/pii/S0923596502000097

[12] D. V. D. Ville, T. Blu, M. Unser, W. Philips, I. Lemahieu, and R. V. de Walle, "Hex-splines: a novel spline family for hexagonal lattices," *Transactions on Image Processing*, vol. 13, no. 6, pp. 758–772, June 2004.

[13] P. Sheridan, T. Hintz, and D. M. Alexander, "Pseudo-invariant image transformations on a hexagonal lattice," *Image and Vision Computing*, vol. 18, no. 11, p. 907917, 2000. [Online]. Available: http://www.sciencedirect.com/science/article/pii/S0262885600000366

[14] L. Middleton and J. Sivaswamy, *Hexagonal Image Processing: A Practical Approach (Advances in Pattern Recognition)*, ser. Advances in Pattern Recognition. Springer-Verlag, 2005. [Online]. Available: http://dx.doi.org/10.1007/1-84628-203-9

Integration of FPGA-based Hardware-acceleration into an Automotive Validation Framework

Reham Tallawi and Stephan Blokzyl and Wolfram Hardt
Chemnitz University of Technology
Faculty of Computer Science
Professorship Computer Engineering
D-09107 Chemnitz, Germany
{reham; sblo; hardt}@hrz.tu-chemnitz.de

***Abstract*—The Elektrobit Automotive Data and Time-Triggered Framework (ADTF) is a powerful software toolchain, which is used to develop, simulate, and validate complex systems in the areas of advanced driver assistance and highly automated driving. The framework offers various capabilities supporting sensor evaluation and measurement, software validation, prototyping, and data acquisition. Moreover, the framework provides the possibility to integrate with other devices and technologies which add more computing power, dynamics, and flexibility to the system under development or test.**

This paper presents the realisation of a novel adapter filter for integrating hardware-acceleration applying Field Programmable Gate Arrays (FPGAs) into the ADTF framework. The proposed system architecture links ADTF and FPGA technology by using Gigabit-Ethernet-based communication for high-performance and reliable data and result dissemination.

The paper introduces implementation details of the software adapter, communication methods, protocols, and the hardware-acceleration framework which is developed in VHDL.

The resulting adapter filter has been validated with a test setup adding hardware-acceleration for high-resolution images data exploitation to ADTF. The proposed solution enables time- and cost-efficient development and testing of hardware-software-co-designed systems for automotive and non-automotive applications.

***Index Terms*—Advanced driver assistance systems; Image analysis; Image processing; Automotive applications; System validation; Field programmable gate arrays**

I. Introduction

The continuously rising number of automotive vehicles on the road includes increasing immanent risks caused by both human and non-human factors. Therefore, the need for safe and reliable traffic participants is essential to maintain public safety, especially when vehicles become more sophisticated and complex. Traffic users shall not only deliver safe and secure services, they shall own intelligence to reduce and manage traffic congestions and allow reliable environment recognition. Hence, modern vehicles use high-technology real-time embedded systems that sense, measure, process, and control, as well as share information with other traffic participants. Powerful sensors like e.g. electro-optical (EO) sensors are very suitable for complex environment recognition tasks and more and more used for automotive applications. EO sensors acquire high-resolution, high-quality, and large-volume data, which makes the management and exploitation of high-volume image data challenging, particularly when using conventional generic software approaches running on embedded architectures.

Accordingly, alternative processing methods become necessary to cope with the substantial amount of data and to provide fast, reliable, high-quality exploitation results. One of the most convenient solutions are hardware-acceleration technologies applying Field Programmable Gate Arrays (FPGAs). These reconfigurable integrated circuits enable the development and implementation of powerful, high-speed, and highly parallelisable digital signal processing and supply high-performance computing capabilities to computational demanding traffic system applications.

Developed by Elektrobit, the Automotive Data and Time-Triggered Framework (ADTF) is a complete development, validation, and visualisation environment dedicated for advanced driver assistance systems and highly automating driving applications [1]. The framework offers cutting edge uses cases and libraries which provide a powerful interactive groundwork to design and develop complex software filter components.

In addition to the software-based development and validation framework, this paper presents a novel solution integrating hardware-acceleration capabilities into the ADTF environment. The resulting adapter filter connects ADTF to an FPGA-based hardware-accelerator and offers an efficient, high-performance software-hardware-interface for flexible communication of a wide range of different data structures and types. Furthermore, the connected hardware-acceleration architecture provides a framework with a standardised Application Independent Interface (AII) for easy integration and validation of arbitrary hardware-acceleration modules.

This paper is organised as follows. Section II will present the system architecture, communication methodologies, and technologies. The software implementation of the adapter filter and the hardware-acceleration architecture are discussed in section III. Section IV and V conclude the achieved results and summarise the integration concept.

II. Design Concept

Figure 1 illustrates the overall system architecture including the different hardware/software components and modules.

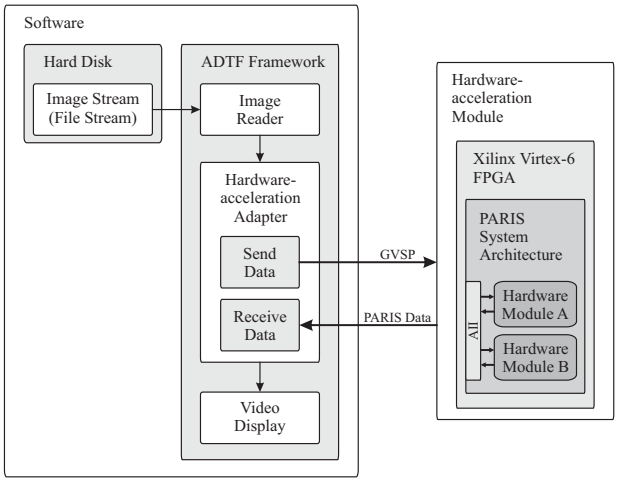

Fig. 1: Overall system architecture

A. System Architecture

From the software point of view, the ADTF framework replays sensor data (here pre-recorded EO sensor data) from a local hard drive. A standard Image Reader filter loads imagery data and forwards media sample-encapsulated image frames to the Hardware-acceleration Adapter. This filter performs the necessary communication between ATDF and an externally connected Hardware-acceleration Module. The incoming image media samples are converted to IP/UDP-based GigE Vision Streaming Protocol (GVSP) datagrams, a high-speed Gigabit Ethernet-based image stream protocol for high-performance, high-resolution camera sensors, and transmitted to the connected PARIS[1] system architecture. The PARIS framework is an FPGA-based solution for modular, flexible, and comfortable parallelisation of real-time image data exploitation. PARIS supports various data and task parallelisation strategies, as well as static and dynamic in-system-reconfiguration [2]. The incoming data packages from the Hardware-acceleration Module base on a user-defined IP/UDP protocol encapsulating all hardware-acceleration results. The successfully received data is forwarded by the Hardware-acceleration Adapter to the Video Display filter for visualisation and validation.

From the hardware side, the FPGA-based hardware-acceleration framework hosts all algorithms and operations, which perform the required processing of the incoming image data, and controls the data/result dissemination from/towards the ADTF environment. A detailed introduction into the PARIS parallelisation architecture for real-time image data exploitation is given in [2].

B. Data Dissemination

The following section discusses the basic concepts and principles of the communication protocols applied for the proposed system. The implementation uses IP/UDP protocol to establish the communication link between ADTF and PARIS system architecture. The User Datagram Protocol (UDP) is a connectionless network protocol that executes on the Internet Protocol (IP) network. The UDP protocol provides port numbers for addressing of source and destination processes and a checksum for data integrity [3]. UDP does not provide handshaking capabilities, but enables simple and fast transmission, which is essential for high-speed data and result dissemination of the hardware-software-co-design architecture. The generic UDP datagram, which is utilised in the proposed system, encapsulates additional user-defined protocols (GVSP, PARIS Data) for reliable, application-specific communication.

1) Data Encapsulation: In communication networks, data encapsulation is a protocol design methodology, in which the process hides or encapsulates non-relevant information of subsequent lower level layers from networking modules at a higher level. Taking the DoD internet architecture model [4] for illustration, the model is composed of four layers of abstraction: Application, Transport, Internet, and Link layer. Each layer encapsulates the preceding datagram by adding a header to the packet. As shown in Fig. 2, the data is prepared in the Application layer and encapsulated by the UDP protocol creating an UDP datagram in the Transport layer. The UDP datagram is encapsulated by the Internet Protocol at the Internet layer. Finally, the Link layer adds an Ethernet frame which concludes the encapsulation process. The datagram is now ready to be dispatched to the according destination over the physical Ethernet network (wire). On the receiving end, the extraction or unwrapping of the payload data is performed by repeating the process in reverse order.

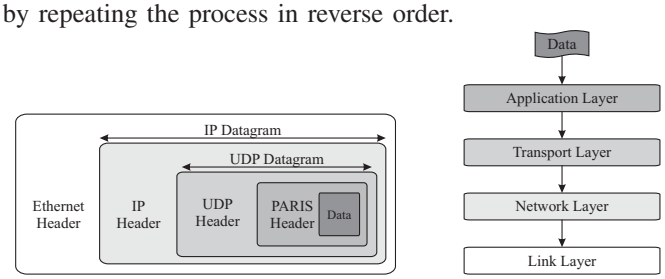

Fig. 2: Datagram encapsulation

2) PARIS Data Protocol: The PARIS data protocol is an Application layer protocol running on top of the UDP stack as shown in Fig. 2. The PARIS data protocol was utilised to overcome the limitations and constraints of the generic UDP, like e.g. congestion control, error recovery, datagram ordering, and datagram tracking. Accordingly, the PARIS datagram compensates these restrictions by introducing an extra PARIS header field (compare Fig. 3).

The PARIS datagram header comprises 16 bit sequence number, 16 bit message length information (in byte), 32 bit source ID, 32 bit destination ID, eight bit message sequence number, 32 bit time stamp, eight control bits, and 16 bit data length information (in byte). Subsequently, the PARIS datagram contains the payload data, optional padding, and 32 bit CRC-32 checksum. Source and destination ID identify the hard- and

[1] **P**arallelisation **A**rchitecture for **R**eal-time **I**mage data exploitation and **S**ensor data fusion

software modules which are co-processing the sensor data and define the data structure type of the PARIS data field. Sequence and message sequence numbers are used for datagram ordering and assembling of fragmented result data. The time stamp field documents the local time of the Hardware-acceleration Module which supports the analysis of runtime behaviour of the hardware architecture. Finally, payload integrity is ensured by a standard Ethernet CRC-32 checksum [5] and if a constant datagram length is required, the PARIS protocol allows 0x00-based padding inside the payload data section.

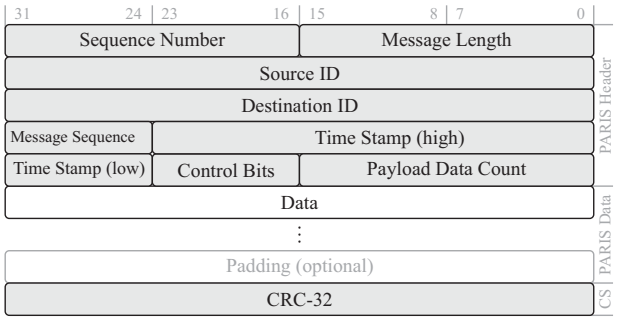

Fig. 3: PARIS datagram

3) GigE Vision Streaming Protocol: The GigE Vision Streaming Protocol (GVSP), is Gigabit Ethernet-based protocol standard, developed specifically for high-performance electro-optical sensors and devices [6]. The protocol is an Application layer protocol that runs on top of IP/UDP. GVSP supports reliable, fast image data transmission with a high bandwidth up to 1,000 Mb/s and data transfer distance up to 100 meters. It serves light-weight communication to high-resolution image data streaming sensors and devices. The GVSP bases on standard Gigabit Ethernet network and maximises transmission throughput of image data packets. The GVSP protocol is utilised for the image data transmission from the Hardware-acceleration Adapter in ADTF to the external Hardware-acceleration Module hosting the PARIS system architecture.

III. Implementation

The core ADTF filter is the Hardware-acceleration Adapter. This filter establishes and verifies the connection to the FPGA-based PARIS architecture and maintains the link to the attached ATDF filters Image Reader and Video Display. The Image Reader filter obtains image data from hard disk and forwards a media sample stream to the Hardware-acceleration Adapter. A transmission thread (Send Data, compare Fig. 1), hosted by the Hardware-acceleration Adapter, transfers the image data to the hardware-acceleration architecture. The Video Display filter visualises the incoming result data that was received and extracted by a nested receive thread (Receive Data) inside the Hardware-acceleration Adapter. All ADTF filters are developed in C/C++, use ADTF SDK libraries and the standard ADTF API in accordance to the guidelines and rules of the ADTF specification.

The Hardware-acceleration Adapter is composed of different subcomponents for sending data packets and data encapsulation, receiving data packets and payload extraction, as well as acquiring and transmitting media samples. The filter implementation uses multi-threading strategies in parallel to the main program thread. This increases the overall system performance as the ADTF framework has not to wait or stall for the external PARIS system architecture. E.g. the Video Display filter can visualise the received (previous) media sample while the external FPGA-based Hardware-acceleration Module processes the subsequent data frame simultaneously.

A. Payload Encapsulation and Data Transmission

Media samples received from the Image Reader filter are copied inside the Hardware-acceleration Adapter to a local buffer. Next, the image data is extracted for the encapsulation into the IP/UDP/GVSP protocol. As the GVSP protocol uses additional control packets, which envelop the image data payload datagrams, these packets have to be built first. The image transmission sequence starts with an Image Data Leader (IDL) and ends with an Image Data Trailer (IDT) [7]. The IDL contains meta information, like status flags, time stamp, pixel format, offset, padding, image width, and height. The IDT indicates the end of an image datagram sequence (also called block) and supports keeping track of the integrity of the datagram sequence. The IDL-IDT-encapsulation ensures that image payload packets are sent completely and in the correct order to the destination (compare Fig. 4). The resulting datagram sequence is transferred via a pre-registered UDP socket and Gigabit Ethernet to the FPGA framework.

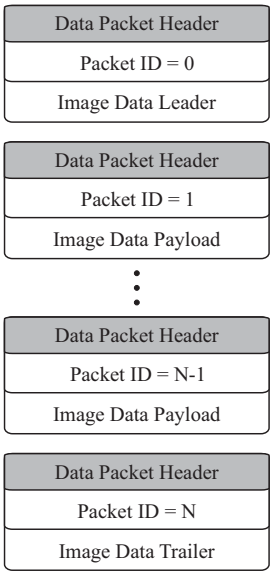

Fig. 4: GigE Vision Streaming Protocol datagram sequence

B. Packet Reception and Payload Extraction

After completion of system initialisation, a child thread is instantiated and registered for data packet reception. The receive thread (Send Data, compare Fig. 1) checks the UPD

socket cyclically for incoming messages and copies available payload to a local buffer. The receive thread validates source address data, byte count, and the CRC-32 checksum (see Fig. 3) of all incoming packets. After successful validation of the received packets, the PARIS datagram payload is extracted, defragmented, and finally forwarded to the Video Display filter.

IV. Results

The Hardware-acceleration Adapter is applied by linking adapter, Image Reader, and Video Display inside the ADTF environment. Fig. 5 shows an example ADTF project configuration. The Image Reader (Image_Reader) feeds image media samples from hard drive to the Hardware-acceleration Adapter (HA_Adapter) which establishes the communication link to the external Hardware-acceleration Module, hosting the FPGA-based PARIS system architecture. The Hardware-acceleration Adapter sends the GVSP-based image stream towards the FPGA, receives the processed results, encapsulates them into media samples, and forwards the media samples to the Video Display filter (Video_Display). The Video Display filter visualises the result image for visual validation.
If the external Hardware-acceleration Module processes non-imagery data of different data type, alternative result visualisation filters can be connected to the generic *dout* port of the Hardware-acceleration Adapter (compare Fig. 5).
For the validation of the Hardware-acceleration Adapter, a simple image scaling operation (1:2) was realised inside the PARIS system architecture. A test video stream with 640×360 pixel resolution was processed using the external hardware-acceleration capabilities. The PARIS result data was received after approx. 1.225 ms (see Fig. 6) which allows a processing rate of more than 800 frames per second with the hardware-accelerated implementation of the image scaling. The value of 800 frames per second is a theoretical number only. Because the ADTF Video Display filter is not able to render hundreds of frames per second with the given resolution. The software-based ADTF framework represents the bottle-neck for the proposed hardware-software-co-designed architecture and the processes for reading sensor data from hard disk, data and result dissemination, as well as result visualisation determine significantly the performance of the overall system.

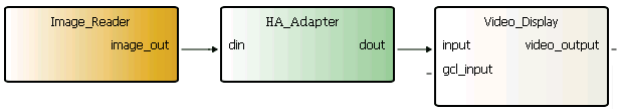

Fig. 5: ADTF filter composition

V. Conclusion

Elektrobit ADTF is a powerful virtual validation framework for development, simulation, and visualisation of software components. Originally designed for automotive software development, ADTF can be used for any kind of applications which focus (multi-) sensor data exploitation and fusion.
This paper presents a novel approach to integrate external hardware-acceleration capabilities to ADTF, which allow both FPGA-based hardware-in-the-loop validation and FPGA-based acceleration of algorithms under test. The presented approach showcases the comfortable, simple integration of FPGA-based hardware-acceleration into ADTF and provides an easy-to-use Hardware-acceleration Adapter to connect the external Hardware-acceleration Module. The flexible, reconfigurable PARIS system architecture on the FPGA serves a powerful Application Independent Interface (AII) to hardware developers to realise and integrate hardware-accelerated algorithms into the ADTF framework. This enables the ATDF software framework to benefit from hardware-acceleration technologies and to develop and validate hardware-software-co-design-based processing concepts. Furthermore, the proposed solution allows the utilisation of the powerful data synchronisation and dissemination management as well as visualisation capabilities of the ADTF toolchain for hardware-acceleration development in the areas of automotive and non-automotive applications.

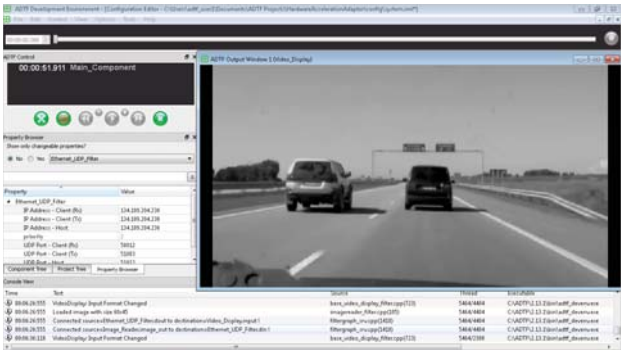

Fig. 6: ADTF GUI with scaling test case

Acknowledgment

The authors gratefully acknowledge the cooperation of our project partners and the financial support of the DFG (Deutsche Forschungsgemeinschaft) within the Federal Cluster of Excellence EXC 1075 ”MERGE”.

References

[1] J. Messner. (2005, December 3). *EB Assist ADTF Automotive Data and Time Triggered Framework* [Online]. Available: https://d23rjziej2pu9i.cloudfront.net/wp-content/uploads/2015/12/09163559/EB_Assist_ADTFTechDay_December2015.pdf
[2] S. Blokzyl, M. Nagler, W. Hardt, “Generic Parallelisation Architecture for Real-time Image Data Exploitation and Sensor Data Fusion on Reconfigurable Integrated Circuits,” unpublished.
[3] J. Postel. (1980, August 28). *User Datagram Protocol* [Online]. Available: https://tools.ietf.org/html/rfc768
[4] V. G. Cerf, E. Cain, “The DoD internet architecture model,” in *Computer Networks*, vol. 7, no. 5, pp. 307-318, 1983.
[5] W. W. Peterson, D. T. Brown, “Cyclic Codes for Error Detection,” in *Proceedings of the IRE*, vol. 49, no. 1, pp. 228-235, 1961.
[6] E. Norouznezhad *et al.*, “A high resolution smart camera with GigE Vision extension for surveillance applications,” in *Proceedings of the Second ACM/IEEE International Conference on Distributed Smart Cameras*, CA, USA, 2008, pp. 7-11.
[7] P. Pellet. (2009, October 15). *ev2 - Linux Embedded applications in Machine Vision* [Online]. Available: http://elinux.org/images/7/73/PascalPellet-e2vELC-E.pdf

Intersection Point Based Power Lines Detecting and Tracking Algorithm

[*]Batbayar Battseren and [+]Hemanth Patchipala and [+]Uranchimeg Tudevdagva and [+]Wolfram Hardt
[*]Power Engineering School
Mongolian University of Science and Technology
Ulaanbaatar, Mongolia
Email: nano.batbayar@gmail.com
[+]Department of Computer Science
Chemnitz University of Technology
D-09107 Chemnitz, Germany
{hemap;utu;hardt}@hrz.tu-chemnitz.de

***Abstract*—In this article, an intersection point based power line detection and tracking method presented. Our concept detects all intersection points of the lines, which are both inside and outside of the image. After that, we will do data exploitation on these intersection points to detect the power line. This method provides both power lines detection and power line tracking direction at once.**

***Index Terms*—UAV, High voltage power line, image processing, line detection, Hough Transform, line intersection.**

I. Introduction

Since the power outage causes significant losses to all consumers of electric power, increasing power system reliability is the one major goal of energy sector. Power system performance directly depends on High Voltage Transmission Line (HVTL) reliability. The HVTL inspection and maintenance are expensive, time consuming and dangerous tasks.

The Unmanned Aerial Vehicle based high voltage power line inspection is becoming more and more popular, and researches have been doing in every corner of the sphere [1]. Currently, according to the low cost, time saving and reliability, the UAV-based method is the best solution for HVTL inspection. Most importantly, it will provide a possibility to do inspection on loaded power line and the safety of the workers could increase significantly. Although, inspection processes and results are still depending on the human ability. To avoid this problem, the UAV based fully automated HVTL inspection system should be developed [2].

UAV based power line inspection is still an emerging approach. In generally, in UAV based aerial inspection, the fault assessment and further analyzing processes done after the flight. In recent years, due to the rapid growth in technology, there are some researches have been done for automated power line inspection and for automated power line detection [3-9].

Most of the methods are based on edge detection. Canny filter is most commonly used for edge detection [10]. There are several other edge detection filters like Pulse Coupled Neural Network (PCNN) and Otsu threshold method [11].

The Hough Transform [9], [12] is the classic method for line detection, also there are several other transformations like Radon Transform, Line Segment Detection algorithm, Edge Drawing [13], Circle-Based Search and many other methods are available for line detection.

In the work of Alexander and Ivan [6], a process for power line detection based on Circle-Based Search approach is defined. In this case, they used Steerable filter instead of Canny filter for better output. Another relevant work for power line detection is Symmetrical partial derivative distribution prior [7] by Cao and Yang, most nature images have symmetry partial derivative distributing. According to this fact, they used radon transformation in partial derivative image to recognize the power lines in the aerial image.

Due to the conventional positioning sensors are not working reliably near to the strong electromagnetic field of the HVTL, there is a high possibility of losing the image of the power line during the flight. The power line detections second main role is image processing based UAV self-navigation

II. The Proposed Method

Like other methods, our proposed algorithm starts with image segmentation and line detection. Afterward, with help of geometric relationship of lines, we will find out the power line and its direction.

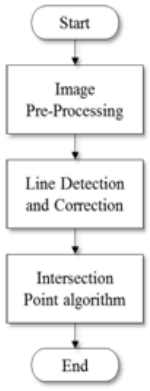

Fig. 1. Step-by-step procedure of The Proposed Method

A. Image Pre-Processing

Original images (see Fig. 3(a)) are transformed from color to gradient image to separate foreground from the noisy background, noisy background is eliminated. Extracting gradient image gives the exact information about edges and image segments. This is an effective process to achieve good results.

Canny Edge Detector is an effective approach [10], which is widely used in image segmentation stage. Canny Edge Detector filter takes less computational time compared to other available filters during segmenting. Steerable Filter is also an option. At the end of this image segmentation process, we will get edges in the image (see Fig. 3(b)).

B. Line Detection and Correction

1) Line Detection: The Hough Transform is widely used in detecting simple shapes in image, such as straight lines, circles and ellipses through mapping each pixel to a new parameter space in which the location and orientation of certain shapes are identified [12].

The Linear Hough Transform uses a 2-dimentional array, to detect the number of lines described by the equation,

$$xcos\theta + ysin\theta = r \tag{1}$$

This is polar representation of lines. Each point (xi, yi) in the xy-plane gives a sinusoid in the (rθ- plane). A line can be detected by finding the number of intersections between curves. The more curves intersecting means that the line represented by that intersection have more points.

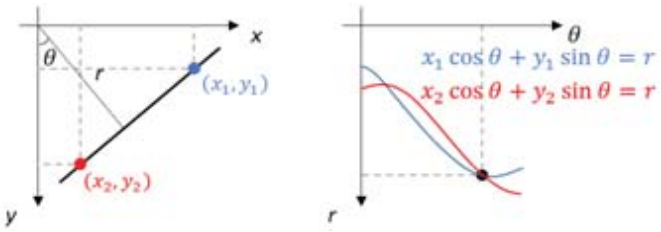

Fig. 2. Line in xy plane (left) and rθ- plane (right)

In general, we can define a threshold of the minimum number of intersections needed to detect a line. Hough Transform keeps track of the intersection between curves of every point in the image. If the number of intersections is above some threshold, then it declares it as a line with the parameters $(ri, \theta$i) of the intersection point. rθ - plane is called Hough Space.

2) Line Correction: After applying Hough Transformation, the output image will contain many different lines and noises (see Fig. 3(c)). For example, in our situation, the line detecting algorithm detects two lines on one power line. The reason is power line has two edges. Also, some lines could be detected like a dashed line.

To decrease the noise and to gain the correct lines, different type of filtering techniques will be used. For instance, we have to merge the close, similar lines to get one perfect line. At the end of this process several main lines will be remain (see Fig. 3(d)).

Fig. 3. Original image (a), Image after Canny filtering(b), Hough Transformed image (c) and Filtered image (d)

III. Intersection Point Algorithm

Where the two lines cross is called their point of intersection. If that two lines are not parallel, they will intersect somewhere. We will use following algorithm to coordinate the all intersections.

1) After Hough line detection, detected lines (ri, θi) parameters will be stored in vector variables. First step is convert it into slope-intercept form.

$$y = ax + b \tag{2}$$

2) Select two lines
3) Set the two equations for y equal to each other.

$$a_i x + b_i = a_j x + b_j \tag{3}$$

4) Solve for x parameter, then based on this parameter solve for y.

This x and y value is the exact intersection coordinate of selected two lines. This algorithm will be repeated on ever pair of lines. There are n lines in a plane no two of which are parallel. They intersect at nC2 distinct points in space.

Lets assume that, there are six lines (a, b, c, d, e, f) detected on the image, as shown in Fig. 4. According to previous process, there will be 15 intersection points (P1-P15), if there are no parallel lines. Although, some lines are the high voltage transmission lines (a, b, c, d) but some of them is unwanted lines (e, f), we call it false lines.

1) Intersection point based power line detection: To rid of this false lines, we need some invariant features which perfectly fits with our condition. Useful invariant features of high voltage power line:

- Lines
- Lines are headed toward one direction

- Power lines will never intersect in the image

In other words, the lines which are not crossed in the frame should be taken and we will focus on the concentrated area of intersection points. Following algorithm will be used for this process:

1) We would not consider the intersection points which are inside of the frame (see Fig. 4, point: P8, P9, P10, P11, P12, P13, P14). Each point which is outside of the frame is represents, that two lines are could be the power line.
2) Find the farthest point (point P1) from the center of frame. It means that two lines (line a and b) have less angular difference.
3) Find the next points (point P2 and P3) which are on that two lines and on that side of the frame. If there are no such point, jump to 5th step.
4) If that two points are belongs to one line, that line is our third line (line c) which is almost same direction with previous two lines. If they are not on same lines, that meant there are two or more lines in that direction (line c and d). Continue until last intersection point on that first two lines.
5) Find next farthest point and do the same process with previous one.

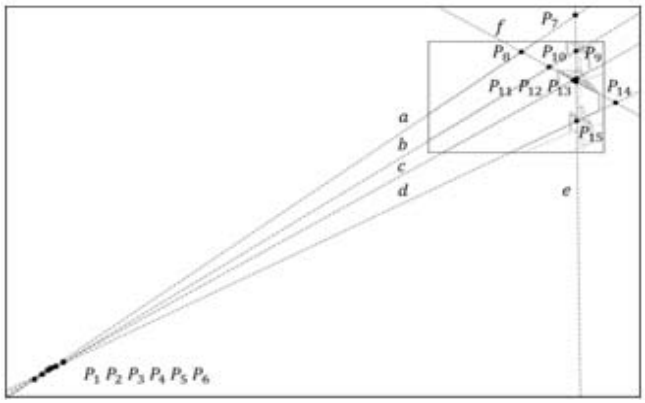

Fig. 4. Lines and intersection points

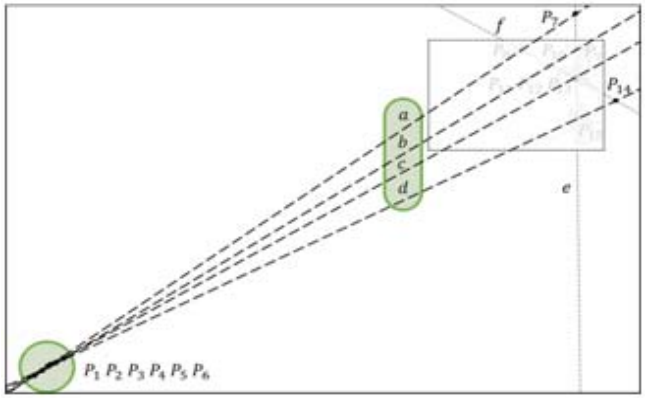

Fig. 5. Intersection point based power line detection

This algorithm provides the correct intersection point concentration. That area represents the possible power line direction and lines in that area are the high voltage power lines.

On our situation, we have only one concentrated area, which represents both high voltage powers line and the heading direction of it. P7 and P14 points are outside of the frame, but there are no concentration and these points are located near to the frame. So, these points are representing the false lines.

IV. Conclusion and Future work

The Intersection Point-based line detection method is suitable for detecting high voltage power lines. This technique requires low computational power, due to the simple mathematical calculations. The next goal of this research is to test it in the numbers of samples and develop the main concept idea.

References

[1] Enkhjargal Khaltar, Uranchimeg Tudevdagva, Chinbat. D, Erdenetsogt. B, Stephan Blokzyl and Batbayar Battseren, The beginning of Unmanned Aerial Vehicle based inspection of HVTL, Power energy and Engineering, vol. 156, Feb 2017, Mongolia, pp. 23-27.

[2] Uranchimeg Tudevdagva, Batbayar Battseren, and Wolfram Hardt. Unmanned Aerial Vehicle Based Automated Inspection System for High Voltage Transmission Lines, Chemnitz University of Technology, Chemnitz, Germany, Power Engineering School, Mongolian University of Science and Technology, Ulaanbaatar, Mongolia, . 2017. 1 (19). . 2832.

[3] Ishino, R., F. Tsutsumi. "Detection system of damaged cables using video obtained from an aerial inspection of transmission lines." In Power Engineering Society General Meeting, 2004. IEEE, pp. 1857-1862.

[4] Jingjing Zhang, Liang Liu, Binhai Wang, Xiguang Chen, "High speed Automatic Power Line Detection and Tracking for a UAV-Based Inspection", Shandong Electric Power Research Institute, Electric Power Robotics Laboratory of State Grid Corporation, Jinan, Shandong, China

[5] Guang Zhou, Jinwei Yuan, I-Ling Yen and Farokh Bastani, "Robust Real-Time UAV Based Power Line Detection and Tracking",Department of Computer Science, University of Texas at Dallas, Texas, USA

[6] Alexander Ceron and Ivan F. Mondragon B and Flavio Prieto, "Power line detection using a circle based search with UAV images", 2014 International Conference on Unmanned Aircraft Systems (ICUAS)May 27-30, 2014. Orlando, FL, USA

[7] Weiran Cao , Xiuyi Yang "Power Line Detection Based on Symmetric Partial Derivative Distribution Prior", International Conference on Information and Automation, Yinchuan, China, August 2013

[8] Carol Martinez, Carlos Sampedro, Aneesh Chauhan, and Pascual Campoy, "Towards Autonomous Detection and Tracking of Electric Towers for Aerial Power Line Inspection", 2014 International Conference on Unmanned Aircraft Systems, May 27-30, 2014. Orlando, FL, USA

[9] Lewis Baker, Steven Mills, Tobias Langlotz, "Power line detection using Hough transform and line tracing techniques", University of Otago, Dunedin, New Zealand

[10] J. Canny, A Computational Approach to Edge Detection, IEEE Transactions on Pattern Analysis and Machine Intelligence, vol.PAMI-8, no. 6, 1986.

[11] Nobuyuki Otsu. "A threshold selection method from gray-level histograms". IEEE Trans. Sys., Man., Cyber. 9 (1): 6266. 1979

[12] Hough, P.V.C. Method and means for recognizing complex patterns, U.S. Patent 3,069,654, Dec. 18, 1962

[13] Cuneyt Akinlar and Cihan Topal, EDLines: Real-time line segment detection by edge drawing (ED), Computer Engineering Department, Anadolu University, Eskisehir, Turk

Multi-Objective Integrated Scheduling Algorithm Based on Allocation Rule Queue

Zhiqiang Xie, Yingchun Xia, Yu Xin
School of Computer Science and Technology
Harbin University of Science and Technology
Harbin, China
hrbust@hotmail.com

***Abstract*—In these years, many integrated scheduling algorithms for complex product based on exact rule methods are proposed, most of them optimize only one objective. Now, we will discuss a multi-objective integrated scheduling algorithm based on allocation rule queue, where the makespan, device load rate and key device load rate are used as objective functions. At first, the scheduling model based on allocation rule queue for the problem is set up. One allocation rule queue corresponds to one scheduling solution. One element of the queue represents a method of selecting a node from available procedure set and allocating a device to the node. Secondly, to evaluate different solutions and select the optimal compromise solution in multi-objective sense, non-dominated sorting method and analytic hierarchy process approach are adopted. Finally, instance result shows that the proposed algorithm is efficient.**

Keywords—integrated scheduling; multi-objective; allocation rule queue; non-dominated sorting; analytic hierarchy process

I. INTRODUCTION

Integrated scheduling problem for complex product concerns the scheduling mode of processing and assembly. A general view of the complex product tree is shown in Figure 1. Each box of the tree means a procedure, and we call it flexibly scheduling problem if a procedure node of the product tree can be processed on different devices flexibly [1].

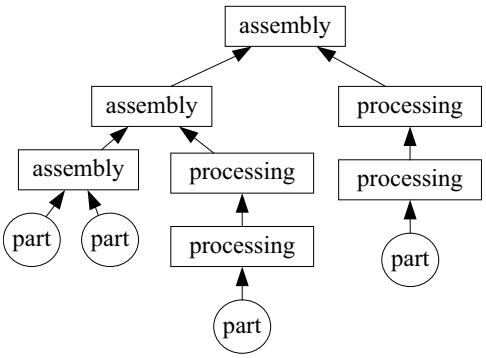

Fig. 1. Integrated mode of processing and assembly

II. PROBLEM MODEL DESCRIPTION

Set n as procedure count of product A, P_x represents a procedure node of the product tree, then we get $A = \bigcup_{x=1}^{n} P_x$. Set m as the processing devices count. Procedure P_x can be processed on different devices flexibly. We could set the mathematical model for the complex product problem as follows:

In the model, X is a scheduling solution of the product.

$$\min\left(f_1(X), f_2(X), f_3(X)\right) \tag{1}$$

$$\text{subject to} \quad f_1(X) = \max \bigcup_{i=1}^{n} end(i) \tag{2}$$

$$f_2(X) = \max \bigcup_{k=1}^{m} \left(\sum_{i=1}^{n} t_{ik} x_{ik} \right) \tag{3}$$

$$f_3(X) = \sum_{i=1}^{n} \sum_{k=1}^{m} t_{ik} x_{ik} \tag{4}$$

$$e(X) < 0 \tag{5}$$

Equation (1) means scheduling goal. Equation (2) is makespan, and $end(i)$ means the completion time of procedure P_i. Equation (3) is objective function of the key device load rate. t_{ik} means how much time it will take when procedure P_i is processed on device k. Set $x_{ik} = 1$ when procedure P_i is allocated to device k, and if procedure P_i is not processed on device k, $x_{ik} = 0$. Equation (4) is the device load rate objective function. Equation (5) means the common constraints of the product tree [2].

III. STRATEGY AND ALGORITHM DESIGN

A. Allocation Rule Queue strategy

Literature [2] only use critical path rule at different stages. Here, we propose an improved strategy of using different rules at different stages, which named Allocation Rule Queue strategy.

B. Rule generator

Random rule generator consists of two pieces: Sorting Rule Generator and Device Allocation Rule Generator. A Rule Generator could return a rule in follows randomly:

1) Shortest Processing Time (SPT).
2) Longest Processing Time (LPT).
3) Critical Path Method (CPM).
4) RANDOM.

C. Pareto sorting strategy

In order to solve the problem that how to estimate different solutions in multi-objective sense, non-dominated sorting method and analytic hierarchy process approach are adopted (AHP) [3].

D. Algorithm Design

According to the above description and analysis, the proposed Multi-Objective Integrated Scheduling Algorithm Based on Allocation Rule Queue is as follows:

Step 1.We will initial solution X_0 by Sorting Rule of SPT and Machine Allocation Rule of SPT, solution X_1 by Machine Allocation Rule of SPT and Sorting Rule of CPM, solution X_2 by Sorting Rule of LPT and Machine Allocation Rule of SPT. Set $i = 0, iteration = 200$.

Step 2.Calculating the objective function values of f_1, f_2, f_3 for solutions of X_0, X_1, X_2.

Step 3.Estimating solutions of X_0, X_1, X_2 by AHP, set $X_b = min\{AHP(X_0), AHP(X_1), AHP(X_2)\}$.

Step 4.According to Rule Generator, random Allocation Rule Queue S is created, decode queue S into a scheduling solution X. Calculating the objective function values of f_1, f_2, f_3 for solution X.

Step 5.Set $X_b = min\{AHP(X_b), AHP(X)\}$. $i = i+1$, if $i < iteration$, go to Step 4, else go to Step 6.

Step 6.The Gantt chart of solution X_b is output.

IV. Instance Analysis

The root element (13/4,10) of the product tree, which is shown in Figure 2, means procedure No.13 can be processed on device No.4, and the processing time on device No.4 is 10 work hours.

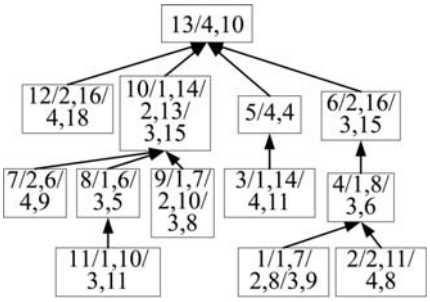

Fig. 2. Product tree of product G1

Figure 3 is the gantt chart ($f_1 = 45$) generated by algorithm of literature [4], and we could get $f_2 = 35, f_3 = 123$, which is calculated by hand. Figure 4 is the gantt chart ($f_1 = 40, f_2 = 33, f_3 = 122$) generated by the proposed algorithm, which is a better solution than literature [4]. The proposed algorithm use random and dynamic strategies, therefore, its generality has been strengthened.

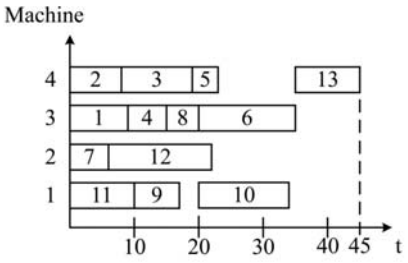

Fig. 3. Gantt chart of product G1

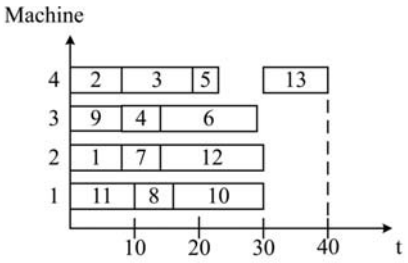

Fig. 4. Gantt chart generated by the proposed algorithm

Conclusions

Aiming at many algorithms for flexible integrated scheduling problem based on exact rule methods optimize only one objective, we have argued a multi-objective integrated scheduling algorithm with three objectives in this paper. Instance result shows that the proposed algorithm is efficient, and the proposed Allocation Rule Queue strategy could strengthen the generality of the algorithm.

Acknowlegment

This project is financed by foundations: National Natural Science Foundation of China (No. 61370086 and No.61602133), China Postdoctoral Science Foundation (No.2016M591541), Postdoctoral Science Foundation of Heilongjiang Province (No.LBH-Z15096), Postdoctoral Scientific Research Start Fund Project in Heilongjiang Province (No.LBH-Q13092), Science and Technology Research Project Foundation of Heilongjiang Province Education Department (No.12531105).

References

[1] Z. Q. Xie, S. Z. Hao, G. J. Ye, and G. Y. Tan, "A new algorithm for complex product flexible scheduling with constraint between jobs," *Computers & Industrial Engineering*, vol. 57, no. 3, pp. 766–772, oct 2009.

[2] Z. Q. Xie, S. H. Liu, and P. L. Qiao, "Dynamic job-shop scheduling algorithm based on acpm and bfsm," *Journal of Computer Research & Development*, 2003.

[3] S. O. Adebiyi, E. O. Oyatoye, and O. L. Kuye, "An analytic hierarchy process analysis: Application to subscriber retention decisions in the nigerian mobile telecommunications," *International Journal of Management and Economics*, vol. 48, no. 1, jan 2015.

[4] Z. Q. Xie, Z. Y. Gui, and J. Yang, "Dynamic parallel integrated flexible scheduling algorithm based on device driver and essential path," *Journal of Mechanical Engineering*, vol. 50, no. 18, p. 203, 2014.

Case study of ICT usage for active learning processes

Danaa Ganbat* and Senden Delgermaa#
Department of Technical Mechanics
Mongolian University of Science and Technology (MUST)
Ulaanbaatar, Mongolia
E-mail: *ganbatda@must.edu.mn; #deegiisenden@must.edu.mn

***Abstract*—In order to improve quality and efficiency of engineering education, modern internet communication technology (ICT) is used for teaching and learning process in fundamental engineering disciplines, such as Engineering Mechanics and Mechanics of Materials for undergraduate students of Mechanical and Construction Engineering specialties at Mongolian University of Science and Technology. Some results of experiments and experiences of using computer and internet technology based tools, for instance, Classroom, Plickers, Socrative are presented in this article. Learning progresses of 195 students are evaluated and followed-up for two semesters. Mid-term and final exam results of 581 students are used for comparison analysis between the traditional teaching methods and the approach based on modern ICT technology. In addition, results for average evaluation parameters of students who studied the course of "Engineering Mechanics" for last seven and eight years were compared to control group students' results.**

Keywords—Classroom, Plickers, Socrative, assessment of student progress, continuous assessment, final evaluation

I. INTRODUCTION

There is an issue in our university - Mongolian University of Science and Technology (MUST), that many students could not receive required scores in both of mid-term and final exams in their first attempt during their study of the fundamental engineering disciplines. For instance, about 27.9%-53.3% of students who studied the course of Engineering Mechanics, passed successfully this subject only after their second or third efforts and 29.1%-48.6% of students failed in each semester Table 1 [2].

Therefore it is needed to find a methodology to increase effectiveness and quality of training process. One of possible way is a regular assessment of students during whole semester and make continues feed-back with them. However, because of large number of students per lecturers it is difficult to make regular evaluation for each students by traditional or conventional methodologies. In order pass this kind of difficulties tried to use competency or result-based active learning method with combination of modern internet and computer based technologies [1], [5].
In other side, nowadays, employers require from the employees not only specialized professional skills, but also transferable skills e.g. potential to use computer and internet technologies [3]. Real-time and continuous use of internet and computer technologies for training processes in higher education stimulate students' self-studying activities and create more opportunities for them, such as communication skills, abilities to use modern internet computer technologies for active learning [4], [6].

Table 1.
Some evaluation parameters of students
who studied course of "Engineering Mechanics"

Academic year	Total number of students	Number of students with the second and third time efforts	Number of failed students based on results of mid-term and final exams
2007-2008	483	130	143
2008-2009	826	282	289
2009-2010	910	382	222
2010-2011	886	380	396
2011-2012	809	419	323
2012-2013	938	496	354
2013-2014	947	498	362

Some results of experiments and experiences using computer and internet technology based tools, for instance, Classroom, Plickers, Socrative for teaching processes in courses of Engineering Mechanics and Mechanics of Materials at MUST are presented in this article.

II. MATERIALS AND METHODS

Three common internet tools used for continuous evaluations of students' progresses during their studies for Engineering Mechanics and Mechanics of Materials courses at the Mongolian University of Science and Technology (MUST): classroom.google.com, plickers.com and socrative.com.

Classroom.google.com. is an online platform tool for various education activities e.g. open information platform is useful for creating and delivering training materials for students, providing easy communication between teachers and their

students in terms of assignments, evaluation and feedback [6]. Using this platform in organizing training process was highly efficient especially for classroom time management.

Plickers.com.is simple and powerfull tool that teachers can assess students in real-time and save collected data. During the real-time assessment, students are required to show their plickers cards with chosen answers to the teacher as shown in Fig. 1 and teacher collects the answers quickly using smartphone with plickers application.

Fig. 1. Using Plickers-Cards for real-time assessment

Socrative.com – is a tool to assess the students with prepared questions. During evaluation process, the questions can be selected randomly and automatically, and each student can be assigned different tasks. The real-assessment can be done for each student.

During the period of two semesters, 195 students, who have attended the "Engineering Mechanics" and "Mechanics of Materials" courses, were assessed by Plickers and Socrative tools every week. Using the data from these tools, comparison analyses were conducted on final exam scores of 581 students who attended these two courses at the MUST. EViews software was used for the statistical analyses, namely one factor model analysis, correlation analysis, and regression analysis.

III. RESULTS

In the one factor model, the data of 581 students with mid-term exam scores from 31 up-to 70 were used.
Correlation analysis was conducted to define a relationship between the mid-term and the final exam scores. Correlation coefficient was determined 0.36 and it is shown that these two parameters have weak relationship. Co-variation matrix is determined as follows:

$$C = \begin{pmatrix} 154.0668 & 38.23879 \\ 38.23879 & 72.28580 \end{pmatrix}$$

Comparison results of mid-term exam and final exam results of 581 students and 195 students in control group are shown in Fig. 2.

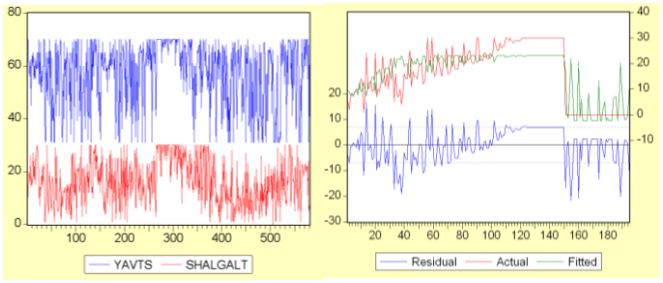

(a). Total students (b). Control group

Fig. 2. Comparison graphs of (a) 581 and (b) 195 students in control group.

Mid-term and final exam scores with statistical parameters are shown in Fig. 3.

Group: UNTITLED Workfile: UNTITLED

View | Procs | Objects | Print | Name | Freeze | Sample | Sheet

	YAVTS	SHALGALT
Mean	57.04475	16.13322
Median	61.00000	15.00000
Maximum	70.00000	30.00000
Minimum	31.00000	0.000000
Std. Dev.	12.42306	8.509432
Skewness	-0.852552	0.078016
Kurtosis	2.501937	1.949765
Jarque-Bera	76.38804	27.29099
Probability	0.000000	0.000001
Observations	581	581

Fig. 3. Statistical parameters of mid-term and final exam scores.

The mean value of the mid-term exam is 57.04 and the median is 61, while for the final exam equals 16.13 and 15, respectively. In the mid-term exam, the skewness value of 0.85 means higher trend than average in the mid-term exam.

Kurtosis values show that sharpness of top of density distribution graphics for statistical series, $K = 2.502$,and $K = 1.95$ for mid-term exam and final exam, respectively. These values show, that the distribution of mid-term and final exam scores have more plain top in comparison with normal distribution.
Standard devations of mid-term and final exams are 57.04±12.42 and 16.13±8.5, respectively (Fig. 4).

Sample: 1 581
Included observations: 581

Method	df	Value	Probability
F-test	(580, 580)	2.131357	0.0000
Siegel-Tukey	(1, 1160)	74.87912	0.0000
Bartlett	1	81.06034	0.0000
Levene	(1, 1160)	85.03759	0.0000
Brown-Forsythe	(1, 1160)	39.25505	0.0000

Category Statistics

Variable	Count	Std. Dev.	Mean Abs. Mean Diff.	Mean Abs. Median Diff.	Mean Tukey-Siegel Rank
YAVTS	581	12.42306	10.36122	9.762478	498.9415
SHALGALT	581	8.509432	7.235216	7.214458	664.0585
All	1162	23.06670	8.798218	8.488468	581.5000

Bartlett weighted standard deviation: 10.64760

Fig. 4. Parameters of standard deviations of mid-term and final exams

Regression analysis was conducted using mid-term exam scores and final exam scores using following model:

Mid-term scores = 0.529 x Final exam scores + 48.510.

Multi-factor analysis was carried out to determine the relationship between mid-term exam scores and final exam scores for 195 students in control group.

Correlation analysis was conducted to determine the relationship between continous assessment scores in every week, mid-term exam scores and final exam scores. Correlation matrix was defined as follows:

$$\begin{pmatrix} 1.000 & 0.983 & 0.753 \\ 0.983 & 1.000 & 0.782 \\ 0.753 & 0.782 & 1.000 \end{pmatrix}$$

The matrix values show (a) very strong relationship between the scores of assesment in every week and mid-term exam scores with correlation coefficient of 0.983; (b) a strong relationship between the scores of assesment in every week and final exam scores since they have correlation coefficient of 0.753; (c) a strong relationship between the mid-term scores and final exam scores since they have correlation coefficient of 0.782.

The mean values of the scores of assesment in every week, mid-term and final exam scores are 24±10.45, 51.33±23.65 and 16.09±11.31, respectively. The median values of the scores of assesment in every week, mid-term exam and final exam scores are 28, 62 and 18, respectively (Fig. 5).

The skewness values ofthe scores of assesment in every week, mid-term exam and final exam scores are (-1.41), (-1.19) and (-0.236), respectively.

The Kurtosis values of the scores of assesment in every week, mid-term exam and final exam scores are 3.65, 3.03 and 1.595, respectively.

EViews Basics - [Group: UNTITLED Workfile: UNTITLED]

File Edit Objects View Procs Quick Options Window Help

View Procs Objects Print Name Freeze Sample Sheet Stats Spec

	NEMELT	YAVTS	SHALGALT
Mean	24.00256	51.32821	16.08718
Median	28.00000	62.00000	18.00000
Maximum	32.00000	70.00000	30.00000
Minimum	0.000000	0.000000	0.000000
Std. Dev.	10.44839	23.64874	11.31998
Skewness	-1.408140	-1.191429	-0.235390
Kurtosis	3.648112	3.026075	1.595218
Jarque-Bera	67.85579	46.13938	17.83474
Probability	0.000000	0.000000	0.000134
Observations	195	195	195

Fig. 5. Statistical parameters of multi-factor analysis

In order to determine how final exam scores are related to the assesment scores in every week and mid-term exam scores, multi-factor regression model is developed as follows:

Final Exam = 0.589 x Mid Exam + 0.495 x Week Assesment - 2.283

From this model we can see that if the mid-term exam score is increased by 1 point, the final exam score is increased by 0.589 point and if the score of assessment in every week is increased by one point final exam score is increased by 0.528 point.

In the Table 2, comparison of evaluation results of continuously assesed control group students with previous year students.

Table 2

Comparison analysis of average evaluation parameters for students who studied the course of "Engineering Mechanics" with the Control group students

Academic year	Mid term scores /70 point/	Final exam scores /30 point/	Average of the final assessment scores /100 point/
2007-2008	51,64	16,14	67,78
2008-2009	59,31	11,35	70,66
2009-2010	51,5	14,5	66
2010-2011	57,22	15,48	72,70
2011-2012	56,33	16,34	72,68
2012-2013	57,11	16,9	74,01
2013-2014	58,1	15,7	73,8
Continously assessed Control Group students	62	18,1	80,1

IV. Discussion

Statistical parameters for scores of the assessment in every week were made by using exam results data from 195 students from the control group, while the mid-term and final exam scores were of 581 students.

Student's *t* test was used to determine the accuracy for comparison analysis on differences of mean values for two statistical parameters. *t* values in mid-term, final exam and in total assessment scores were t=0.103 (p<0.05), t=0.167 (p< 0.05), t=0.224 (p< 0.05), respectively. This implies that all of these statistical parameters have importance level of (p< 0.05) or 5% and true differences of mean values of these two groups have probability of 95%. Therefore, if students are assessed every week it would positively influence the students' scores in mid-term and final exam and consequently total scores for evaluation of knowledge on the subjects [4].

This study shows that the modern ICT technologies, such as classroom, plickers and socrative are effective tools that support more close collaboration between teachers and students during education/training processes. They provide many advantages for instance, more effective and open communication and information sharing, easier distribution of training materials, tasks and assignments, scheduled assessments etc. [8].

As shown in Table 2, the results of this study show the importance of continuous assessment during education processes. Continuous assessments and providing feedback based on the assessment results help students to systemize their knowledge, understand the contents and concepts of each topic. Online education platforms classroom, plickers and socrative provide opportunities for students' self-tests, quizzes, make possible every week continuous assessments for them, and mainly stimulate students to gain in deep knowledge of the subjects and have good results in the exams [9], [10].

V. Conclusions

The results of this study confirmed that there is a positive relationship between continuous assessments for the students' learning process and final exam performances, or regular assessments led to improvements in students' mid-term and final exam scores. In addition, the regression model and correlation results confirmed this positive trend even though only one control group was checked in this case study. In the future, it is needed to check our regression model in more control groups as increasing number of teaching courses with number of students.

References

[1] Badarch D. Innovation on Higher Education Reform.Ulaanbaatar, 2013; 213-235.

[2] Delgermaa.S "Some issues on improvement of methods for assessing student knowledge, abilities and skills" Doctoral dissertation, 2015, NUM, Mongolia.

[3] UNESCO World Conference on ESD 2014; 374

[4] Dneprovskaya N. and Komleva N. Open Reseources for Education. 2014; 86-88.

[5] Narantsetseg N. and Tuguldur E. Education Management. Ulaanbaatar, 2010; 43-56.

[6] Unurnasan. Education Evaluation System based on Internet. Ulaanbaatar, 2010; 67-86.

[7] Beadle, P. How to Teach: The ultimate (and ultimately irreverent) look at what you should be doing in your classroom if you want to be the best teacher you can possibly be. Crown House Publishing, 2010; 164-172.

[8] J. Scott Armstrong. Natural Learning in Higher Education. Encyclopedia of the Sciences of Learning, 2010; 112-139.

[9] White, M., Distance education in Australian higher education-a history', Distance Education, Vol. 3, 1982; 89-91.

[10] RDI, UK university courses now offered on Mobile Devices, Retrieved. 2009; 125-128.

Support of Inclusive Education of Student with Hearing Disabilities based on Computer Sign Language Translation System

Michael Grif, Yuliya Manueva
Department of Automation and Computer Engineering
Novosibirsk State Technical University
Novosibirsk, Russia
juleno4eknot1@rambler.ru

Abstract –**In this paper, the problem support of inclusive education deaf students is observed. One of possible solution of this problem is a computer sign language translation system. Currently translation from Russian sign language to Russian-sounding language is difficult because of inadequate attention to hardware recognition sign language. The translation system from Russian-sounding language to Russian sign language is considered. A new method for constructing a semantic unit of the computer system of sign language is shown. The result of the semantic analysis system is a list of correspondence "word-gesture." Among the many alternatives to words based on semantic analysis algorithm, every word is assigned a unique lexical meaning.**

Keywords— inclusive education, Russian Sign language, computer Sign language translation, semantic analysis, homonyms, lexical meaning

I. INTRODUCTION

The modern system of education is aimed to training highly qualified personnel, who have a great creative potential. For fruitful work in one area requires knowledge and related areas. Almost every tenth Russian has hearing problems, so higher education this population is difficult due to the lack of barrier-free communication between the university community and the hearing impaired student.

In Russia at the present time a lot of attention is paid to the firmware support inclusive education of persons with hearing disabilities. These tools include a computer Sign language translation system, which in the near future will successfully overcome the barriers in communication between the deaf and hearing citizens (students), as well as to ease the shortage of Russian Sign language interpreters [5].

Within the concept of inclusive education in the Russian system of computer sign language should include a module of semantic analysis and translation module on sign language, which will take into account its features.

II. INCLUSIVE EDUCATION OF STUDENTS WITH HEARING DISSABILITIES

The society rethinking and government the ratio for persons with disabilities, the recognition of their rights to equal rights with other opportunities in different areas of life, including education, led to the active development of inclusive forms of education, training and rehabilitation of this category of citizens at all levels and stages education.

The Federal Law of the Russian Federation dated December 29, 2012 N 273-FZ "About education in the Russian Federation" inclusive education is defined as the provision of equal access to education for all students, given the diversity of special educational needs and individual capabilities [6-7].

In accordance with the law of the person with disabilities an opportunity to study in an ordinary group of students. To enable persons with disabilities in the educational process must take into account their psychological and physical abilities. For each type of activity limitations (hearing impairment, visual impairment, mental retardation, and disorders of the musculoskeletal system) is supposed to own approach for higher education on a par with ordinary students.

We single out the main features of hearing impaired students in teaching in higher education. Hearing loss leads to a significant restriction of communication with others. There is a difference in the mental development rate [8,10].

The educational process of hearing students is an integral part of the attraction sign language interpreter (sign language interpreter). Prior to the implementation of inclusive education sign language interpreter was the decision of problems of communication students with disabilities by ear and teachers. At the moment, hearing-impaired student has the opportunity to study with students who do not have hearing problems. The obvious solution to the problem is to attract the same sign-language interpreter.

At first glance, the best solution is a sign language interpreter, an assistant teacher. Thus, every teacher in the class should have a sign language interpreter. But here there is a significant problem: for example, the number of teachers at the Novosibirsk State University has about 1,750, and the number of sign language interpreters in the this university is only 8 people [1].

There are three main approaches to the organization of educational process of the students with special needs. The first approach is the training in specialized educational institutions. An example of this approach is the Institute of social technologies and rehabilitation of the Novosibirsk State

Technical University, which was founded in 1992 as a specialized educational institution conducting the training of students with disabilities. At the moment, the Institute trained about 300 students from various regions of Russia [2].

By the second method, we put the distance learning technology. For student and teacher interaction, a system of remote sign language translation is applied.

Number of sign language interpreters is often limited. For the smooth operation of the program must be a sufficient number of sign language interpreters. Active human intervention in remote sign language interpreter is the main drawback of this system. In addition, significant investments are required not only in the software part, but also in the hardware.

This lack of a system devoid of computer sign language to Russian-sounding language to Russian sign language and vice versa (Figure 1). In the role of the translator in this case is a computer program sign language, which is a closer look at in the next section.

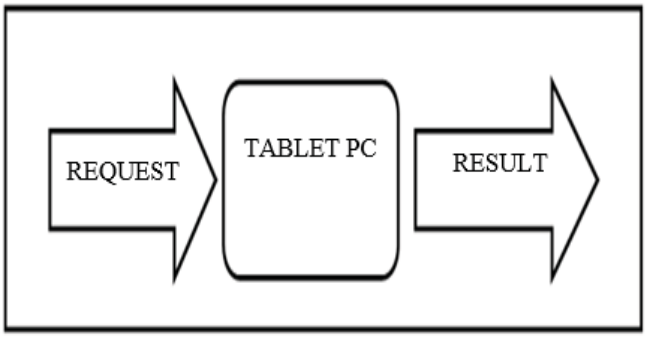

Fig. 1. Entering the sentence into the system

III. COMPUTER SIGN LANGUAGE TRANSLATION SYSTEM

In Novosibirsk, it was developed translator to translate speech to Russian sign language. The purpose of this development is that the way people with hearing disabilities can communicate with other people. Firstly, speech recognition is execute, then the analysis of text is carried out and then result of it is translated to Russian sign language [8].

The translation process is completed by the working of animated personage. Translation is made by the rules of Russian sign language, in contrast to the majority of cases, when a loan translation is performed. Sign language speakers do not understand this translation. The Sign language computer translation system consists of two interrelated systems, forward and reverse translation.

The main problem in the translation from Sign language to sounding speech is gesture recognition problem. For a competent analysis of individual gesture recognition is not enough, it is necessary to recognize gestural speech, gestures change the dynamics for the correct transmission of proposals sense. For gesture recognition are the two groups of devices: devices based on image data and devices that use the accelerometer, magnetometer, gyroscope.

The greatest interest is the translation system from Russian-sounding language to sign language. Computer sign language translation system consists of four subsystems [1]. First part is a recognition system of Russian-sounding language, based on the development of Google voice recognition company. Second is a Russian text analysis system, including morphological, syntactic and semantic analysis. This module is based on freely available code (Dialing System) [4]. Third part is a syntax conversion system from Russian language to Russian Sign language. The translation processes ends by systems of display Russian Sign language. There are two embodiments of the visualization of gesture: photographing models, demonstrating certain gestures, and stores them in a database system; the creation of a virtual character to demonstrate the gestures [3].

In step of speech recognition, text string is obtained for subsequent analysis. At the stages of morphological and syntactic analysis is determined by a set of necessary morphological and syntactic features. To improve the quality of translation semantic analysis system has been developed.

The sense of unity of the Russian language depends on its relationship with other units of the language and its lexical and syntactic compatibility with them.

The problem of lexical ambiguity resolution is one of the priority issues in the process of translation from one language to another, because of the proper operation of the module depends on the semantic meaning of the text. Of particular interest in this regard are homonyms and idioms. To determine the meaning of words used Dictionary made by Vitaliy Tuzov [9].

Semantic analysis unit starts its operation after the morphological and syntactic analysis. The main task of semantic analysis is building a list of alternatives and independent calculation of semantic-grammatical type of each alternative, part of the description. These transformations are carried out in several stages. The first step is to search for all alternative meanings for each word in a sentence search alternatives. In the second phase, the following ancillary jobs are numbered and identified all the alternatives of each word, to make a semantic class number words from the semantic description of all the arguments submitted.

Built description consists of a set of alternatives, each of which contains two main parts: morphological semantic class indicating words and semantic. The first part contains information about alternatives is to what words can join this word, the second part - which words it can attach. When assembling the interaction take two standing next to the structure.

The next stage of the semantic module is processing of phraseology. The semantic dictionary idioms are defined in the individual alternatives. Therefore, they are processed in the first place, to further reduce the number of scanned values. The process of prepositions processing consists of two phases. First searches prepositional-case combinations. The correct choice of semantic description pretext of envy from the related noun.

As a result, we find that each correspond to a single preposition semantic description. Further operation of the analyzer depends on the type of offer. We distinguish two types of proposals: the first - the proposal as part of that one word has several alternatives, the second time - in the sentence of a few words. In the first case there is no loop, and only one word is analyzed. The analysis depends on the parts of speech ambiguous word. To date, the analyzes: verbs, nouns,

adjectives, infinitives, participles, gerunds, adverbs. in each case different algorithms are applied.

IV. CONCLUSION

In this paper, the problem of inclusive education deaf students in higher professional education is analyzed. As a solution to this problem, a system of remote computer Sign language translation and computer Sign language interpretation system are proposed. Currently translation from Russian Sign language to Russian-sounding language is difficult because of inadequate attention to hardware recognition of Sign language. The translation system from Russian-sounding language to Russian Sign language is considered. A new method of construction of semantic unit in the computer translation system of Sign language is developed. The result of the semantic analysis system is a list of matches "word-gesture." Among the many alternatives to words based on semantic analysis algorithm, every word is assigned a unique lexical meaning. For simple sentences designed and implemented semantic analysis algorithms. The most priority directions of the modification of the semantic analysis module include the following: broadening the base of gestures, the implementation of parsing complex sentences, add the account in the algorithm analyzes the specifics of Russian Sign Language.

REFERENCES

[1] Grif M.G., Manueva J.S., Kozlov A.N. Development of computer interpretation system - Postroinie sistemi kompiuternogo surdo-perevoda. SPIIRAS Proceedings - Trudy SPIIRAN –, 2014, no. 6 (37), pp. 170–183.

[2] Grif M.G., Timofeeva M. K. The problem of automation of sign language from the perspective of applied linguistics - Problemi avtomatizacii surdoperevoda s pozicii prikladnoi lingvistiki. Siberian Journal of Philology Sibirckii filologiskii gurnal, 2012, no.1, pp. 211-219.

[3] M.G.Grif, J.S.Manueva Historical aspects of computer interpretation system to sign language – Istoricheskie aspecti rasvitiya sistem komputernogo surdoperevoda. NSTU Proceedings – Sbornik nauchyh trudov NGTU, in press.

[4] Sokirko A.: Semantic vocabularies in automatic text processing (based on DIALING system papers). PhD thesis, MSPIFL. Moscow, p. 108 (2000)

[5] Grif M.G., Korolkova O.O.: [Development of computer sign language interpreter sounding speech at conversational Russian sign language]. In: Informatika:problemi, metodologiya, tehnologii. Materiali XI meshdunarodnoi nauchno-metodicheskoi konferencii [Computer science: problems, methodology, technology. Proceedings of the XI International Scientific Conference], pp. 206-208 (2011) (In Russ)

[6] Grif M.G., Korolkova O.O., Panin L.G., Timofeeva M.K.,Tsoi E.B.: Leksicheskie i grammaticheskie aspect razrabotki kompyuternogo surdoperevodchika russkogo yazika: monografiyu [Lexical and grammatical aspects of the development of computer sign language Russian language: monograph]. Novosibirsk: NGTU, p. 292 (2013) (In Russ).

[7] Grif M.G., Demyanenko Y.A., Korolkova O.O., Tsoy Y.B.: Development of Computer Sign Language Translation Technology for Deaf People. In: Proc. of the 6th Internation Forum of Strategic Technology (IFOST 2011), pp. 674-677 (2011)

[8] Grif M.G., Korolkova O.O., Tsoy Ye.B.: On Peculiarities of the Russian Language Computer Translation into Russian Sign Language for Deaf People. In: Proc. of the 2-nd IndoRussian Joint Workshop on Computational Intelligence and Modern Heuristics in Automation and Robotics. Novosibirsk, NSTU, pp. 219-222 (2011)

[9] Tuzov V.A.: Computer semantics of Russian language, tutorial. Saint-Petersburg, SPSU, p. 391 (2003)

[10] Korolkova O.O.: Russian Sign Language Morphology. In: Modern linguistics and intercultural communication: monograph, Book 3.: O.A. Berezina, N.V.Bizyukov, O,O, Korolkova and others. Krasnoyarsk, Research and Innovation Center, pp. 60-87 (2011)

The Computational Method for Self-Diagnostical System

Yumchmaa Ayush* and Grif M.G#
Faculty of Automation and Computer Engineering
Novosibirsk State Technical University
Novosibirsk, Russia
*yumchmaa@must.edu.mn, #grifmg@mail.ru

***Abstract*— This paper describes the interrelation of the symptoms of separate diseases which a based on human constitutions by representation as a computational method. Our research focused to create a medical expert system which combines traditional medicine of Asian countries like Tibet, Chine, and Mongolia with European medical symptom based diagnostics. During last three years research we found out that to produce hardware for such us medical expert system need contribution of many other researchers of different fields. Based on this state we reduced frame of our research focus more to objective target. This is the interrelation of the symptoms of separate diseases which a based on human constitutions by representation as a computational method.**

***Keywords*— human; three constitutions; wind; bile; phlegm; relation between constitutions and diseases**

I. Introduction

In traditional medicine, the human is an entire system that can define by individual features which are called wind, bile and phlegm. According to eastern medicine, from the first day of human's life in the womb, three constitutions begin to arise in the human body. In most case, one of these three features dominates the others. The combination of those three elements indicates the personal character, life-style, health and disease.

There are numbers of self-diagnostic system has been developed by the cooperation of doctors and computer engineers in last few years [1].

The medical diagnostic expert system susceptible as to a natural language of doctors and patients and as the formalized computer language has to be developed. It will allow come to the heuristic diagnosis which will be a basis of medical artificial intelligence [2].

II. Aspects of Human Three Constitutions

A. Human and Nature

In traditional medicine doctor-lama considers relations between human and the mother world. The three main constitutions are the major aspects of human health. The human body has a unique capability to resist different types of pathogenic factors also to maintain a relative balance inside the body and with the outside world.

Some researchers consider that in three levels:

1. The first is actually wind, bile and phlegm in an organism.
2. The second — these terms are meant as all processes in organism somehow connected with wind, bile and phlegm. (For example, the system of bodies, such, as digestive, a liver, a gall bladder etc. can be understood as bile).
3. The third — these terms any processes (cosmo-physical, natural, etc.), somehow similar on action call.

B. Basic principles of basic three elements

Philosophical idea of these three elements is based on the initial five elements which are wind, fire, earth, space, water. As in traditional medicine, all living thing in universe, for example seed, plant, insect, animal and even human have same principle which is evolutionary cycle [3]. Every element has their own purpose and imbalance of these things could cause variety of mental and physical diseases and pain.

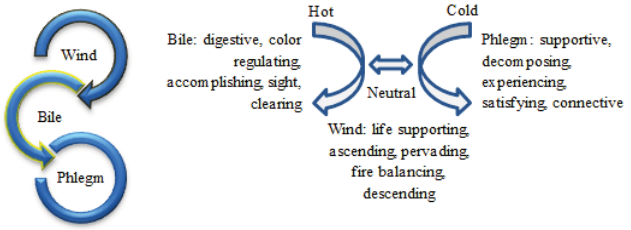

Fig .1 Basic three elements and their 5 aspects

In addition, each element has 5 different types and each of them located in the different parts of human body (Fig.1). Wind is in the lower body, the Bile is in the middle and the Phlegm is in the upper body. For instance, cause is the major concept of diseases in Eastern medicine. In this case, they elements are the immediate causative factor which is due to seasonal factors, harmful evil spirits, improper eating and behavior, that result in increase, decrease or disturbance of the three elements that eventually rules the body and mind [4].

In addition, it depends on the age of human. Example, element Wind gets bigger at old age.

But, private physical properties of human don't change at all. Some modern traditional doctors distinguish on their book

about three main constitutional types of human: wind, bile and phlegm [5]. It means like differences of human types at the Western medicine.

III. Interrelation between Human Constitutions and Diseases

The constitutions are generally determined by human body type and external features for example, height, weight, proportions of the various body measurements. These are established by anthropometric measurements. Also, human morphology is affected by the major constitutions. In most case, one or two constitutions dominate. In very rare condition, some people does not have any dominant constitution, which means the main three elements are balanced equally and we believe that man or woman is physically and mentally strong and healthy human. According to the constitutions ratio, all human beings can be categorized as 3 dominants, 3 combined and 1 complicated. Also, in the practice, there hasn't any evidence that someone has only one or two constitutions.

TABLE I. Some special features of human dominant constitutions

	Types of basic human constitutions	*Special features*
1	Wind	Stooped, skinny, dark blue complexion, over talkative, unable to endure cold and wind, shuffling of joints when walk, small in stature, poor strength of the body, little sleeper, love to sing, to dance, grapple and to bet. Like sweet, sour and bitter foods.
2	Bile	Tend to be more rounded often hungry and thirsty, yellow complexion, yellow hair, intelligent, arrogant, sweaty with putrid smell, middle in stature and strong. Like sweet, bitter, eager, fresh drink.
3	Phlegm	Little heat in the body, heavy, pale complexion, with the thrown back arrogant, burly, able-bodied, able to endure protracted hunger and thirsty, sleeper, quiet. Like sour, musty, heavy foods.

In many ancient books, there are numbers of scripts about the diseases, their cause and treatments, which are divided according to these three basic constitutions.

In Table I, it shows some special features of each type of human dominant constitutions. For combined and complicated constitutions, it's possible to know what kind of human from their mixed physical properties.

TABLW II. Number of questions and expression values their characters

Questions	*A (Wind)*	*B(Bile)*	*C (Phlegm)*
Q1	QA1	QB1	QC1
Q2	QA2	QB2	QC2
Q3	QA3	QB3	QC3
Q4	QA4	QB4	QC4
Q5	QA5	QB5	QC5
Q6	QA6	QB6	QC6
Q7	QA7	QB7	QC7
Q8	QA8	QB8	QC8
Q9	QA9	QB9	QC9

If human have a dominant constitution then he has special features more than other constitutions. In that case, human can determine your constitution by questioning based on the own feeling.

TABLE III. Questions and their points for definition human constitutions.

Constitutions	**Wind**			**Bile**			**Phlegm**		
Questions	**Yes**	**No**	**Maybe**	**Yes**	**No**	**Maybe**	**Yes**	**No**	**Maybe**
Q1	10	0	5	10	0	5	10	0	5
Q2	10	0	5	10	0	5	10	0	5
Q3	10	0	5	10	0	5	10	0	5
Q4	10	0	5	10	0	5	10	0	5
Q5	10	0	5	10	0	5	10	0	5
Q6	10	0	5	10	0	5	10	0	5
Q7	10	0	5	10	0	5	10	0	5
Q8	10	0	5	10	0	5	10	0	5
Q9	10	0	5	10	0	5	10	0	5
Total points	**90**			**90**			**90**		

Example:

TABLE IV. Answers according to the given question

Constitutions	**Wind**			**Bile**			**Phlegm**		
Questions	**Yes**	**No**	**Maybe**	**Yes**	**No**	**Maybe**	**Yes**	**No**	**Maybe**
Q1	10					5		0	
Q2		0			0			0	
Q3	10					5		0	
Q4			5	10				0	
Q5	10					5		0	
Q6	10					5		0	
Q7			5	10				0	
Q8	10				0		10		
Q9	10					5			5
Total points	**60**		**10**	**20**		**25**	**10**		**5**

From Table 4 can be built decision trees and can be easily converted into *IF THEN Rules*.

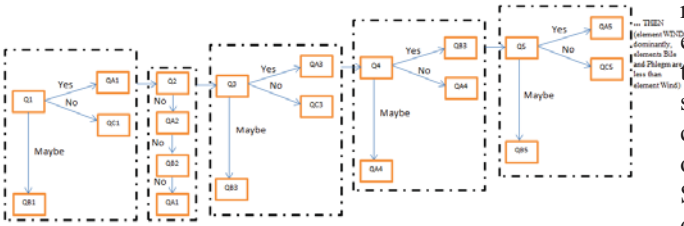

Fig .2 Decision tree for definition of different types human constitutions.

IF (QA1>5 OR QB1=5 AND QC1<5) THEN Q2,
IF (QA2<5 AND QB2<5 AND QC2<5) THEN Q3,
IF (QC3>10 OR QB3>5 AND QC3<0) THEN Q4,
IF (QA4<5 OR QB4>5 AND QC4<5) THEN Q5,
IF (QA5>5 OR QB5=5 OR QC5<0) THEN Q6,
IF (QA6>5 AND QB6=5 OR QC6<5) THEN Q7,
IF (QA7=5 OR QB7>5 AND QC7<5) THEN Q8,
IF (QA8>5 OR QC8>10 OR QB8<0) THEN Q9
IF (QA9>10 OR QB10=5 OR QC9=5) THEN (element WIND dominantly, elements Bile and Phlegm are less than element Wind) [6].

In that case, this person is element Wind dominantly and attributes of elements Bile and Phlegm are less than element Wind.

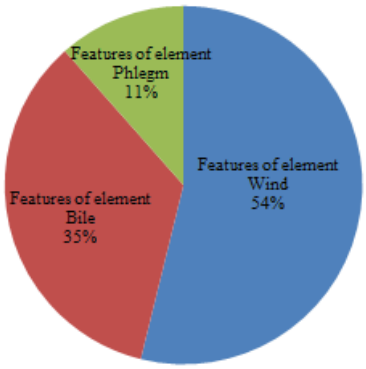

Fig .3 Example of human constitutions which element Wind dominantly

Previously, in the books written about cause of diseases depends on the human constitution and their balance. In Fig. 3, it's shown one example of human constitutions which is element Wind dominantly by diagram.

Example, element Wind is considered as the backbone of many diseases and it is an air. Air is vital human survival and its quality is active. It more supports activity of nervous system and cardiovascular system of human. It is the vital spirit passing through all things, giving life to all things, moving and filling all things. Accordingly, this affects to emotion, attitude yourself and the environment. In there, must to diagnose diseases by manifestations or by observing symptoms and signs. In fact, the element Wind is most common cause of all diseases, because contains the attributes of elements Bile and Phlegm and locates at each parts of body. So, it is highly important event for treatment to know about disturbance of element Wind. Therefore, in the recent time, the some Eastern medical modern books are written about that if human dominates element Wind then it's in higher risk to suffer mental and cardiovascular diseases [1].

I.

CONCLUSION

The self-diagnostic system can be used during the practical work in out-patient departments, for training in higher education institutions and in the research purposes. The new system allows researchers to intend for the visual analysis of data of constitutionally diagnosis, and also for formation of the expert description and the conclusion about a human's health state.

The most important step is to create abstract rules from a number of questions and answers. It will give to make decision based on the human's own information about their private physical properties by criteria Eastern medicine. The symptoms of diseases based on human constitutions are introduced into the knowledge base of medical diagnostic system and used for definition of diseases based on the fuzzy and probabilistic models.

REFERENCES

[1] T. Uranchimeg, S. Uyanga, A. Yumchmaa, "A Prototype of Expert System for Rural Medical Centers," 7th International Conference on Frontiers of Information Technology, Applications and Tools, and the 4th PT-ERC International Symposium on Personalized Medicine, FITAT/ISPM 2014, 29 July – 01 August 2014. Thailand, 2014, pp. 23-26.

[2] A.Yumchmaa, R.Davaasuren, "Object Oriented Medical Technical Expert System", International Summerschool Computer Science 2014, Proceedings of Summerschool 7-13.July, Germany, 2014, pp.44-47.

[3] Ch.Baavgai, B.Boldsaikhan, Mongolian Traditional Medicine. UB: State Publ., Mongolia, 1990.

[4] Kh.Tumba, Four fundamentals of medical science. UB: State Publ., Mongolia, 1991.

[5] S.G.Choijinimaeva, Tibetan medicine: unity of a body, reason and spirit. About diseases wind, bile and phlegm. St.Peterburg: Piter, Russia, 2015.

[6] M.G.Grif, Yu.Ayush, "Application of expert systems by pulse diagnostics", Transaction of scientific papers of the Novosibirsk state technical university, no. 3 (81), pp. 114–133, 2015.

The design of high efficiency personal computer power supply

Yu-Bo Liu, Xu-Dong Wang, Xiao-Li Wang
Institute of Electrical and Electronic Engineering
Harbin University of Science and Technology
Harbin, 150020, China
e-mail: yubo_ryan@yahoo.com

***Abstract*— In this paper, the key problem of personal computer power supply is studied to improve the efficiency of power supply. The power supply design for the personal computer(PC), which adopt LLC resonant converter and synchronous rectification as core topology, can reduce the volume and improve the efficiency. The analysis of basic principle of the proposed converter will be presented. The output voltage regulation of LLC resonant converter using a PID controller in feedback loop for the personal computer is proposed. The dominant pole and phase margin tuning system PID is used in controller. Experimental results demonstrate that the method of tuning PID parameters accurately, the LLC resonant converter can achieve a significant efficiency improvement in a 300W prototype converter.**

Keywords—personal computer, power supply, LLC resonant converter, PID tuning

I. INTRODUCTION

With the increasing popularity of computers, computer performance requirements are getting higher and higher, the power level of computer power supply is also growing. When the PC was introduced, it was used only for performs various works, such as text, music, video, entertainments, programming, graphic and so on. Conwequently, current PC requires more electric power and the importance of the PC power supply unit (PSU) has been increased significantly.The switching loss of the conventional computer hard switching power supply is very large. The power density of the conventional PC PSU is small, and the efficiency is low.Therefore, a LLC resonant converter is proposed as the topology of the PC PSU. The LLC resonant converter has the advantages of simple structure, high power density and high conversion efficiency. It can achieve the zero voltage switching (ZVS) of the switches in the full voltage input range and the full load range. The PC PSU based on LLC resonant converter has the advantages of high efficiency and small volume. Therefore, it has a very bright application prospect in the future[1][2].

Dominant pole and phase margin method proved to be a very effective method of PID parameters tuning[3][3][5]. This method has been widely used in PID controller. The output voltage of the converter is regulated using PID controller in feedback path. The PID controller regulates the output voltage by adjusting frequency of the gate pulses of the MOSFETs. The operational principle, analysis, design and experimental results are presrnted to confirm the validity of the proposed converter.

II. DESIGN OF THE PROPOSED CONVERTER

LLC resonant converter has gained a lot of attention and has been widely discussed in literature for having simple structure and several desirable features like high power density, reduced switching losses at high frequencies, high efficiency, zero voltage switching (ZVS), zero current switching (ZCS), low electromagnetic interference (EMI) and elimination of reverse recovery of the output rectification diodes[6]. LLC resonant converter circuit simplified is shown in fig. 1.

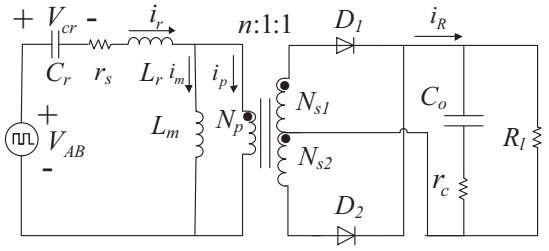

Fig. 1 Equivalent circuit of the LLC resonant converter.

LLC resonant circuit switch network is simplified to ac square wave voltage source, and its amplitude is V_{AB} , its frequency is equal to the LLC switching frequency. The circuit has four energy storage elements, L_r , L_m , C_r and C_o . L_r is the inductance of the transformer leakage inductance. L_m is the transformer magnetizing inductance, and the transformer model is the ideal model which only represents the ratio of the former to the side. Inductor currents and capacitor voltage are chosen as the state variables of the system. r_s is the resonant capacitor equivalent series resistance, r_c is the output filter capacitor equivalent resistance.

For LLC series resonant converter there are two resonant frequencies, the first involves L_r and C_r and the second involves L_m also and are given by

$$f_{r1} = \frac{1}{2\pi\sqrt{L_r C_r}} \tag{1}$$

$$f_{r1} = \frac{1}{2\pi\sqrt{(L_r + L_m)C_r}} \tag{2}$$

Equation (1) is always true regardless of load but (2) is true only at no load. Mostly LLC resonant converter is designed to operate in the vicinity of resonant frequency f_{r1}. For the above two resonance frequencies $f_{r2} < f_{r1}$ and, the separation between f_{r1} and f_{r2} depends upon the inductance ratio $k = L_m/L_r$ and increases with increase in k. The switching frequency f_s controls the power flow from input to the load which increases with the decrease in f sw and vice versa. The LLC resonant converter's nonlinear circuit is replaced by a linear and time-invariant circuit. This approximation model simplifies the analysis of the main complex circuit and illustrates variations of the output voltage by changing the load and frequency.

The converter specifications for the design are given as follows:

Table I. Main Parameters of the LLC resonant converter

Parameter	Nominal value
Input DC Voltage range	255 V ~ 375 V
Output Voltage range	12 V
Maximum output power P_{max}	300W
Series resonance capacitance	20.1nF
Series resonance inductance	74.6μH
Parallel resonant inductance	223.8μH
Switching frequency range	95.69 kHz ~ 200 kHz

The voltage gain of the converter is given as follows [10]:

$$G(Q,k,f_n)=\frac{1}{\sqrt{(1+k-\frac{k}{f_n^2})^2+(f_n^2-\frac{1}{f_n^2})Q^2}} \quad (3)$$

With the parameters:

$$Q=\frac{Z_0}{R_{ac}}=\frac{\sqrt{\frac{L_r}{C_r}}}{R_{ac}} \quad \text{where} \quad R_{ac}=n^2\frac{8V_o^2}{\pi^2 P_o} \quad , \quad \text{Normalized frequency:} \quad f_n=\frac{f_s}{f_{r1}}.$$

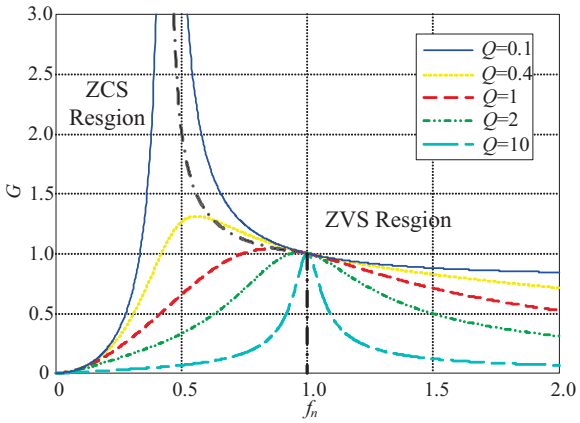

Fig. 2. Operating regions of LLC series resonant converter.

Using (3) the DC characteristics of LLC resonant converter can be derived, and are divided into ZCS and ZVS regions, as illustrated in Fig. 2. Below f_{r2} is the ZCS region and is not preferred for power MOSFET application due to the loss of ZVS operation[7].

III. DESIGN OF OUTPUT VOLTAGE CLOSED LOOP CONTROLLER

The closed loop control block diagram of voltage as shown in Fig.2.

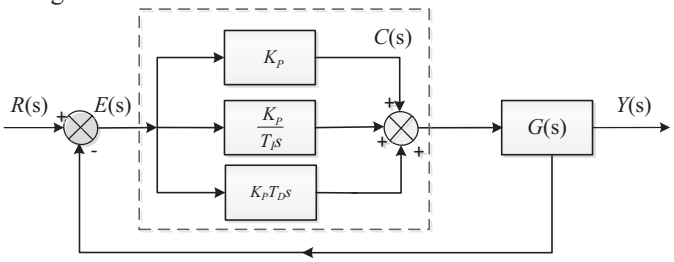

Fig. 3 Control block diagram of the system.

A. *The method of Dominant pole and phase margin*

Controlled object function is known, use the unit feedback structure of closed loop control circuit, the PID controller transfer function is:

$$C(s)=K_P(1+\frac{1}{T_I s}+T_D s) \quad (4)$$

Where

$$K_I=\frac{K_P}{T_I}, K_D=K_P T_D.$$

The second order time domain performance index of the closed-loop system is transformed into a dominant pole :

$$p_{1,2}=a\pm jb \quad (5)$$

It is follows from (4) (5) and $1+G(p_1)C(p_1)=0$ that

$$aK_P+K_I+(a^2-b^2)K_D=Re[-\frac{p_1}{G(p_1)}] \quad (6)$$

$$bK_P + 2abK_D = Im[-\frac{p_1}{G(p_1)}] \tag{7}$$

$G(jw_c)C(jw_c) = e^{j\varphi_m}$,where φ_m is the specified phase margin, ω_c is the cut-off frequency. So there are:

$$K_p = Re[\frac{e^{j\varphi_m}}{G(j\omega_c)}] \tag{8}$$

$$-\frac{K_I}{\omega_c} + K_D\omega_c = Im[\frac{e^{j\varphi_m}}{G(j\omega_c)}] \tag{9}$$

A PID controller is designed to enable a dominant pole make (6)-(9) was founded at the same time. It follows from (6)-(8) and (9) that

$$K_D = \frac{1}{2ab} Im[-\frac{p_1}{G(p_1)}] - \frac{1}{2a} Re[\frac{e^{j\varphi_m}}{G(j\omega_c)}] \tag{10}$$

$$\begin{aligned} K_I = {} & Re[-\frac{p_1}{G(p_1)}] - \frac{(a^2-b^2)}{2ab} Im[-\frac{p_1}{G(p_1)}] \\ & -\frac{(a^2+b^2)}{2a} Re[\frac{e^{j\varphi_m}}{G(j\omega_c)}] \end{aligned} \tag{11}$$

$$\begin{aligned} K_I = {} & \frac{\omega_c^2}{2ab} Im[-\frac{p_1}{G(p_1)}] - \frac{\omega_c^2}{2a} Re[\frac{e^{j\varphi_m}}{G(j\omega_c)}] \\ & -\omega_c Im[\frac{e^{j\varphi_m}}{G(j\omega_c)}] \end{aligned} \tag{12}$$

Simultaneous (11) and (12), It solves equations about ω, the solution of K_I and ω. It follows from (9) (10) and (11) that

$$K_p = \frac{2a}{(a^2+b^2)}(Re[-\frac{p_1}{G(p_1)}] - \frac{(a^2-b^2)}{2ab} Im[-\frac{p_1}{G(p_1)}] - K_I) \tag{13}$$

$$K_D = \frac{1}{a^2+b^2}(\frac{a}{b} Im[-\frac{p_1}{G(p_1)}] - Re[-\frac{p_1}{G(p_1)}] + K_I) \tag{14}$$

And then calculate the PID parameters about T_I and T_D .

B. The procedure of PID parameter

The transfer function contains a right half plane zero, but out of the design bandwidth, so the stability of the LLC converter will not be impacted. Therefore, it is necessary to consider a pair of low frequency double poles of the left half plane and a ESR zero caused by output filter capacitance[8][9]. The transfer function of the LLC resonant converter is obtained as:

$$G(s) = \frac{1.235e^{-9}s + 3.502e^{-5}}{3.953e^{-9}s^2 + 6.206e^{-7}s + 1} \tag{15}$$

This paper builds the LLC converter resonance frequency to 120KHz. The cut-off frequency of the LLC resonant converter system is usually one tenth of the switching frequency. In this paper, the cut-off frequency $\omega_c = 12\text{KHz}$.

In order to design a controller the overshoot volume should be less than 15% and the settling time is no longer than 0.5ms. According to the second order under-damped system dynamic performance index, we can get a pair of conjugate complex poles which meet the requirements, $p_{1,2} = -0.28 \pm j0.41$. A phase margin $\varphi_m^* = 60^\circ$ is set, which is normally used in practice. According to the dominant pole and phase margin method, resulted PI controller is

$$C(s) = 240100(1 + \frac{113040}{s}) \tag{16}$$

Formula (16) is for PI controller's transfer function of the system.

Using the mtthod for tuning the parameters of PID controller.The PI controller is obtained as

$$C(s) = 240100(1 + \frac{113040}{s} + \frac{1}{42265}s) \tag{17}$$

Formula (17) is general PID controller's transfer function of the system.

Research[10][11] proposed incomplete differential function. Formula (18) is incomplete differential PID controller's transfer function of the system.

$$C(s) = 240100(1 + \frac{113040}{s} + \frac{\frac{1}{42265}s}{\frac{1}{302333}s + 1}) \tag{18}$$

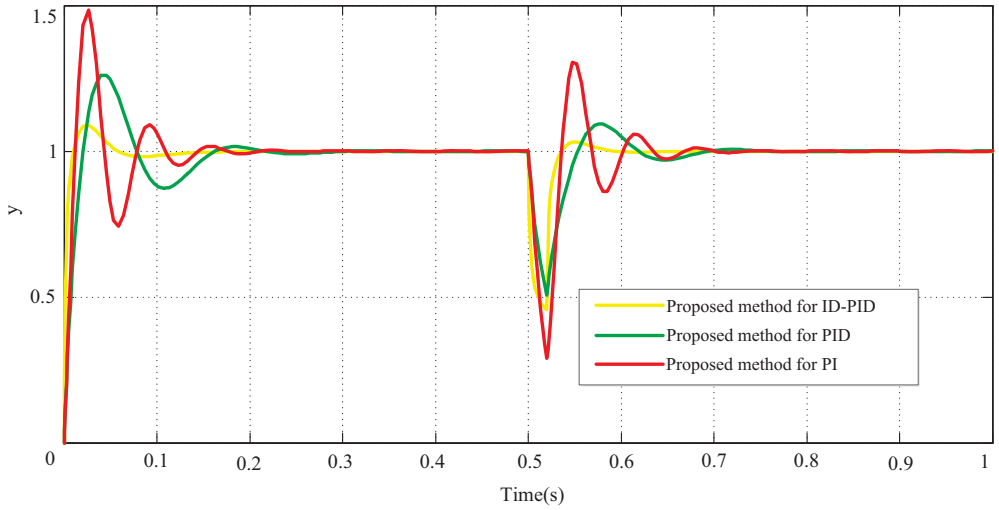

Fig. 4 Responses for PID tuning methods.

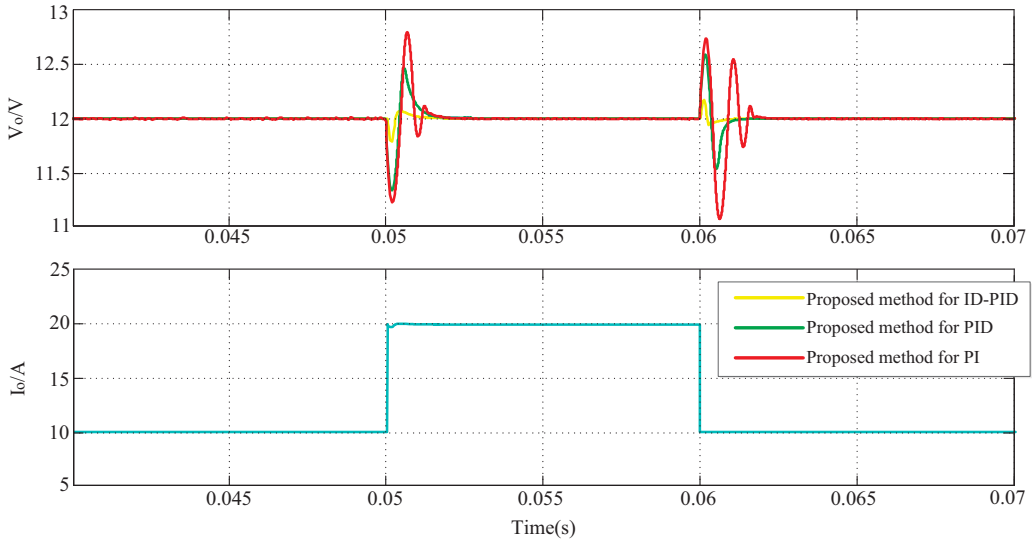

Fig. 5 Output voltage waveforms of load variation by four PID controllers.

IV. Simulation Result

Assume that the value of the input signal is the unit step and the disturbance of magnitude 0.5 at t=0.5ms are exhibited in system. Comparing the above three step response of PID/PI controllers. The corresponding response curve as shown in fig. 4. It follows from Fig. 4 that the incomplete differential PID controller of the method of dominant poles and phase margin has the best performance.

Fig. 5 shows the performance of controller for variation in load at 12V. It can be seen from the figure that the output voltage is adjusted due to the load variations for both increase and decrease in load. The output current variation is shown in Fig. 5.

V. Experimental Result

Beasd on the design guidelines in the preceding section, a prototype of a 12V, 300W converter is constructeed using the conponents as shown in table 1.

Fig. 6 shows the key waveforms of the proposed converter at full losd condition. Fig. 6 shows that v_{AB} is the voltage between two points (A and B) of the bridge arms, i_{Lr} is resonant inductor current, v_{Cr} is resonant capacitor voltage, and v_{D1} is rectifier diode D_1 terminal voltage. The experimental results show that the converter can work well under in the PFM mode under the closed-loop control of the output voltage.

Fig. 7 shows the comparative efficiency with respect to the load variation. As shown in fig. 7, the proposed LLC resonant converter always has about 5% higher efficiency than the conventional converter with symmetric control scheme in entire load range.This high efficiency indicates the significant reduction of the switching losses for the entire load by enploying the converter. Therefore, the LLC resonant converter is suitable for PC PSU.

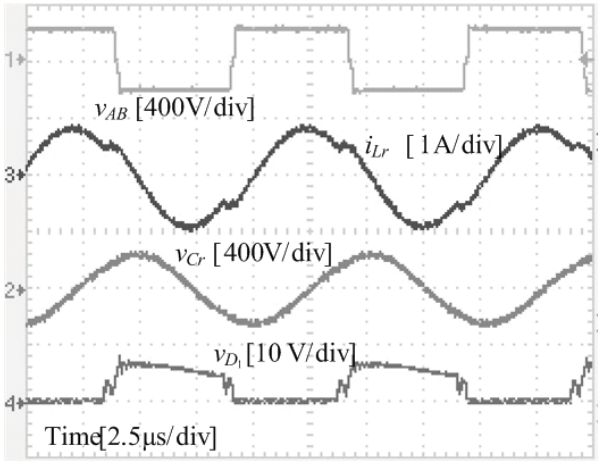

Fig. 6 Key waveforms of the LLC resonant converter

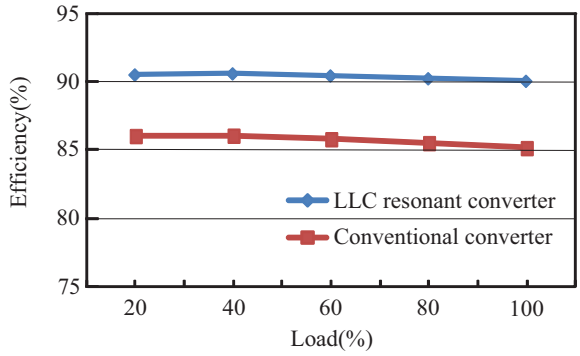

Fig. 7 Measured efficiency

VI. CONCLUSIONS

PID tuning method of dominant pole and phase margin is proposed in this paper. It is applied with voltage closed loop control in the LLC resonant converter of PC PSU. The expermental results showed the controller performance for adjustment of output voltage for load variations. It is shown that the controller has adjusted the effects of step variations in load. The method of tuning parameters makes PC PSU have a superior performance and strong robustness. The experimental results show that the efficiency of LLC power supply for the entire load is kept at 90%, its power factor is above 0.92. Compared to the conventional 80% efficiency of computer power supply, both from the volume or power point of view, the advantages of LLC is obvious. Therefore, the proposed LLC resonant converter is very suitable for high efficiency and low cost PC PSU.

REFERENCES

[1] A.I.Pressman,K.Billings,andT.Morey, *SwitchingPowerSupplyDesign*, 3rd ed. New York, NY, USA: McGraw Hill, 2009.

[2] F. O. Ongondo, I. D. Williams, and T. J. Cherrett, "How are WEEE doing? A global review of the management of electrical and electronic wastes,"*Waste Management*, vol. 31, no. 4, pp. 714–730, 2011.

[3] Emre Dincel and Mehmet Turan Söylemez, "Limitations on dominant pole pair selection with continuous PI and PID controllers," *2016 International Conference on Control, Decision and Information Technologies(CoDIT)*, Malta, 2016, pp. 741-745.

[4] Wei Tang, Junmei Huang, Jie Wu and Qing-Guo Wang, "A PID method based on dominant poles and phase mafgin," *Proceedings of the 29th Chinese Contorl Conference*, Beijing, 2010,pp. 3402-3405.

[5] Mikuláš Huba, "Triple real dominant pole tuning of a filtered PI controller," *Proceedings of the 28th International Conference 2016 Cybernetics & Informatics(K&I)*, Levoča, Slovakia, 2016, pp. 1-5.

[6] R. Beiranvand, B. Rashidian, M. R. Zolghadri, and S. M. H. Alavi, "Adesign procedure for optimizing the LLC resonant converter as a wide output range voltage source," *IEEE Trans. Power Electron*., vol. 27, no.8, pp. 3749–3763, Aug. 2012.

[7] Ray-Lee Lin; Chiao-Wen Lin, "Design criteria for resonant tank of LLC DC-DC resonant converter," *IECON 2010 - 36th Annual Conference on IEEE Industrial Electronics Society*, vol., no., pp.427-432, 7-10 Nov.2010.

[8] M.Imran Shahzad, Shahid Iqbal, Soib Taib, "LLC series resonant converter with PID controller for battery charging application," *2014 IEEE Conferrnce on Energy Conversion(CENCON)*, Johor Bahru, 2014, pp. 84-89.

[9] Brian Cheng, Fariborz Musavi, William G. Dunford, "Novel small signal modeling and control of an LLC resonant converter," *2014 IEEE Applied Power Electronics Conference and Eeposition-APEC 2014*, Fort Worth, Texas, 2014, pp. 2828-2834

[10] Na Guo, Jingtao Hu, "Velocity control sysytem with variable universe adaptive fuzzy-PD method for agricultural vehicles," *Procceeding of the 11th World Congress on Intelligent Control and Automation*, Shenyang, China, 2014, pp. 2148-2154.

[11] Yingzhe Wu, Hui Li, Ye Bi and Bo Guo, "Study on missile rudder servo system based on Mixed Fuzzy-PID control algorithm," *2011 IEEEInternational Conference on Mechatronics and Automation*,Beijing, 2011, pp. 2072-2077.